The physics of simple metal clusters: self-consistent jellium model and semiclassical approaches

Matthias Brack

Institut für Theoretische Physik, Universität Regensburg, D-93040 Regensburg, Germany

The jellium model of simple metal clusters has enjoyed remarkable empirical success, leading to many theoretical questions. In this review, we first survey the hierarchy of theoretical approximations leading to the model. We then describe the jellium model in detail, including various extensions. One important and useful approximation is the local-density approximation to exchange and correlation effects, which greatly simplifies self-consistent calculations of the electronic structure. Another valuable tool is the semiclassical approximation to the single-particle density matrix, which gives a theoretical framework to connect the properties of large clusters with the bulk and macroscopic surface properties. The physical properties discussed in this review are the ground-state binding energies, the ionization potentials, and the dipole polarizabilities. We also treat the collective electronic excitations from the point of view of the cluster response, including some useful sum rules.

CONTENTS

I. Introduction 677
II. From the Quantal Many-Body Problem to Semiclassical Jellium Drops: A Hierarchy of Approximations 679
A. The quantal many-body problem 679
B. Quantum chemistry 680
C. Molecular dynamics and static pseudopotential models 681
D. Jellium model 682
E. Phenomenological shell models 682
F. Semiclassical and classical approaches 683
III. The Self-Consistent Jellium Model 684
A. Basic concepts 684
B. Kohn-Sham-LDA calculations 685
1. Spherical jellium model 686
2. Deformed jellium model 688
3. Finite-temperature effects 691
C. Beyond LDA 692
1. Hartree-Fock calculations 692
2. Explicit evaluation of long-range correlations 692
3. Self-interaction correction 694
4. Weighted-density approximation 694
5. Gradient expansions of the xc functional 694
D. Extensions of the jellium model 695
1. Simple patches 695
2. Structureless pseudopotential models 695
IV. Electric Dipole Response of Metal Clusters 696
A. Linear-response theory 696
B. Linear-response calculations 697
1. Static dipole polarizabilities 697
2. Dipole resonances and the dynamic response 699
3. General discussion 701
C. Sum-rule approach 702
1. Sum-rule relations and classical limits 702
2. Coupling of surface and volume plasmons 704
V. Large Clusters: A Step Towards the Bulk? 707
A. Shells and supershells 707
1. Shell effects in finite fermion systems 707
2. Electronic supershell structure in large alkali clusters 709
3. From electronic to ionic shells 713
B. Semiclassical theory and large-N expansions: links to the macroscopic world 713
1. Semiclassical density-variational calculations 714
2. Liquid-drop model expansion of the energy 714
3. Asymptotic behavior of ionization potentials and electron affinities 716
VI. Summary and Conclusions 718
Acknowledgments 719
Appendix A: Mean-Field Theories 720
1. Hartree-Fock theory 720
2. Density-functional theory 721
a. Hohenberg-Kohn theorem and density-variational equations 721
b. Kohn-Sham equations 723
c. Local-density approximation 724
d. Pseudopotentials 724
e. Car-Parrinello equations 725
Appendix B: Linear-Response Theory 725
1. RPA and TDLDA 725
2. Sum rules and relations to classical hydrodynamics 726
a. Sum-rule expressions 726
b. Scaling model interpretation of moments m_3 and m_1 727
c. Local-current RPA, fluid dynamics, and normal hydrodynamics 728
References 729

I. INTRODUCTION

The theoretical description of metal clusters has recently undergone a sort of phase transition. Until less than a decade ago, metal clusters were either small micromolecules consisting of a few atoms, treated with molecular physics and quantum-chemical methods, or small particles in the mesoscopic domain, which were essentially pieces of bulk metal and could be described using the approaches of solid-state and statistical physics (Kubo, 1962; Denton *et al.*, 1973; for a review, see Halperin, 1986). With the discovery of electronic shell structure in free alkali clusters by Knight *et al.* (1984, 1985), a new era has started in which emphasis is put on the quantized motion of the delocalized valence electrons in the mean field created by the ions. The detailed ionic

 0034-6861/93/65(3)/677(56)/$10.60

structure often does not seem to affect very much the properties of alkali and other simple metal clusters. Carried to the extreme, this behavior suggests the jellium model, which is defined by a Hamiltonian that treats the electrons as usual but the ionic cores as a uniform positively charged background. This naturally leads to a description of the electron density in terms of single-particle wave functions that extend over the entire cluster. The mean field of the electrons can either be calculated self-consistently in the simple spherical jellium model (Ekardt, 1985a, 1985b), yielding the correct shell-closing numbers of electrons in many cases, or be phenomenologically parametrized including the effects of deformations (Clemenger, 1985a, 1985b) in analogy to the nuclear shell model. In this way, using relatively simple-minded approaches to the many-body problem, a wealth of experimental data on simple metal clusters can be classified and often be theoretically reproduced at least semiquantitatively (see de Heer, Knight *et al.*, 1987, for a review).

Metal clusters today provide a convenient and relatively inexpensive tool for studying the properties of finite fermion systems with increasing sizes all the way from atomic to mesoscopic dimensions, and hopefully soon to the macroscopic domain as well. The recent observation by Pedersen *et al.* (1991) and other groups of the so-called supershell structure in alkali clusters with up to three thousand atoms represents a milestone in this development.

This review article is devoted to some of the theoretical approaches used for the description of simple metal clusters. It has been conceived and prepared in close contact with Walt de Heer, whose review on experimental techniques and results appears as an adjacent article in this issue. De Heer also discusses many theoretical models and physical pictures and compares their results to the experimental data. The present article is meant to provide some background of the theory, mainly based on the microscopic mean-field and density-functional approaches. We shall be discussing the results of different theoretical models and approximations and, of course, we also have to look at experimental data in order to assess the differences. But for the detailed comparison between experiment and theory, we recommend that the reader consult de Heer's review.

We cannot possibly give an account of all theoretical aspects of metallic clusters. This would be a truly interdisciplinary task, involving atomic, molecular, and solid-state physics, quantum chemistry, and many aspects of nuclear physics as well. The author of this article is, in fact, a nuclear physicist and a certain bias in the selection of the presented material cannot be denied.

One of our aims here is to build bridges: from sophisticated quantum mechanics to simple phenomenological models on the one hand, and from atoms and "simple" molecules to the infinite bulk metal on the other hand. We also put some emphasis on semiclassical approximations and asymptotic expansions for very large particle numbers N. As a matter of fact, in order to describe the structure of clusters with many thousands of atoms one is strongly encouraged by the sheer numerical size of the quantum calculations to use statistical or quasiclassical methods. Besides, it is our belief that even for medium-sized systems in which microscopic effects play an important role, semiclassical approaches often allow for a more transparent interpretation of many phenomena than the purely microscopic theories and therefore offer better insights into the important physical mechanisms.

The jellium model has proven to be an almost ideal theoretical instrument for approaching the above goal: it is simple enough to be applied to spherical metal clusters containing up to several thousand atoms, but still allows for a self-consistent microscopic description of the average field felt by the valence electrons, correctly rendering many of the observed shell structures. At the same time it allows one to extract parameters from finite clusters that can be directly compared to those of the bulk or of plane metal surfaces for which it has been applied already over twenty years ago (Lang and Kohn, 1970, 1971, 1973). Its success in describing the "supershell" structure in very large alkali clusters, for which none of the more structural models have any chance to compete, speaks for itself.

The obvious flaw of the jellium model is its complete neglect of ionic structure. In order for the model to work, several conditions must be satisfied. First, the valence electrons must be strongly delocalized, a condition met in metals that are good conductors. Second, the ionic background must respond very easily to perturbations, to permit the electronic single-particle energies to determine the structure. This is obviously most likely to be satisfied when the valence electron has an s-wave character with respect to the ionic cores, since then there is no directionality to the binding.[1] Thus the jellium model has its main applicability in the group Ia metals, particularly sodium, potassium, and the heavier alkalis, and to some extent the Ib metals such as copper and silver.

Even in elements that slow the jellium behavior most clearly, the model cannot compete quantitatively with *ab initio*[2] quantum-chemical methods or molecular dynamics in explaining many finer experimental details of microclusters with some 20 or fewer atoms where these structural methods can be applied. For detailed accounts of the techniques and achievements of some of these methods, we refer the reader to the recent literature: Bonačić-Koutecký, Fantucci, and Koutecký (1991) have presented an extensive and very valuable review on quantum-chemical methods, and a comprehensive review on the molecular dynamics method has been given by Galli and Parrinello (1991).

---

[1]This is certainly not a sufficient condition; cf. the structure of elemental hydrogen.

[2]We use the term *ab initio* meaning a calculation using the full electron Hamiltonian with the unmodified Coulomb interaction.

The jellium model on one side and the quantum chemical approaches on the other side represent two almost diametrically opposed points of view, a situation that has led to a great deal of debate. Even their relative degrees of difficulty can be debated. Quantum chemistry has a clear and simple concept of treating the many-body problem, but in practice is computationally very complex and requires sophisticated approximations even for small molecules. The jellium model is an easy-to-use and rather effective tool for the largest clusters also, but its limitations are hard to exceed and its physical applicability is difficult to judge. Even though researchers on both sides seem to agree that either approach has its merits and its limitations, the question remains when and where to use them for those cluster sizes in which both methods can be applied. We tend to believe that, ultimately, this dispute can only be resolved empirically. Careful analyses of the *ab initio* results in terms of mean-field quantities are certainly also very useful in partially settling these questions.

In Sec. II we try to given an overview of some of the facets of the quantum many-body problem posed by the phenomena seen in metal clusters. We shall go through the successive approximations and simplifications used in the various approaches, starting from the purely microscopic *ab initio* description and ending up with semiclassical mean-field theory. We hereby hope to give the uninitiated reader a guide to the various theoretical approaches that one meets when scanning through the literature on metal clusters. Some of the general and more formal aspects of mean-field and linear-response theory have been put into appendices.

Section III deals extensively with the microscopic jellium model and its results. We hope to demonstrate that in its recent deformed versions, it yields results that are strikingly close to those of quantum chemistry and molecular dynamics. An important approximation for dealing with the jellium Hamiltonian is the local-density approximation (LDA). We also review briefly some attempts to go beyond the LDA and some extensions of the jellium model that aim at a partial inclusion of the ionic structure without sacrificing its simplicity.

There is a wealth of interesting experimental data on the electric dipole response of metallic clusters, and we devote the whole of Sec. IV to their description, using linear-response theory. Results of microscopic and semiclassical jellium model calculations are compared to those of the quantum chemical and to the structural models employing pseudopotentials. We also establish links between microscopic theories and their classical counterparts, and discuss the coupling of collective surface and volume modes.

The final section, Sec. V, is devoted to very large metal clusters. In Sec. V.A we discuss, after some general considerations on shell structure, one of the most fascinating aspects: the so-called supershell structure and its explanation in terms of a semiclassical quantization of the electronic orbits. Average cluster properties and their asymptotic behavior are discussed in Sec. V.B, in order to provide links from the microscopic to the macroscopic world. Starting from self-consistent semiclassical calculations, we show how to extract the asymptotic large-N expansion of the energy and other observables, and how some of the coefficients in these expansions are directly linked to properties of the bulk metal.

It should be clear from our emphasis that we have not been able to review and discuss all relevant theoretical papers on simple metal clusters. In particular, concerning the structural approaches, we have simply cited several important references without a detailed discussion. We apologize to all whose work is not assessed appropriately or not mentioned at all.

II. FROM THE QUANTAL MANY-BODY PROBLEM TO SEMICLASSICAL JELLIUM DROPS: A HIERARCHY OF APPROXIMATIONS

This section is an introduction and guide to the different levels of sophistication of theoretical approaches to metal clusters and to the various approximations used in different contexts. We also take the occasion here to review some selective literature on those approaches that will not be further discussed in the remaining sections.

A. The quantal many-body problem

Let us start by writing down the exact Hamiltonian for a neutral cluster consisting of N nuclei with Z electrons each:

$$\hat{H}=\sum_{\alpha=1}^{N}\left\{\frac{\mathbf{P}_\alpha^2}{2M}+\sum_{i=1}^{Z}\frac{\mathbf{p}_{\alpha_i}^2}{2m}+\sum_{\beta=1}^{N}\left[\frac{1}{2}\frac{(Ze)^2}{|\mathbf{R}_\alpha-\mathbf{R}_\beta|}+\sum_{i=1}^{Z}\left[-\frac{Ze^2}{|\mathbf{r}_{\beta_i}-\mathbf{R}_\alpha|}+\frac{1}{2}\sum_{j=1}^{Z}\frac{e^2}{|\mathbf{r}_{\alpha_i}-\mathbf{r}_{\beta_j}|}\right]\right]\right\}, \tag{2.1}$$

where M, $\mathbf{P}_\alpha$, $\mathbf{R}_\alpha$ are the mass, momenta, and coordinates, respectively, of the nuclei, m, $\mathbf{p}_{\alpha_i}$, $\mathbf{r}_{\alpha_i}$ are those of the electrons in the αth atom, and self-interactions must be left out of the double sums. This constitutes a system of $N(Z+1)$ charged particles interacting via the Coulomb forces. Although the Hamiltonian (2.1) is exactly known, it is impossible to solve the corresponding Schrödinger equation.

Luckily, the different scales of nuclear and electronic masses allow a rather clear separation of their treatment. According to the Born-Oppenheimer hypothesis, the dynamics of the nuclei may either be neglected altogether,

as in the quantum-chemical approaches (see Sec. II.B), or treated classically as a slow, adiabatic motion (see Sec. II.C), whereas the electrons must be treated quantum mechanically.

Considerable simplification is achieved by explicitly treating only the w valence electrons of each atom quantum mechanically and including the core electrons with the nuclei as ions of charge $+we$. The assumption "atom=ion+w valence electrons" generally works quite well, even for materials in which the valence electrons are not strongly delocalized, and provides the basis for a large proportion of calculations for molecules and clusters. The total Hamiltonian then is reduced to that of N interacting ions ($\hat{H}_I$) and wN interacting valence electrons ($\hat{H}_{\rm el}$) in the external field V_I provided by the ions:

$$\hat{H}=\hat{H}_I+\hat{H}_{\rm el}\ , \tag{2.2}$$

with

$$\hat{H}_I=\sum_{\alpha=1}^{N}\left\{\frac{\mathbf{P}_\alpha^2}{2M}+\frac{1}{2}\sum_{\beta(\neq\alpha)=1}^{N}\frac{(we)^2}{|\mathbf{R}_\alpha-\mathbf{R}_\beta|}\right\}, \tag{2.3}$$

$$\hat{H}_{\rm el}=\sum_{i=1}^{wN}\left\{\frac{\mathbf{p}_i^2}{2m}+V_I(\mathbf{r}_i)+\frac{1}{2}\sum_{j(\neq i)=1}^{wN}\frac{e^2}{|\mathbf{r}_i-\mathbf{r}_j|}\right\}, \tag{2.4}$$

where the ionic potential

$$V_I(\mathbf{r}_i)=\sum_{\alpha=1}^{N}V_{\rm ps}(|\mathbf{r}_i-\mathbf{R}_\alpha|)\ . \tag{2.5}$$

couples the electronic and ionic degrees of freedom. Although the core electrons are no longer explicit degrees of freedom in the wave function, they still influence the valence electrons by screening and Pauli exclusion effects. The ion potential $V_{\rm ps}$ in Eq. (2.5) is a smoothed function that includes the influence of the core electrons, and is called a "pseudopotential" in physics and an "effective core potential" in chemistry. (See Appendix A.2.d for further discussion.)

Even when the nuclear (or ionic) part of $\hat{H}$ is ignored or treated by classical equations of motion (Sec. II.C), the electron-electron interactions in Eq. (2.1) or Eq. (2.4) still constitute an unsolvable quantal many-body problem. The most common method for dealing with it is the mean-field approximation, which has been widely used for treating many-fermion systems in all branches of physics: one determines self-consistently an average potential in which the electrons move as independent particles.

One starts from a Slater determinant built of electronic single-particle wave functions and determines these by an energy variational principle. This leads to the familiar Hartree-Fock (HF) approximation (see Appendix A.1). Thus the average part of the electronic repulsion is included in the mean field (or potential), which, due to the nonzero range of the Coulomb interaction, is nonlocal. Extensions of the HF approximation are obtained by inclusion of many-particle/many-hole excitations and their interactions in perturbation theory. This constitutes, at least formally, the scheme for a complete microscopic treatment of the many-electron problem and is the basis of the quantum-chemical approaches (see Sec. II.B).

An alternative version of the mean-field approach is obtained in the framework of the density-functional theory, in which exchange effects and correlations going beyond the HF approximation can be included approximately in a local mean field. A major part of the microscopic calculations for metal clusters so far has been done using density-functional theory by solving the so-called Kohn-Sham equations (see Appendix A.2 for a brief outline of density-functional theory). In principle, density-functional theory applies only to static ground-state properties. But some information about excitation processes, like ionization potentials and electron affinities, can be gained from static calculations just by combining energy differences of clusters with different numbers of electrons.

The mean-field concept allows one to describe most of the electronic shell effects and many other static properties of metallic clusters, at least semiquantitatively, and provides the common basis for the approaches sketched in Secs. II.C–II.E below and discussed more extensively in the remaining sections III–V.

Collective excitations of the valence electrons in metal clusters have been both observed and theoretically discussed extensively. The microscopic framework for their description within mean-field theory is the random-phase approximation (RPA); its practitioners call it the time-dependent local-density approximation (TDLDA) in the context of density-functional theory. See Sec. IV.A. and Appendix B for the formal basis of this theory. In essence, it is a linear-response theory using particle-hole excitations from the determinantal ground state as the basic degrees of freedom. RPA theory was originally developed for infinite electronic systems in solid-state physics, but has been used successfully also for finite fermion systems in molecular and nuclear physics, where collective excitations play an important role. It has recently been extensively used for analyzing the optical response of metal clusters, starting from *ab initio* quantum-chemical or density-functional results for the ground state. In Sec. IV.B we review the corresponding literature and compare the different predictions.

B. Quantum chemistry

The ambitious goal of the quantum-chemical *ab initio* approach is to treat all the electronic degrees of freedom in Eq. (2.1) fully quantum mechanically. This can only be done at the cost of "freezing" the positions $\mathbf{R}_\alpha$ of all nuclei. The Born-Oppenheimer approximation thus is used to vary adiabatically the positions of the nuclei, letting the electrons adjust their motion at any time to the instantaneous external field of the nuclei, until the total static energy is minimized. This is a strict zero-temperature treatment; no zero-point motion of the nuclei is included.

Since the quantal many-electron problem is too complicated for an exact solution, one starts from the Hartree-Fock (HF) approximation (see Appendix A.1) for the electronic wave functions to obtain a self-consistent mean field; the correlations are then included perturbatively in a hierarchy of n-particle/n-hole configuration interactions or, alternatively, by superposing several Slater determinants ("multiconfigurational HF"). The pure *ab initio* treatment of all electrons is limited to very small clusters ($N \lesssim 10$); for larger systems further simplifications, using density-functional methods and/or pseudopotentials, must be made.

A detailed discussion of the quantum-chemical approaches and their results is outside the scope of our present review. We refer the reader to a very recent and exhaustive review article by Bonačić-Koutecký, Fantucci, and Koutecký (1991) on the theory and application of quantum-chemical methods for the description of metal clusters. As a few selected references for the history and development of these methods for metal clusters, let us just mention here Marinelli *et al.* (1976), Beckmann *et al.* (1980), Fantucci *et al.* (1984), Garcia-Prieto *et al.* (1984), Martins *et al.* (1985), Rao and Jena (1985), Boustani *et al.* (1987), and Bonačić-Koutecký *et al.* (1988–1991). Later in this review we shall compare some *ab initio* predictions to the results of other approaches.

C. Molecular dynamics and static pseudopotential models

In this subsection we briefly review density-functional calculations which investigate explicitly the ionic geometry of metal clusters, making use of pseudopotentials. We start with the most up-to-date, fully dynamic theory, and then discuss its static limits and some of its precursors. It is important to note that, for many purposes, and indeed for our applications here, the dynamics of the ionic motion is irrelevant to the quantities calculated. We shall discuss only properties of the clusters that are static with respect to the ionic motion. The quality of the results will depend on the form of the Hamiltonian and the approximations used to treat the electronic part. In principle, all that is required here of the dynamics is to locate the stable structures.

The molecular-dynamics (MD) method, developed by Car and Parrinello (1985), includes the dynamics of the ions by solving their classical Newton equations, coupled to the quantum-mechanical Kohn-Sham equations for the electrons (see Appendix A.2.e). This goes beyond the quantum-chemical approaches in that it is able to treat the systems dynamically (although only in the adiabatic limit due to the basic restrictions of density-functional theory; see Appendix A.2.). It also allows one to extract thermodynamic properties of complex molecular systems, at least approximately. The price one pays is that not all electrons can be treated fully quantum mechanically. Instead, the valence electrons are treated in density-functional theory, most frequently in the local-density approximation (see Appendix A.2), and the core electrons are represented by pseudopotentials (see Appendix A.2.d).[3]

On large computers, the MD method is usually combined with the simulated annealing technique of Kirkpatrick *et al.* (1983): the finite temperature is used as a technical means to allow the system to relax into the lowest minimum of its Born-Oppenheimer energy surface and thus to determine the optimal ground-state geometry of the ions.[4] This is very time consuming but crucial in view of the fact that the number of isomeric minima to which the simpler steepest-descent method can lead increases very rapidly with the number of ions (Hoare and McInnes, 1983). In view of the above remarks, we shall refer to these calculations as pseudopotential calculations, emphasizing the approximation in the Hamiltonian, rather than as Car-Parrinello or MD calculations, which would emphasize the search for the stable structures.

As examples of MD calculations for the ionic structure of small metal clusters and their thermal properties, we mention that Ballone *et al.* (1989) studied Na_{20} and $Na_{10}K_{10}$ clusters; Na_N clusters with $N \leq 20$ were investigated by Röthlisberger and Andreoni (1991). Jones (1991) has investigated the ground-state geometries of small Al clusters with N up to 10. The fission of a small doubly charged sodium cluster was investigated in MD calculations by Barnett *et al.* (1991).

The pseudopotential approach represents today perhaps the most effective tool for treating molecules and clusters containing up to several tens of atoms with their full ionic structure, in the adiabatic limit also for the inclusion of their dynamics. For a recent comprehensive review on the pseudopotential approach we refer the reader to Galli and Parrinello (1991). A short status report on MD calculations for small metal and semiconductor clusters was given by Andreoni (1991).

Generally, it can be said that the ionic ground-state structures of small metallic clusters obtained in MD calculations are practically identical to those found in *ab initio* quantum-chemical calculations.

Another approximation scheme to include electron-ion correlations dynamically is the so-called "effective medium theory" developed some time ago by Nørskov and Lang (1980) and Nørskov (1982). The effect of an "embedding" electron density ρ_e on the binding of an

---

[3]The name "*ab initio* molecular dynamics," which is often used in the literature, should not be mistaken as indicating an all-electron theory, which in this dynamical form would be impossible even for small clusters. It is merely used to indicate that *ab initio* pseudopotentials, derived from first-principles quantum-chemical calculations, have been employed.

[4]A modified version of the simulated annealing method was used by Manninen (1986b) to calculate the ionic ground-state structures of Na microclusters with $N \leq 8$.

atom is first studied microscopically in density-functional theory with LDA, leading to an energy functional of the atom that depends on ρ_e as an external parameter. Then this functional is used for a metal to include in each Wigner-Seitz cell the effects of the (superposed and averaged) electronic density tails of all neighboring cells. In this model, the Wigner-Seitz radius and the cohesive energy of a given metal can be explicitly calculated.

So far the effective medium theory has been applied mostly to metallic bulk and surface properties, particularly to the process of melting. For a recent review, we refer the reader to Jacobsen and Nørskov (1988). Christensen *et al.* (1991) have presented the first application of the theory to small Cu clusters. The electronic shell effects were calculated from a tight-binding Hamiltonian and included in a way that is reminiscent of the shell-correction theory of Strutinsky (1968) (see end of Sec. V.B.1). Their model allows one to describe in a self-consistent, albeit approximate, way the interplay of ionic and electronic shell effects. Nielsen *et al.* (1992) have used it to simulate the melting of a Cu cluster with 16 727 atoms. This method appears rather promising, but no calculations for simple metal clusters have been reported so far.

As precursors to MD or simulated annealing calculations, many static investigations of the structure of small clusters have been performed over the last decade, using more or less sophisticated pseudopotentials. Since the ionic structure requires a fully three-dimensional solution of the electronic Kohn-Sham equations, and the optimal geometry of the ions must, in principle, be searched systematically by minimizing the total energy, even purely static investigations are very complex and time consuming. With the present-day generation of computers, this is most elegantly done by the simulated annealing technique.

We discuss some of the results of static structural calculations when comparing them to other calculations in later sections. Let us mention here some approximate investigations in which the ionic structure has been simplified. Small cubic crystals were studied by Iñiguez *et al.* (1986). Martins *et al.* (1981) and Baladron *et al.* (1985) introduced a spherical averaging of the pseudopotentials in order to have spherical symmetry. Manninen (1986a) imposed spherical symmetry only on the electronic density; he minimized the classical part of the total energy (the "Madelung energy"), varying the full three-dimensional geometry of the ions. A systematic series of studies with spherically averaged pseudopotentials (the "SAPS model") was started by Iñiguez *et al.* (1989, 1990) and López *et al.* (1990) and recently extended to include simulated annealing (Borstel *et al.*, 1992). For the applications of the spherically averaged pseudopotential model to metal clusters, we refer the reader to the recent reviews of Balbás and Rubio (1990) and of Borstel *et al.* (1992). Finally, we note that a semiclassical version of the spherically averaged pseudopotential model using variational trial densities (see Sec. V.B) was developed by Spina and Brack (1990).

D. Jellium model

The most dramatic but efficient simplification is to ignore the ionic structure totally, replacing the charge distribution of the ions by a constant background charge in a finite (spherical or deformed) volume. This is the three-dimensional, finite-size version of the jellium model which was successfully used long ago for the description of metallic bulk and surfaces properties (Lang and Kohn, 1970–1973). The self-consistent mean field of the electrons can be calculated microscopically in this model including the shell effects due to their quantization. It requires, however, the density of the ions (or, correspondingly, the Wigner-Seitz radius r_s) as an external parameter, which characterizes the nature of the metal.

The total neglect of the ionic structure is better justified than one might think at first sight: the pseudopotentials (see Appendix A.2.d) have no singularities and their sum in V_I [Eq. (2.5)] is, indeed, a rather smooth function. This is the combined effect of screening and the Pauli principle, coming from the inner core electrons that fill the lowest orbitals in the Coulomb-like potentials of the individual nuclei. We refer the reader to textbooks on solid-state physics (e.g., Ashcroft and Mermin, 1976) for a more detailed discussion.

For finite clusters, a wealth of papers initiated by Ekardt (1984a, 1984b) and independently by Beck (1984a, 1984b) has shown that a self-consistent and essentially parameter-free microscopic jellium model calculation can account qualitatively, and in many cases even quantitatively, for many experimentally observed properties of metal clusters, in particular those of alkali metals (see the review of de Heer, 1993). Deformations of the jellium background (axial or triaxial) or a finite temperature of the electrons can be included at reasonable cost in the jellium model. The self-consistent jellium model will be reviewed in Sec. III and some of its applications in Secs. IV and V.

The justification of the jellium model for the description of clusters is, and probably will remain, an object of much debate and research. However, its undoubted virtue is that it can also be applied to large clusters with many hundreds or thousands of atoms, where the more structural models cannot be used for practical reasons. The most beautiful example is the explanation of the "supershells" in large alkali clusters, which we shall discuss in Sec. V.A.

E. Phenomenological shell models

Many shell and single-particle effects do not depend very crucially on the microscopic self-consistency of the total mean field, such as is obtained by iteratively solving the Hartree-Fock or the Kohn-Sham equations. One may therefore give up the self-consistency by simply parametrizing the total average potential in an easy-to-use form and then solving just once the Schrödinger equation, in order to obtain single-particle spectra and

wave functions. This leads, of course, to a considerable gain in numerical simplicity. The cost of such simplicity is a less fundamental description, since contact with the two-body interaction is lost and the parameters of the model have to be determined by fits to experimental observables. The advantage is a greater flexibility, allowing closer contact with the measured data.

The prototype of such a phenomenological shell model is the Woods-Saxon potential, which was successfully introduced into nuclear physics by Maria Goeppert-Mayer (1949) and independently by Haxel, Jensen, and Suess (1949). After inclusion of a strong spin-orbit coupling term, it became possible for the first time to explain the so-called magic numbers of nucleons responsible for the extra stability of certain nuclei like $^{208}_{82}Pb^{126}$ (cf. Sec. V.A.1). The nuclear shell model has been successfully used to explain many single-particle properties of spherical nuclei, despite the lack of an underlying Hartree-Fock basis in the context of realistic nucleon-nucleon interactions. After the discovery of nuclear deformations through low-lying rotational excitations, Nilsson (1955) introduced a shell model for deformed nuclei, which is based on an axially deformed harmonic-oscillator potential including a spin-orbit coupling term and an attractive term proportional to the square l^2 of the single-particle angular momentum operator that simulates a steeper wall. The Nilsson model was very successful in explaining the ground-state deformations of many nuclei and their single-particle excitations (Mottelson and Nilsson, 1955; see also Bohr and Mottelson, 1975). It is rather remarkable that one is able to predict shapes with a model that uses only a single-particle Hamiltonian, and a very oversimplified one at that. The explanation for nuclear physics seems to be that self-consistency in shape between particle density and the potential field is a very powerful constraint, and that shell closure effects can occur as a function of deformation as well as of particle number (see also Sec. V.A.1).

Clemenger (1985a, 1985b) adapted the Nilsson model to small axially deformed Na clusters by dropping the spin-orbit term and readjusting the coefficient of the l^2 term. This model has since been frequently used in metal cluster physics and is usually referred to as the Clemenger-Nilsson model. The model seems to work quite well in reproducing the overall shapes of clusters as calculated by pseudopotential or *ab initio* methods. We shall not discuss it here any further; it is well explained and extensively used in the reviews by de Heer, Knight *et al.* (1987b) and de Heer (1993). Reimann *et al.* (1993) have proposed an extension of the Clemenger-Nilsson model, fitted to spherical Kohn-Sham spectra, and applied it to large deformed sodium clusters with $N \lesssim 800$ (see Sec. V.A.1).

The three-dimensional harmonic-oscillator potential without l^2 term was used by Saunders (1986) to describe triaxially deformed clusters.

Nishioka *et al.* (1990) have introduced a spherical Woods-Saxon potential for Na clusters particularly in connection with calculations of the so-called supershell structure, which we shall discuss in Sec. V.A. They determined the parameters of their potential by fitting it directly to the Kohn-Sham potentials obtained in the self-consistent jellium model calculations of Ekardt (1984b) for Na clusters with $N \leq 192$. Clemenger (1991) has adapted the Woods-Saxon potential to a variety of metals and studied the scaling properties of the supershell structure as a function of the Wigner-Seitz parameter r_s. Frauendorf and Pashkevich (1993) have adapted the Woods-Saxon potential to deformed clusters with $N \lesssim 300$.

The omission of the spin-orbit term in all these shell models for metal clusters seems to be empirically justified by the fact that no strong evidence of spin-orbit splittings has been observed so far. This can be theoretically understood considering the relativistic effects in a jellium potential. First, relativistic effects in atoms and molecules are generally much smaller than in nuclei. Secondly, the Thomas term, which one obtains from a nonrelativistic reduction of the Dirac equation for fermions moving in a spherical electrostatic potential $V(r)$, is proportional to $(1/r)dV/dr$. In atoms, this is strongest near the center where the potential is proportional to $1/r$ and thus affects most strongly the electrons in the lowest orbits. In clusters, $V(r)$ is flat in the interior so that dV/dr is practically zero. In the surface, where the gradient is large, the extra factor $1/r$ gives an extra suppression, which varies as $N^{-1/3}$. Detailed relativistic Kohn-Sham calculations (Schöne, 1991) confirm, indeed, the smallness of spin-orbit splittings within the jellium model.

F. Semiclassical and classical approaches

One more simplification can be made that leads to a considerable gain of efficiency in treating very large systems: the neglect of shell effects. This is done automatically by the explicit use of semiclassical approximations to the kinetic-energy functional $T_s[\rho]$ (see Appendix A.2.a). The density-functional formalism can then be exploited for direct density-variational calculations: one no longer varies many electronic single-particle wave functions, but one single function, the electronic density $\rho(\mathbf{r})$ (or, if relevant, two spin densities). By doing this one sacrifices the single-particle structure, and thus shell effects, but the advantage is an enormous gain in simplicity and calculational speed, and this can still give significant results for average properties of the considered system. The famous prototype of such a model is the Thomas-Fermi (TF) model of the atom.

Extensions of the Thomas-Fermi model (the TFW model, ETF model, etc.; see Appendix A.2.a) were developed long ago and have been successfully used for finite fermion systems in many branches of physics. The variation of the density $\rho(\mathbf{r})$ can either be done exactly, leading to an Euler-Lagrange type (integro-) differential equation, or in restricted variational spaces using trial density functions. In fact, the first self-consistent jellium model calculations for spherical metallic clusters were

carried out using such a semiclassical density-variational method by Cini (1975).

Many average properties of metal clusters can be described in such density-variational calculations, which we shall review in Sec. V.B. A more formal and fundamental interest of this approach is the possibility of connecting the microscopic models to purely classical ones. In the large-N limit, the clusters become classical spheres or drops, and a systematic expansion, the so-called "leptodermous" expansion, can be developed to determine the surface and curvature energies from semiclassical theory. This leads to the self-consistent foundation of a liquid-drop model similar to that in nuclear physics (see, for example, Myers and Swiatecki, 1969). Likewise, the asymptotic behavior of electronic ionization potentials and affinities and their classical limits, which have received much attention in the literature, can be studied rigorously using this technique. These recent developments will also be reviewed in Sec. V.B.

Just as for the static energetics of finite fermion systems, so for their linear-response behavior one can obtain links to classical models by the use of semiclassical and large-N limits of the RPA method. An approximate theory extracted from the RPA under the assumption of local currents (Reinhard *et al.*, 1990) leads to the connection with classical hydrodynamics (or, to use a more appropriate term, Fermi-fluid dynamics). From this point of view, several aspects of surface plasmons can be discussed qualitatively, and the physics becomes more transparent than in the purely microscopic RPA approach. Section IV.C is devoted to these topics.

The gross structure of the shell effects in the single-particle spectrum and the total energy of a finite fermion system can also be described rather well by semiclassical techniques that are based on the quantization of classical trajectories. The well-known prototype of this idea is the old Bohr-Sommerfeld quantization rule. In its modern version, it has become very successful in explaining the beating pattern of the so-called supershells in large alkali clusters. This will be discussed in Sec. V.A.

III. THE SELF-CONSISTENT JELLIUM MODEL

A. Basic concepts

The basic idea of the self-consistent jellium model is to replace the distribution of the ionic cores by a constant positive background or jellium density[5] ρ_{I0} in a finite volume and to treat only the valence electrons explicitly in the mean-field approximation, either microscopically, as described in this section, or semiclassically (see Sec. V.B). The jellium background may be spherical, ellipsoidal, or arbitrarily deformed.

Almost all jellium calculations so far have been performed within density-functional theory, the formal aspects of which we have summarized in Appendix A.2. (For some recent Hartree-Fock calculations, see Sec. III.C.1.) In density-functional theory the total energy of the cluster is expressed as a functional of the local electron density $\rho(\mathbf{r})$:

$$E[\rho]=T_s[\rho]+E_{\rm xc}[\rho]+\int\left\{V_I(\mathbf{r})\rho(\mathbf{r})+\frac{1}{2}\rho(\mathbf{r})\left[e^2\int\frac{\rho(\mathbf{r}')}{|\mathbf{r}-\mathbf{r}'|}d^3r'\right]\right\}d^3r+E_I\ . \tag{3.1}$$

Here $T_s[\rho]$ is the (noninteracting) kinetic-energy density and $E_{\rm xc}[\rho]$ the exchange-correlation energy density (see Appendix A.2); the fourth term is the direct (Hartree) Coulomb energy of the electrons. $V_I(\mathbf{r})$ is the ionic background potential, related to the background jellium charge density $\rho_I(\mathbf{r})$ by

$$V_I(r)=e^2\int\frac{\rho_I(\mathbf{r}')}{|\mathbf{r}-\mathbf{r}'|}d^3r'\ . \tag{3.2}$$

The jellium density is usually assumed to be uniform, i.e., $\rho_I(\mathbf{r})=\rho_{I0}$ inside the cluster and zero outside. The potential (3.2) here replaces the ionic potential (2.5) used in the pseudopotential models. The E_I in Eq. (3.1) is the electrostatic energy associated with the jellium background. It does not depend on the electron density but is included so that $E[\rho]$ (3.1) represents the total binding energy of the cluster. The density $\rho(\mathbf{r})$ must be normalized to the total number wN of valence electrons:

$$\int\rho(\mathbf{r})d^3r=wN\ , \tag{3.3}$$

where w is the valence factor (number of valence electrons per atom).

If the electron density is written in terms of single-particle wave functions $\varphi_i(\mathbf{r})$ as

$$\rho(\mathbf{r})=\sum_{i=1}^{wN}|\varphi_i(\mathbf{r})|^2 \tag{3.4}$$

—which is always possible for physical (i.e., non-negative and normalizable) densities due to the so-called Coleman theorem (Gilbert, 1975)—then the noninteracting kinetic-energy functional $T_s[\rho]$ is

$$T_s[\rho]=\int\tau(\mathbf{r})d^3r=\frac{\hbar^2}{2m}\int\left\{\sum_{i=1}^{wN}|\nabla\varphi_i(\mathbf{r})|^2\right\}d^3r\ . \tag{3.5}$$

[5]Throughout this paper, we denote by ρ the particle densities and not the charge densities. The charges (in multiples of e) appear explicitly in all formulae with their correct signs.

By a variation of the energy $E[\rho]$ (3.1) with respect to the $\varphi_i^*(\mathbf{r})$, one then arrives at the so-called Kohn-Sham equations, whose solutions will be discussed in Sec. III.B.

A direct variation of the energy with respect to the function $\rho(\mathbf{r})$ is also possible if one is satisfied with semiclassical approximations for the kinetic-energy functional $T_s[\rho]$. This is at the cost of neglecting the shell effects, but has the advantage that one is varying only one function $\rho(\mathbf{r})$ instead of wN wave functions $\varphi_i(\mathbf{r})$, and still allows one to obtain average cluster properties self-consistently. We shall discuss this approach and the corresponding calculations in Sec. V.B.

Most applications of the jellium model to metal clusters so far have been restricted to the local-density approximation (LDA) for the exchange-correlation (xc) functional $E_{\rm xc}[\rho]$. As discussed in Appendix A.2.c, this approximation consists in using locally the exchange-correlation energy per electron $e_{\rm xc}(\rho)$ obtained in many-body calculations for an infinite system of electrons with constant density ρ, i.e., $e_{\rm xc}(\rho)$ is taken at the local value $\rho=\rho(\mathbf{r})$ everywhere in the finite system. By construction, this approximation is exact in those regions of space where the density $\rho(\mathbf{r})$ is constant, and it is badly justified where the density varies strongly, such as in the surface region of metal clusters. In spite of its simplicity, the LDA in connection with the Kohn-Sham approach has met with considerable success in almost all branches of physics.[6]

Metal clusters (besides metal surfaces) present perhaps one of the most crucial testing grounds for the LDA, since their surfaces are typically much steeper than those of atoms or small molecules. However, the success of the LDA in conjunction with the jellium model in describing surface energies and work functions for metal surfaces (Lang and Kohn, 1970, 1971; Monnier *et al.*, 1978)—at least for alkali-like metals—has encouraged, and to some extent also justified, its application to metallic clusters. We shall briefly discuss some extensions of the LDA in Sec. III.C below and, in particular, report there on an encouraging test of the exchange part of the LDA functional by means of a Hartree-Fock calculation for finite metal clusters (Sec. III.C.2).

One essential point of the jellium model is that it contains only one single parameter, namely, the Wigner-Seitz radius r_s, which characterizes the metal. It is related to the jellium density ρ_{I0} by

$$\rho_{I0}=\left[\frac{4\pi}{3}r_s^3\right]^{-1} . \tag{3.6}$$

Otherwise, the model is completely free of parameters, since the electron density is determined variationally. Usually, one takes the bulk value for r_s corresponding to the ionic lattice in the crystal. Naturally, this is only justified for large clusters. In the jellium model, however, we have no way to determine the finite-size variation of r_s theoretically, so that the simplest choice is that of the bulk value.

A remark about the internal consistency of the jellium model might be appropriate here. If we consider the inner part of a large neutral cluster and neglect the surface effects, the energy per electron $e(\rho)$ as a function of the (constant) density ρ is given by

$$e(\rho)=\frac{\hbar^2}{2m}\kappa\rho^{2/3}+e_{\rm xc}(\rho) , \tag{3.7}$$

where the first part is the kinetic energy per electron [see Eq. (A19) of Appendix A.2.a]. The Coulomb energies cancel exactly if the density ρ is chosen to be equal to the jellium density ρ_{I0}, which must be done to ensure charge neutrality. If we now search for a minimum of $e(\rho)$ in Eq. (3.7) with respect to varying ρ (and, with it, ρ_{I0}), we find it for values $r_s\simeq 4$–4.3 a.u., depending somewhat on the detailed LDA exchange-correlation functional used. For example, for the functional of Gunnarsson and Lundqvist (1976) [see Eq. (A.33) in Appendix A.2.c], which has often been used for metal cluster calculations, this minimum is at $r_s=4.08$ a.u. Very similar values are obtained with all other exchange-correlation functionals in the literature. In such a variational calculation there is, of course, only one metal that has a stationary value of its density in the bulk region. It is perhaps no coincidence that the jellium model works best for alkali metals, in particular sodium, with r_s values close to this minimum. It has, indeed, already been observed by Lang and Kohn (1970) that good surface energies are obtained in the jellium model only for metals with $r_s \gtrsim 4$ a.u. (see also Sec. V.B.2). In fact, the model completely breaks down for $r_s \lesssim 2.3$ a.u., in that it gives negative surface energies for the corresponding metals (e.g., aluminum). This should not be forgotten when applying the jellium model to finite clusters, in particular when their shape is not kept spherical. A negative surface energy means that the cluster is not stable against deformation, so that, in the jellium model, the energetically most stable configuration for a finite aluminum system is not a sphere but alu-foil!

B. Kohn-Sham-LDA calculations

The variation of the energy $E[\rho]$ (3.1) with respect to the single-particle wave functions $\varphi_i^*(\mathbf{r})$,

$$\frac{\delta}{\delta\varphi_i^*(\mathbf{r})}E[\rho(\mathbf{r})]=0 \tag{3.8}$$

with the subsidiary condition that the $\varphi_i(\mathbf{r})$ be normalized, leads to the Kohn-Sham equations (see Appendix A.2)

$$\{\hat{T}+V_{\rm KS}(\mathbf{r})\}\varphi_i(\mathbf{r})=\varepsilon_i\varphi_i(\mathbf{r}) . \tag{3.9}$$

$\hat{T}$ is the kinetic-energy operator; the local potential

[6] See, for example, Jones and Gunnarsson (1989) or Dreizler and Gross (1990) for its applications to electronic systems, and Sprung (1972) for a discussion of the LDA in nuclear physics.

$V_{\rm KS}(\mathbf{r})$ is a sum of three terms:

$$V_{\rm KS}(\mathbf{r})=V_{\rm KS}[\rho(\mathbf{r})]=V_{\rm xc}[\rho(\mathbf{r})]+V_H[\rho(\mathbf{r})]+V_I(\mathbf{r}) , \tag{3.10}$$

of which the first is due to the exchange and correlation contributions:

$$V_{\rm xc}[\rho(\mathbf{r})]=\frac{\delta}{\delta\rho(\mathbf{r})}E_{\rm xc}[\rho] ; \tag{3.11}$$

$V_H[\rho]$ is the Hartree potential of the electrons, given in the square brackets in Eq. (3.1) above, and V_I is the jellium potential (3.2). The constants ε_i in Eq. (3.9) are the Lagrange multipliers used to fix the norm of the ith state; their interpretation as single-particle energies is not justified in general as discussed in Appendix A.2.

Since V_H and $V_{\rm xc}$ depend on the density $\rho(\mathbf{r})$, the Kohn-Sham equations (3.9) are nonlinear in the φ_i and must be solved by iteration until self-consistency is reached (i.e., until the results do not change any more upon iteration). In general, (3.9) are partial differential equations in the three spatial coordinates and their solution is not trivial. However, if symmetries are assumed or imposed, the problem simplifies considerably. A large majority of Kohn-Sham calculations so far have been performed assuming spherical symmetry of the clusters. The calculation then becomes one-dimensional and is relatively easy to do, even for clusters with up to $N\simeq 3000$ electrons (Genzken and Brack, 1991). We review spherical Kohn-Sham calculations in Secs. III.B.1; their extension to finite temperatures is discussed in Sec. III.B.3 and their application to very large clusters in Sec. V.A.2.

When major electronic shells are only partially filled, the mean field tends to be deformed, as is well known from nuclear physics (see also Sec. V.A.1). The spherical jellium model therefore must be generalized to include deformed ionic background densities, in order to minimize the total energy of such "nonmagic" systems. In an average sense, this simulates the nonspherical distributions of the ions known from *ab initio* and molecular-dynamics calculations. In Sec. III.B.2, jellium calculations in two and three dimensions are reviewed, corresponding to axially and nonaxially deformed clusters, respectively.

1. Spherical jellium model

In the spherical jellium model, the ionic background density $\rho_I(r)$ is that of a uniformly charged sphere with radius R_I:

$$\rho_I(r)=\rho_{I0}\Theta(r-R_I) , \quad R_I=r_sN^{1/3} , \tag{3.12}$$

in which the value of R_I is fixed by the number N of ions. The ionic potential $V_I(r)$, which replaces the sum of individual ionic potentials (2.5), is then easy to evaluate and is given by

$$V_I(r)=-\frac{wNe^2}{2R_I}\left[3-\left[\frac{r}{R_I}\right]^2\right] \quad \text{for } r\le R_I$$

$$=-\frac{wNe^2}{r} \quad \text{for } r\ge R_I , \tag{3.13}$$

and the ionic energy E_I is simply

$$E_I=\frac{3}{5}\frac{(wNe)^2}{R_I} . \tag{3.14}$$

If the electron density is also assumed to have spherical symmetry, the total Kohn-Sham potential (3.10) is spherical and the single-particle states $\varphi_i(\mathbf{r})$ will have good angular momentum quantum numbers l_i,m_i, their angular parts being given by $Y_{l_im_i}(\theta,\phi)$ in polar coordinates (r,θ,ϕ). Equations (3.9) can then be reduced to radial Schrödinger equations for the radial parts $R_{n_il_i}(r)$ of the wave functions and solved numerically on a one-dimensional mesh in the variable r (Beck, 1984a, 1984b; Ekardt, 1984a, 1984b). As a variational precursor of this model we mention that of Martins *et al.* (1981). In their treatment, which is not fully self-consistent, they replaced the Kohn-Sham potential (3.10) by a simple variational square-well potential.

During the last eight years, many papers have been published with results of spherical jellium model calculations. We cannot cite them all here; many of them are referred to when we compare their results with experimental data or with results of other models. The results of several groups have been summarized by Balbás and Rubio (1990). All authors, except those cited in Sec. III.C, used LDA functionals for the exchange-correlation part of the energy.

As an illustration, we show in Fig. 1 (upper part) the Kohn-Sham potentials of three alkali clusters with $N=40$, obtained in some early jellium model calculations by Chou *et al.* (1984). Their shape is similar and scales essentially with the Wigner-Seitz radius r_s. The minimum near the surface is related to the fact that the electronic density always has a maximum there as a consequence of the Friedel oscillations (Lang and Kohn, 1970). Some of the Kohn-Sham single-particle levels ε_i are shown in the lower part of Fig. 1 directly as functions of r_s; their positions for the respective metals are marked by the dashed vertical lines.

The successes and failures of the spherical jellium model have been discussed extensively by de Heer (1993) while comparing its results with experimental data. Let us summarize here some general trends and add a few remarks:

(i) Spherical-shell closings: The most prominent "magic numbers" observed in mass abundances, ionization potentials, and electron affinities correspond to the filling of major spherical shells and are in general correctly reproduced for alkali metals, some noble metals, and, to some extent, also for Al clusters. A problem exists with the atomic numbers 34 and 40: The self-consistent jellium

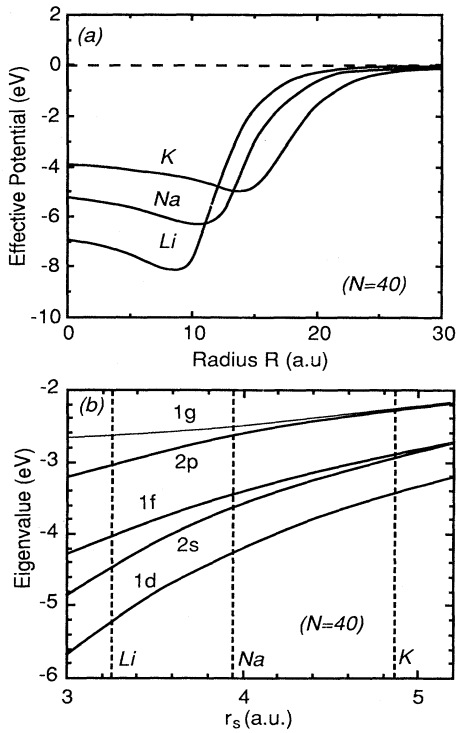

FIG. 1. Potentials and electronic single-particle energies ε_i for three alkali clusters with $N=40$, obtained in the self-consistent spherical jellium model by Chou *et al.* (1984): upper part, total Kohn-Sham potentials versus radius r; lower part, electronic Kohn-Sham levels ε_i of the $1d-1g$ shells vs Wigner-Seitz radius r_s. Values for the three metals Li, Na, and K, respectively, are indicated by the vertical dashed lines.

model for Na clusters (and, to a lesser extent, for Li clusters) gives $N=34$ as a stronger spherical shell than $N=40$, contrary to experiment. This is due to too large a splitting between the $1f$ state and the $2p$ state lying above it (see Fig. 1 above). Some remedies for this failure are discussed in Sec. III.D below. The phenomenological Clemenger-Nilsson model does better here (see also de Heer, 1993), but this is just due to a suitable choice of the l^2 term. Similarly, a Woods-Saxon-type potential is better, since it is flat in the inner part and does not exhibit the "Friedel dip" near the surface (see Fig. 1), which in the self-consistent model leads to some extra attraction for higher-l states and thus pulls the $1f$ state down more than the $2p$ state. (Similar discrepancies are found for larger spherical shells and subshells; we refer the reader to Sec. V.A.2 in connection with very large alkali clusters.) In general, it can be said that the detailed ordering and spacing of single-particle levels near the Fermi surface, and therefore the correct prediction of "magic numbers," can be rather sensitive to the radial shape of the potential. Of course, the ionic structure also plays a role when it comes to these details. Indeed, Kohn-Sham calculations by Borstel *et al.* (1992) including the ionic structure schematically in the so-called spherically averaged pseudopotential model (see Sec. II.C) also yield a reduction of the $2p$-$1f$ gap.

(ii) Deformed-shell closings: In principle, the imposed spherical symmetry does not allow one to treat clusters in the regions between the major spherical shells. From the analogous situation in nuclei, we know that such clusters are deformed (see also the general discussion on shell effects in Sec. V.A.1). This is, indeed, the case and will be discussed in the next subsection.

(iii) Ionization potentials (IP) and electron affinities (EA): The jellium model with LDA gives a reasonable qualitative description of these quantities, namely their approaching the bulk work function W like $1/R$ for large N and their sawtooth-like behavior at major shell closings. (For an extensive discussion concerning the asymptotic slopes of IP and EA plots versus $1/R_I$, see Sec. V.B.3.) However, in Na and K, the average values of the IP are too large. This is related to the bulk values W, which are too large in the jellium model, as is well known since the pioneering calculations of Lang and Kohn (1971). It can partially be remedied by inclusion of the ionic structure via pseudopotentials (Lang and Kohn, 1971; Monnier *et al.* 1978). Moreover, the finer details of IPs and EAs are not correctly explained in the spherical jellium model; the experimentally observed odd-even staggering is missing and the amplitude of the shell fluctuations is exaggerated by a factor of up to two. For small clusters ($N \lesssim 12$), the *ab initio* and the pseudopotential models with local-spin-density approximation (LSDA) clearly give a better quantitative description. Some of the fine structure is partially improved in the spheroidal model discussed below. [An improvement over the LDA results, both for neutral and for the particularly critical negatively charged clusters, was obtained in jellium model calculations using a nonlocal weighted-density approximation to the *xc* energy (WDA; see Sec. III.C.4) by Rubio *et al.* (1989, 1991a) and Balbás *et al.* (1989, 1991). On the other hand, very recent Hartree-Fock plus perturbation-expansion calculations by Guet *et al.* (1993) seem to confirm the validity of the LDA for both exchange and correlation effects, by yielding almost identical ionization potentials to those of the Kohn-Sham-LDA approach for a series of Na clusters.]

(iv) Dipole polarizabilities and photoabsorption cross sections: We discuss these quantities and their description in the jellium model extensively in Sec. IV.

It is clear that in clusters with up to $N \sim 20$ atoms the jellium model is not quantitatively competitive with quantum-molecular methods or spin-dependent LDA calculations with pseudopotentials. For very large clusters with hundreds or thousands of atoms, however, the jellium model will presumably remain the only tractable way to make theoretical predictions. The agreement obtained recently with the experimentally observed supershell structure (see Sec. V.A) is, indeed, very encouraging. It is therefore interesting to ask to how small a size the jellium model can be extrapolated.

Some points of comparison with respect to *ab initio* and pseudopotential theory will be mentioned here.

First, the basic starting assumption of delocalized single-particle wave functions seems to be rather well satisfied for alkali-metal clusters. For example, in the configuration-interaction (CI) calculation of Na_6 by Bonačić-Koutecký *et al.* (1991), the leading ground-state configuration has an amplitude of 0.91 in the CI wave function. This is despite the fact that correlation effects are known to be crucial to obtain binding of alkali-metal clusters. Evidently the LDA is a rather good approximation. Secondly, the electron densities in these more microscopic calculations are seen to concentrate on the interstices of the ionic lattice rather than on the atoms or on the lines between neighboring atoms. This shows a degree of delocalization not present in ordinary chemical binding. Also, the large-scale nodal structure of the single-particle wave functions exactly duplicates that of the jellium model. This is particularly striking in the highly symmetric clusters such as $Na_8(T_d)$, where the occupied s and p jellium states as well as the empty s and d orbitals can be identified with the corresponding molecular orbitals. Finally, Röthlisberger and Andreoni (1991) have compared the spherically averaged densities and mean potentials of their pseudopotential calculations with those of the spherical jellium and phenomenological models. We shall come back to this comparison in the context of the deformed jellium models discussed in the next section.

2. Deformed jellium model

Some of the shortcomings of the spherical jellium model can be removed, or at least reduced, by relaxing the spherical shape of the clusters. Indeed, as discussed extensively by de Heer (1993), there is good evidence that clusters are deformed in regions between the major spherical shell closures. The deformed shell model of Clemenger (1985a, 1985b) allows one to interpret the fine structure of mass abundance spectra and the splitting of the dipole resonances in sodium clusters in the mass regions $8 < N < 18$ and $20 < N < 40$. In this model (see the Appendix of de Heer, 1993, for details) the potential depends on a deformation parameter, and the equilibrium (ground-state) shape of each cluster is calculated simply by minimizing the sum of occupied single-particle energies with respect to this parameter. Obviously, such a model is not self-consistent in two respects: First, the density distribution of the electrons is not guaranteed to have the same shape as that of the potential (although this is approximately the case at the shapes of minimal total energy; see, for example, Bohr and Mottelson, 1975).

Second, the sum of single-particle energies is far from representing the total binding energy of an interacting system. As is well known from HF theory [cf. Eq. (A15) in Appendix A.1], the sum of occupied ε_i contains the potential energy twice, and there is *a priori* no reason to expect it to have the correct deformation behavior.[7] The errors introduced by just summing the occupied ε_i increase with the number of particles; this gives an upper limit to the usefulness of the simple Clemenger-Nilsson model in determining the correct ground-state deformations. This situation is well known in nuclear physics: the breakdown of the Nilsson model in describing the deformation energies of heavy nuclei, in particular at the large deformations occurring in the fission process, has made it necessary to correct for its missing self-consistency. An approximate but very powerful tool for achieving this was introduced by Strutinsky (1968); his shell-correction theory is mentioned briefly at the end of Sec. V.A.1.

It is therefore of basic theoretical interest to verify the phenomenological potential of the Clemenger-Nilsson model by microscopic, self-consistent calculations in the framework of density-functional theory. In the deformed jellium model, one uses the spirit of the Born-Oppenheimer approach underlying the quantum-chemical and molecular-dynamics calculations (see Secs. II.B, II.C): one varies the shape of the jellium density distribution and lets the electrons adjust themselves in the corresponding deformed ionic potential (including their interaction and exchange-correlation effects in LDA, as usual). The ground-state configuration is then found by minimizing the total energy with respect to the jellium shape. Practically, one parametrizes the shape of the jellium density in terms of one or several deformation variables. These variables take the roles of the ionic positions $\mathbf{R}_\alpha$ of the *ab initio* approaches [see Eq. (2.1)]. Allowing for a sufficient number of shape degrees of freedom for the jellium therefore should bring this model closer to the more realistic approaches, the main difference being that here only the averaged geometry of the ions is varied.

One technical problem in the deformed jellium model is that the background jellium potential $V_I(\mathbf{r})$ is no longer a simple analytical function as in the spherical case; cf. Eq. (3.13). It must therefore be calculated numerically either by direct integration over the jellium density or by solving the Poisson equation. Similarly, the Kohn-Sham equations become more complex with decreasing symmetry of the cluster and have to be solved in two or three spatial dimensions explicitly.

The existence of axially deformed equilibrium shapes within the framework of the self-consistent jellium model has been confirmed in Kohn-Sham calculations for spheroidal clusters by Ekardt and Penzar (1988, 1991; Penzar and Ekardt, 1990). These authors use an axially symmetric ellipsoidal jellium density with constant

[7] In a pure harmonic-oscillator model, from which the Clemenger-Nilsson model does not much differ, one can obviously exploit the virial theorem to correct for this double counting. But realistic self-consistent potentials are quite different from harmonic-oscillator potentials.

volume and half-axes z_0, ρ_0 given in terms of a single deformation parameter δ, restricted by $-2<\delta<2$, and the cluster radius R_I (3.12)

$$z_0=\left[\frac{2+\delta}{2-\delta}\right]^{2/3} R_I\ ,\quad \rho_0=\left[\frac{2-\delta}{2+\delta}\right]^{1/3} R_I\ . \qquad (3.15)$$

The electronic density is assumed to have axial symmetry, too, and the Kohn-Sham equations are solved in spheroidal coordinates, again using the LDA functional of Gunnarsson and Lundqvist (1976) for the exchange-correlation energy [see Eq. (A33) in Appendix A.2.c]. The total energy of the cluster must be calculated for each deformation δ, and the ground state is found by minimizing the resulting energy with respect to δ. The shell structure obtained by this model for the IPs and EAs of Na and Cu clusters is somewhat reduced by the deformation effects, but still exaggerated with respect to experiment. An interesting result is that the odd-even staggering in these quantities, a striking feature observed in clusters up to $N\simeq 92$, can to some extent be explained by polarization effects of the odd electrons. The results of Ekardt and Penzar (1991) for collective photoabsorption spectra obtained in the axially deformed model are discussed in Sec. IV.B.

Nonaxial deformations of small sodium clusters have recently been investigated in the self-consistent Kohn-Sham framework by Lauritsch *et al.* (1991). Here, a triaxial ellipsoid with constant volume was assumed for the jellium density; for reasons discussed in Sec. III.D.1 below, the jellium density was given a diffuse surface with a width of one atomic unit. The Kohn-Sham equations (in the LDA) were then solved numerically on a three-dimensional mesh for each given deformation of the jellium background. Potential-energy surfaces of these triaxially deformed clusters were presented as functions of the two quadrupole degrees of freedom β and γ introduced by Hill and Wheeler (1953): $\beta\geq 0$ measures the overall quadrupole deformation ($\beta=0$ corresponding to spherical shape), and γ measures the axis ratios of the ellipsoid ($\gamma=0°$ giving prolate axial, $\gamma=60°$ oblate axial, and $0°<\gamma<60°$ triaxial shapes).

As an example we show in Fig. 2 the Born-Oppenheimer energy surface of Na_{16} in the (β,γ) space, obtained with the model of Lauritsch *et al.* (1991). It has its minimum at $\beta=0.38$, $\gamma=33°$, corresponding to a triaxial shape. This supports the predictions of Saunders (1986) using the triaxial harmonic-oscillator potential [see also Fig. 4(a) of de Heer, 1993]. The shapes of the other clusters with $8<N<20$ of that model are confirmed, too, in the self-consistent jellium model: Na_{12} has a triaxial shape, whereas Na_{10}, Na_{14}, and Na_{18} are axially deformed. Thus while filling the $1d$ shell, there is a transition from spherical ($N=8$) to prolate (10) to oblate (18) shapes; the crossover goes through $0°<\gamma<60°$, leading to triaxial shapes (12, 16). The case $N=14$ is rather critical: the two axial minima (prolate and oblate) are nearly degenerate and their energy difference depends crucially on details of the model (see Lauritsch *et al.*, 1991). In fact, this difference has been found to be very sensitive to hexadecapole deformations (Hirschmann *et al.*, 1993). The same transition, prolate→triaxial →oblate, is again expected on the grounds of the phenomenological shell models for $20<N<40$ while filling the $1f$ and $2p$ shells.

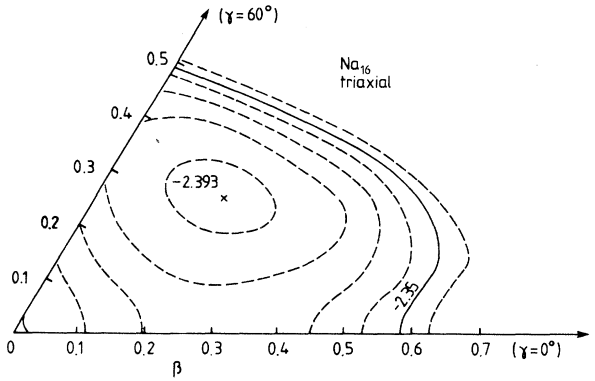

FIG. 2. Deformation energy surface of Na_{16}, obtained by Lauritsch *et al.* (1991) in the triaxially deformed self-consistent jellium model. β and γ are the Hill-Wheeler quadrupole deformation parameters. The contour lines correspond to increments of 0.01 Ry of the total energy of the cluster. The lowest energy ($E=-1.393$ Ry) is found for $\beta=0.38$, $\gamma=33°$, corresponding to a triaxially deformed ground state.

In recent photoabsorption measurements on positively charged Na clusters by Lützenkirchen *et al.* (1993), the transition from prolate to oblate shapes in the regions $12<N<20$ and $20<N<40$ has been observed. For $N>40$ (i.e., filling the $1g$ shell), however, the shapes seen to be oblate again (see also Borggreen *et al.*, 1993); it is a challenge to explain this in further self-consistent calculations.

An interesting result of Lauritsch *et al.* (1991) is the occurrence of several almost degenerate isomers with different spherical, axial, or nonaxial shapes, separated by barriers of $\sim 0.5-1$ eV. Indeed this shape isomerism recalls that found in *ab initio* quantum-chemical and molecular-dynamics calculations, although the heights of the barriers between are overestimated in the jellium model due to the missing residual interactions. Nevertheless, these results show that a lot of qualitative, averaged features of the *ab initio* approaches can also be obtained in the self-consistently deformed jellium model even for small clusters.

In Fig. 3 we show the energy per particle for the region of sodium clusters with $8\leq N\leq 20$, obtained in self-consistent Kohn-Sham-LDA calculations in three successive approximations with decreasing symmetry. The uppermost line corresponds to the spherical jellium model. The next-lower line gives the energies obtained in the axially symmetric model, whereas the lowest line is that obtained in the triaxial jellium model. The latter two differ only for the two nonaxial clusters with $N=12$ and 16. (Odd values of N have no significance in these calculations, in which the spin degrees of freedom were not in-

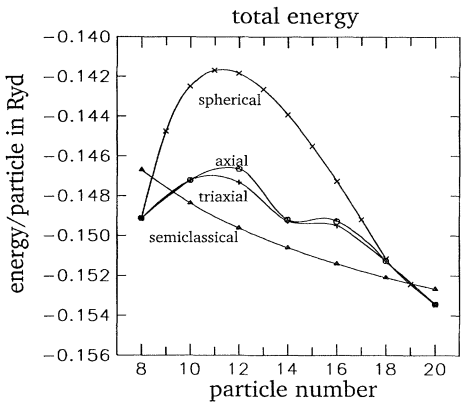

FIG. 3. Total energy per electron E/N vs N for sodium clusters with $8 \leq N \leq 20$, obtained by Hirschmann *et al.* (1993) in the self-consistent triaxial diffuse jellium model of Lauritsch *et al.* (1991): ×, spherical model; ○, axial (spheroidal) model; +, triaxial (ellipsoidal) model; ▲, semicalssical spherical model (cf. Sec. V.B).

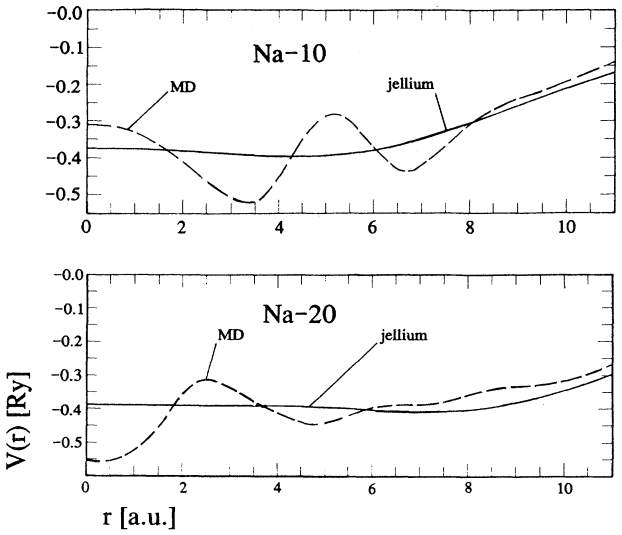

FIG. 4. Spherically averaged total Kohn-Sham potentials for the sodium clusters Na_{10} and Na_{20}: dashed lines, results of molecular-dynamics (MD) calculations by Röthlisberger and Andreoni (1991); solid lines, self-consistent jellium model results by Hirschmann *et al.* (1993), using the diffuse-surface jellium model of Lauritsch *et al.* (1991). Note that Na_{20} is spherical in the jellium model, whereas Na_{10} is prolate axially deformed.

cluded explicitly; the results therefore do not exhibit any odd-even effects.) One observes that quite an appreciable gain in energy is brought about by the deformation of the clusters, except close to the spherical closed-shell numbers 8 and 20. Also shown in Fig. 3, by the dotted curve, is the result of a semiclassical density-variational calculation (see Sec. V.B). It is seen to interpolate nicely between the microscopic curves and represents, in fact, a rather good approximation to these results including deformation, although in the semiclassical approximation all clusters remain spherical.

It is of interest at this point to compare the jellium model results to those of pseudopotential calculations that include the ionic structure. In Fig. 4 we show the spherically averaged total Kohn-Sham potentials obtained by Röthlisberger and Andreoni (1991) for the clusters Na_{10} and Na_{20} and compare them to those obtained by Hirschmann *et al.* (1993) in the diffuse jellium model of Lauritsch *et al.* (1991). Although the pseudopotential results show important oscillations, their average trend is rather well reproduced by the jellium model.

In Fig. 5 we compare the spherically averaged electronic densities obtained in the two approaches for the clusters Na_{18} (which is oblate axially deformed in the jellium model) and Na_{20}. The pseudopotential (left part) are given for three different temperatures; the jellium results (right part) at $T=0$ only. The agreement between the $T=0$ results is almost quantitative, which is rather surprising in view of the potentials shown in Fig. 4 above. It shows that the electrons average out the ionic structure of the pseudopotentials by their motion, so that their density distribution is almost unaffected and is very well reproduced by the jellium model.

The single-particle energies for Na clusters in the region $8 \leq N \leq 20$ are shown in Fig. 6. Here we compare the Kohn-Sham levels ε_i obtained in the spheroidal jellium model of Ekardt and Penzar (1988), the triaxial jellium model of Lauritsch *et al.* (1991), and those of the MD results of Röthlisberger and Andreoni (1991) using the Car-Parrinello method. The jellium model results agree astonishingly well with the pseudopotential results where the ionic structure is included.[8]

An interesting detail that can be observed in Fig. 6 is the relative closeness of the $1p$ and $1d$ type levels around $N=14$. Since they have opposite parity, a static octupole (or more generally, any left-right asymmetric) deformation would mix these levels, which could lead to a lowering of the energy. Such situations are known also from atomic nuclei. Hamamoto *et al.* (1991) have shown that an octupole instability in typically quadrupole-deformed regions are a rather general trend of finite fermion systems and can lead to shell effects of comparable importance to those induced by the nonaxial quadrupole deformations.

In conclusion we can say that the jellium model is able to describe surprisingly well the average trends of potentials, energy levels, and densities in the structural pseudopotential calculations, when a sufficiently flexible deformation is included, even for such small clusters as Na_8–Na_{20}. This is encouraging for the application to larger systems in which molecular dynamics becomes more and more time consuming and one is bound to rely on the jellium model predictions.

[8]A similar study of Kohn-Sham levels, obtained in pseudopotential calculations for Mg clusters with $8 \leq N \leq 20$, was recently presented by Delaly *et al.* (1992), who also confirm the general trends of the jellium model predictions.

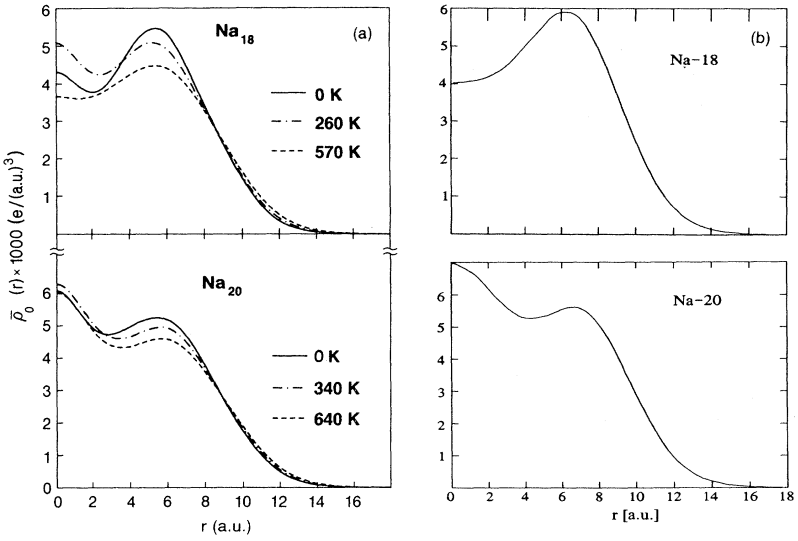

FIG. 5. Spherically averaged electron densities for the sodium clusters Na_{18} and Na_{20}: left part (a), results of molecular-dynamics (MD) calculations by Röthlisberger and Andreoni (1991) at various temperatures; right part (b), results of the self-consistent jellium model as in Fig. 4 above, at zero temperature. (Note that Na_{18} is oblate axially deformed in the jellium model.)

3. Finite-temperature effects

In many experiments, clusters are produced at finite temperatures of up to several hundred Kelvin or even more (see Sec. III.A of de Heer, 1993). The manifestation of shell structure in the abundance spectra of cluster-beam experiments is thought to be a result of evaporation of neutral atoms by the hot clusters: the closer the number of valence electrons gets to a number corresponding to a filled major shell, the more stable the cluster will be and the smaller the probability for evaporation of a further atom, so that finally at the time of detection—when the beam has cooled off—the closed-shell species are the most abundant (Bjørnholm *et al.*, 1993).

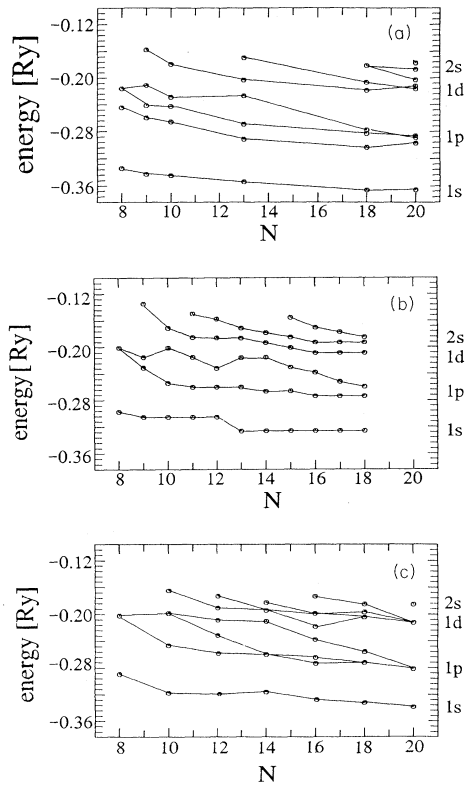

FIG. 6. Kohn-Sham single-particle levels in Na clusters with $8 \leq N \leq 20$, calculated in different models. (a) molecular-dynamics (MD) results (Röthlisberger and Andreoni, 1991); (b) spheroidal jellium model (Ekardt and Penzar, 1988); (a) triaxial diffuse-surface jellium model (Lauritsch *et al.*, 1991). From Hirschmann *et al.*, 1993.

The question therefore arises to what extent a finite temperature affects the magnitude of the electronic shell effects themselves. Shell effects are weakened at finite temperature for two reasons. Most of the excitation energy will be in the structural degrees of freedom, namely, in the vibrations, distortions, and liquefaction of the cluster. The amount of phase space associated with high-symmetry shapes that produce electronic shell closures will then be reduced. Independent of this, the occupation of the electronic orbitals will be smeared out as in the Fermi-Dirac distribution. This will also smooth out shell effects, as is well known from nuclear physics (Bohr and Mottelson, 1975; Brack and Quentin, 1981).

At first sight, one might think that even several hundred degrees are small on the scale of the electronic single-particle energies, so that this second effect should be negligible. This is certainly true for clusters with fewer than a hundred atoms, in which the main spacing between electronic levels corresponds to several thousand degrees. However, in very large clusters in the mass region $N \simeq 1000-3000$, which now have become available in expansion sources, the spectra are much more compressed and the temperatures in question do have a noticeable effect. Furthermore, the detailed shape of the abundance spectra depends in a rather subtle way on first and second differences of the total free energies with respect to the atomic number, so that the temperature

smearing effects can, indeed, become visible (Bjørnholm *et al.*, 1991; Pedersen *et al.*, 1991).

The effects of occupation-number smearing were addressed recently in finite-temperature Kohn-Sham-LDA calculations for sodium clusters in the spherical jellium model (Brack, Genzken, and Hansen, 1991a, 1991b; Genzken and Brack, 1991). The electrons were treated as a canonical system in the heat bath of the ions, and the appropriate density-functional theory for $T>0$ (see Appendix A.2.) was used. The canonical partition function was calculated exactly in terms of the Kohn-Sham single-particle energies, and the relevant thermodynamical quantities were derived from it self-consistently. Since the most important results of these calculations concern the supershell structure in very large alkali clusters, we shall discuss them in Sec. V.A.2 below.

Only the temperature of the electrons can be treated rigorously in the jellium model; the ions are not accessible microscopically. This is a serious restriction, since a dominant fraction of the thermal energy in cluster beams is carried by the ions. However, the ionic part of the thermal energy can be assumed to be a smooth function of the particle number. Therefore the shell-structure oscillations coming from the valence electrons and their temperature dependence can also be studied in the jellium model.

C. Beyond LDA

In this section we review a few approaches that go beyond the local-density approximation. The discussions here are brief and outline only the basic ideas. Results for experimentally measured observables, as far as they have been obtained, are discussed and compared to those of Kohn-Sham-LDA calculations in Secs. III.B and IV.B.

We first review two sets of calculations that were performed explicitly to test the LDA by computing the exchange exactly in the Hartree-Fock approximation and by computing explicitly the leading correlations in finite clusters.

1. Hartree-Fock calculations

Since the Coulomb exchange is treated exactly in Hartree-Fock theory, the standard LDA exchange functional Eq. (A.31) can, in principle, be easily tested with HF calculations. It is just a question of numerical effort to treat the jellium model in a HF approximation; due to the nonlocal nature of the Fock potential $\hat{V}_F$ (see Appendix A.1), the calculations become considerably more complicated and time consuming than in the Kohn-Sham-LDA approach.

The problem is that the HF approximation is known to be rather poor for metallic systems, since the correlations are responsible for an appreciable part of their binding, and one must include corrections. A compromise, already suggested by Kohn and Sham (1965), consists in adding a LDA (or LSDA) functional for correlations only to the total HF energy. However, the inclusion of LDA correlations along with a HF treatment of the exchange goes against the empirical "rule of thumb" that exchange and correlation effects should always be kept together at the same level of approximation (see, for example, Jones and Gunnarsson, 1989). To be more specific: once one goes beyond the HF approximation, Pauli and other types of correlations (also of RPA type; see Appendix B) cannot be disentangled, and therefore adding a correlation functional to HF risks double counting.

HF calculations for spherical sodium clusters within the jellium model were performed by Hansen (1989), Guet and Johnson (1992), and by Hansen and Nishioka (1993). Hansen (1989) investigated the addition of correlations in LDA. Since these authors addressed themselves mainly to the electric response properties of sodium clusters, we shall discuss their results in Sec. IV.B below.

2. Explicit evaluation of long-range correlations

Starting from the HF approximation, one can in principle include all correlations that go beyond the simple exchange systematically in perturbation theory, as is done in the quantum-chemical approaches (see Sec. II.B). In an infinite system, the results can be expressed in terms of an effective mass of the electron, which has both a momentum and an energy (or frequency) dependence. The momentum dependence ("k mass") is due mainly to the nonlocality of the exchange (Fock) potential (see Appendix A.1), which is due to the finite range of the Coulomb force and tends to reduce the effective mass.[9] The energy dependence ("ω mass") comes predominantly from the coupling of the electron to collective vibrations through the long-range correlations and tends to increase the effective mass. Pictorially speaking, the electron is "dressed" by a plasmon cloud that increases its inertia. The two effects have a tendency to cancel each other in infinite systems, so that the net effective mass can become close to the free mass (see, for example, Mahan, 1981).

For finite systems there is no unique way to define an effective mass; it is more appropriate to speak of the self-energy of the electron and of the screened Coulomb interaction. The effect of the correlations can also be studied by looking at the density of the "dressed" single-particle levels, the so-called quasiparticle energies. In the pure HF approximation without long-range correlations, this density is known to be too low at the Fermi energy, resulting in too large an energy gap between the highest

[9]Note that this effect is automatically included in a full Hartree-Fock calculation. The pseudopotentials are often angular momentum dependent, which introduces an additional momentum dependence to the delocalized electron energies. This effect is not accounted for in the jellium model.

occupied and the lowest unoccupied orbitals. The correlations tend to close this gap.

We shall not go into the gory details of many-body theory or use any diagrams here. Let us just mention that an appreciable part of the long-range correlations can be obtained, in both homogeneous and—with considerably more effort—inhomogeneous systems, by summing an infinite series of bubble diagrams, i.e., by iterating the process of creating particle-hole pairs around the Fermi surface and destroying them again. (This is exactly the basic excitation process used in the RPA method; see Appendix B.1.) These RPA correlations are the dominant part of the correlation effect included in most LDA exchange-correlation energy functionals. A systematic approach to the inclusion of these correlations in the electron propagator is given by the so-called GW approximation (Hedin and Lundquist, 1969).

Reinhard (1992) has recently checked the LDA by computing explicitly the RPA-correlation contributions to the ground-state energies and rms radii of closed-shell Na clusters ($N=8$, 20, 40, and 80) in the jellium model using a pseudopotential-folded positive charge density (see Sec. D.2 below). He started from the Kohn-Sham approach including only the exchange-energy LDA functional (thus omitting explicitly the correlation energy). He compared his results to those obtained in the standard Kohn-Sham-LDA approach, employing the correlation energy functionals of Gunnarsson and Lundqvist (1976) and of von Barth and Hedin (1972) (see Appendix A.2.c), thus using exactly the same methods for treating the RPA correlations as the respective authors of these two functionals. The differences were smaller than 10% for Na_8 and smaller than 1% for all larger clusters. This surprising agreement seems to be a strong confirmation of the validity of the LDA, at least for global properties such as energy and radii, even for very small jellium spheres.

The jellium-HF calculations of Guet and Johnson (1992) have recently been extended (Guet *et al.*, 1993) to include the RPA correlations in the ionization potentials of alkali clusters with $N=9$, 21, and 41. Here the electronic self-energies were calculated with the fully screened Coulomb interaction by iterating the Dyson equation to all orders. Again, the results were in the same good agreement with those of Kohn-Sham-LDA calculations, i.e., within a few percent for $N=9$ and less than one percent for the larger systems (see also Sec. III.B.1). In a similar earlier work, Saito *et al.* (1990) evaluated the electronic self-energies only to first order in the screened Coulomb interaction and investigated the quasiparticle energies in closed-shell alkali clusters up to $N=40$. They concluded that their treatment gave a better agreement of the quasiparticle energies with experimental ionization potentials than the Kohn-Sham-LDA results. The iteration to all orders performed by Guet *et al.* (1993) reduces the discrepancy with the Kohn-Sham-LDA results appreciably. In fact, these authors show that the inclusion of the lowest-order diagram alone overestimates the correlation effect by as much as 50%. Saito *et al.* (1990) also compared their results to those obtained with the self-interaction correction (see Sec. III.C.3 below).

Bernath *et al.* (1993) also addressed the question of the density of quasiparticle energies in Na_{40}. Their approach is more phenomenological in the sense that they used an approximate RPA method to obtain the lowest-order contribution to the self-energy, using a fitted separable interaction and selecting its leading multipolarities. (Physically speaking, this corresponds to an explicit coupling of the valence electrons to surface dipole, quadrupole, and octupole vibrations.) They found that the original HF single-particle spectrum, as obtained by Hansen and Nishioka (1993), is compressed—without, however, reducing much the "bandgap" at the Fermi surface—in the direction of the Kohn-Sham-LDA spectrum. They also extracted an ω-dependent effective mass that was found to be of the order of 40% larger than the free-electron mass.

Here we should also mention recent work by Koskinen *et al.* (1992), who did a configuration-mixing calculation in the jellium model for small Na clusters with $N \leq 10$, using nuclear shell-model codes. The jellium Hamiltonian including the full electron-electron interaction was diagonalized in a (partially truncated) many-particle space constructed from a set of harmonic-oscillator single-particle states, including the orbits $1s$, $1p$, $2s$, $1d$, $2p$, $1f$, $2d$, and $1g$. Up to $N=4$ the full space, containing up to 6164 configurations, could be diagonalized. This approach goes beyond both HF and Kohn-Sham-L(S)DA; it becomes exact in the limit of an infinite set of single-particle orbits. Both ionization potentials and total binding energies were calculated and their convergence upon increasing the configuration space was demonstrated. In those cases where convergence could be approximately reached, a close agreement with Kohn-Sham-LSDA results was obtained. Koskinen *et al.* (1992) also calculated the photoabsorption cross sections for Na_8–Na_{10} with similar results to those for the Kohn-Sham-LDA-RPA calculations discussed in Sec. IV.B.2. In particular, they obtained a splitting of the resonance in Na_9 and Na_{10}, showing that a sufficiently large single-particle configuration space, even in a spherical basis, can describe the effects of a deformed mean field.

All these recent results yield a rather positive test of the Kohn-Sham approach using the LDA, even for very small jellium spheres. The question therefore remains to what extent one should expect these correlation effects amongst the valence electrons to depend on the presence of the ionic structure or the core electrons, or how much the results might be modified by additional correlations between the valence electrons and the other charges.

As far as the jellium model is concerned, one is encouraged to conclude that extensions beyond the LDA might not be important. At least, it seems that the errors made in the LDA to the exchange-correlation energy are much smaller than those due to overall neglect of the ion-

ic structure in the total energy functional.

For completeness, however, we shall review below three extensions of the LDA that have been studied extensively for atoms within the Kohn-Sham approach and partially applied recently to metal clusters.

3. Self-interaction correction

One serious breakdown of the local-density approximation to the exchange energy affects the asymptotic behavior of the Kohn-Sham potential for Coulombic systems. In HF theory, where the Coulomb exchange is treated exactly, it is well known that the mean field asymptotically falls off like $1/r$ far outside the surface of a spherical system; this is simply the field of the remaining spherical charge distribution seen by one electron that is taken far away. This is no longer so in the Kohn-Sham theory when the exchange is treated in the LDA. As stated at the end of Appendix A.1, the Hartee potential V_H (A9) contains spurious self-interaction contributions of the electrons, which are exactly canceled when the Fock potential (A10) is added to it. However, with the LDA one makes a crude approximation to the Fock potential, whereas the Hartree potential is left intact, so that this cancellation no longer takes place. As a consequence, one obtains too much screening and the Kohn-Sham potential falls off much faster than $1/r$.

A "self-interaction correction" to remedy this failure of the LDA has been proposed by Perdew (1979) and further elaborated and tested for atomic systems by Perdew and Zunger (1981) with considerable success. It makes the Kohn-Sham potential state-dependent and thereby complicates the self-consistent calculations appreciably; the Kohn-Sham orbitals $\varphi_i(\mathbf{r})$ are no longer orthogonal and must, at least in principle, be reorthogonalized. Since the exchange corrections apply only to electrons with parallel spins, one must start from the spin-dependent LDA to use the self-interaction correction properly.

The self-interaction correction scheme cannot be systematically improved or extended in terms of perturbation theory; it is rather an *ad hoc* prescription that one must take or leave. We refer the reader to Dreizler and Gross (1990) for a detailed discussion and some variations of the scheme, and to Moullet and Martins (1990) for some comparisons in atoms and diatomic molecules. For metal clusters the self-interaction correction has so far been used only in the LDA-jellium model; cf. Stampfli and Bennemann (1987), Saito *et al.* (1990), and Pacheco and Ekardt (1992) (cf. Sec. IV.B).

4. Weighted-density approximation

The weighted-density approximation (WDA), introduced by Alonso and Girifalco (1977) and Gunnarsson *et al.* (1977), makes use of an explicitly nonlocal functional for the exchange-correlation energy $E_{\rm xc}[\rho]$ in terms of approximated forms of the pair-correlation (i.e., the two-electron-correlation) function. It can be constructed (Przybylski and Borstel, 1984a, 1984b) to give the correct asymptotic $1/r$ falloff of the Kohn-Sham potential for a neutral atom or cluster. We refer the reader to Dreizler and Gross (1990) for a discussion of the WDA and its application to atomic and molecular systems.

Using the WDA with an approximate pair-correlation function developed by Chacón and Tarazona (1988), Balbás *et al.* (1989, 1991) and Rubio *et al.* (1989, 1991a) studied the static properties of metal clusters, in particular for negative ions in which the LDA is known to be doubtful. Both for ionization potentials (see Sec. III.B.1) and for static electric polarizabilities (see Sec. IV.B.1), they obtained a considerable improvement in the agreement with experiment over the results obtained in the LDA.

5. Gradient expansions of the xc functional

Another way of including nonlocal effects for exchange and correlations consists in expanding the exact, nonlocal energy functional in terms of gradients and higher-order derivatives of the density $\rho(\mathbf{r})$. This was proposed from the beginning of the density-functional theory by Hohenberg and Kohn (1964). (Applied to the kinetic-energy functional $T_s[\rho]$ this leads to the extensions of the Thomas-Fermi model discussed at the end of Appendix A.2.a.) They also suggested that one study the partial resummation of the series obtained by the gradient expansion; this idea has received much attention in the literature and led to the so-called generalized gradient approximations (GGA).

Although nonlocal effects are included in this approach, it has the advantage that it still leads to a local xc potential in the Kohn-Sham equations. We refer the reader again to Dreizler and Gross (1990) for an extensive review of a large variety of gradient expansions and the techniques used to derive them. Some recent versions of generalized gradient-approximations that have been used for atoms, small molecules, and metal surfaces were proposed by Langreth and Mehl (1983), Perdew (1986), Perdew and Wang (1986), Becke (1988), Engel *et al.* (1992), and Perdew *et al.* (1992); for a recent review see Perdew (1991a, 1991b). The asymptotic falloff of the xc potential obtained in the generalized gradient approximation has recently been discussed by Ortiz and Ballone (1991).

No results with generalized gradient approximation functionals seem to be available yet for jellium model calculations of finite clusters. Delaly *et al.* (1992) recently used the functionals of Perdew (1986) and Becke (1988) in pseudopotential calculations for magnesium clusters with $N \leq 20$.

A more systematic use of generalized gradient approximation functionals for metal clusters would be highly desirable, since their steep surfaces give a crucial test for the validity of density-gradient expansions. Some prelim-

inary studies (Brack, 1988) using the semiclassical density-variational method (see Sec. V.B) seemed to indicate that the variational use of such functionals—which often have been tested only perturbatively using, for example, HF densities—can lead to instabilities of the surface of small jellium clusters. However, Perdew *et al.* (1992) with their new generalized gradient approximation functional found stable solutions in semi-infinite jellium. We note in this context that the density-gradient expansion of the kinetic energy up to fourth order gives no problems and has been quite successfully used in variational calculations for both metal clusters and atomic nuclei (see Sec. V.B).

D. Extensions of the jellium model

The most significant shortcoming of the jellium model is its lack of ionic structure. We review here very briefly a few attempts to include schematically some effects of the ionic geometry without losing the simplicity of the jellium model. Some of them are simple phenomenological *ad hoc* patches (Sec. III.D.1) and some have a more solid basis built on pseudopotential theory (Sec. III.D.2).

1. Simple patches

Lange *et al.* (1991), in an attempt to simulate the effect of an oxygen ion embedded in $Na_N O$ clusters, introduced a modification of the jellium density by adding a bump at its center. They observed that in Kohn-Sham-LDA calculations this improves the situation of the spherical shell closings that we discussed above in Sec. III.B.1: the gap between the $1f$ and $2p$ levels is reduced and thereby the stability of the $N=34$ cluster is reduced in favor of the $N=40$ cluster. Similarly, the stability for $N=186$ is reduced in favor of $N=196$ or 198. A partial remedy for some of the systematic failures of the spherical jellium model can thus be achieved. Essentially, the trick consists in an increase of the surface diffuseness of the Kohn-Sham potential, which pushes states with higher angular momentum l upwards with respect to those with smaller l.

Yannouleas and Broglia (1991b) introduced a similar perturbative correction of the jellium potential, representing the "nonjellium behavior" of small clusters, which could be fitted to the position of the surface plasmon. This helped to repair the lack of red shift of the dipole resonance systematically obtained in all jellium-LDA calculations (see Sec. IV.B.2).

Such simple patches represent little more than punctual remedies obtained by fitting *ad hoc* parameters and have no predictive power at all. They show, however, that some of the results of the jellium model are very sensitive to modifications of the jellium density distribution.

A more systematic variational approach was taken by Rubio *et al.* (1991b) in spherical Kohn-Sham-LDA calculations. These authors introduced a parametrization of the jellium density with a diffuse surface and determined the diffuseness parameter by minimization of the total energy for each cluster. The resulting diffuseness was found to be of the order of ~ 1 a.u. for all clusters in the range $8 \leq N \leq 40$. The effects of the increased surface diffuseness of the clusters are very beneficial to several of their properties (see also Balbás and Rubio, 1991). As in the case of Lange *et al.* (1991), the shell-closing situation is improved in the right direction, $34 \rightarrow 40$. At the same time the ionization potentials of Na clusters, which are systematically too high in the standard jellium model (see Sec. III.B.1), are reduced. Furthermore, the increased spillout of the electrons increases the static dipole polarizabilities and reduces the surface-plasmon energies; these effects, too, bring the theoretical results closer to experiment (cf. Sec. IV.B).

The introduction of a diffuse surface of the jellium density also has the technical benefit of easing the numerical calculations in the ellipsoidally deformed self-consistent jellium model (see Sec. III.B.2). Lauritsch *et al.* (1991) used a Fermi function with a constant diffuseness of 1 a.u.

Although the diffuse jellium surface can be determined variationally, as was done by Rubio *et al.* (1991b), so that no fit parameter is needed, it has not yet been given a microscopic justification.

2. Structureless pseudopotential models

A step towards the inclusion of pseudopotential effects has been taken by Reinhard *et al.* (1992) and Genzken *et al.* (1993), who relate the diffuseness of the jellium density to the ionic pseudopotentials. They use a convolution of the steplike jellium density with the ionic density distribution corresponding to a "soft-core" pseudopotential of the type introduced by Ashcroft (1966) [see Eq. (A34) in Appendix A.2.d], which is just a surface delta function peaked at the radius $r=r_c$. This leads to analytical expressions for the jellium density and the background potential $V_I(r)$ that can easily be incorporated in spherical Kohn-Sham-LDA calculations. The empty-core radii r_c determined from bulk and surface properties are taken from the literature, and thus no new parameters have to be determined either variationally or by *ad hoc* fits. The results of this pseudopotential-folded jellium model for alkali clusters are similar to those found by Rubio *et al.* (1991b) mentioned above: one obtains at the same time an increase in the static electronic polarizability and a corresponding decrease in the dipole resonance energies (cf. Sec. IV.B), as well as a reduction of the ionization potentials and electron affinities.

A similar and more systematic approach has been proposed by Perdew *et al.* (1990) in their "stabilized jellium model," which is an extension of the "pseudojellium model" introduced earlier by Utreras-Díaz and Shore (1984, 1989). The effects of the ionic cores, represented again by the empty-core pseudopotential of Ashcroft (1966), are included here in a modified exchange-

correlation energy functional. This approach retains all the simplicity of the jellium model and has been used successfully for metal surface properties, yielding work functions and surface energies in good agreement with experiment (cf. Sec. V.B.2). Due to an explicit ionic structural term in the energy functional, this model also yields the correct cohesive energy of bulk metal—a quantity that is not accessible in the simple jellium model. Brajczewska *et al.* (1993) have recently calculated binding and ionization energies of Al, Na, and Cs clusters with $1 \leq N \leq 20$ using the stabilized jellium model and solving the Kohn-Sham-LSDA equations. In particular for aluminum, which is not accessible in the standard jellium model, they found a reasonable agreement with experimental ionization energies.

IV. ELECTRIC DIPOLE RESPONSE OF METAL CLUSTERS

A. Linear-response theory

Linear-response theory is the most convenient tool for studying the interaction of a system with an external, not too strong field. In connection with metal clusters, it has been extensively used to calculate static dipole polarizabilities and photoabsorption cross sections. In the present section we address calculations that have been done using the random-phase approximation (RPA) or the equivalent time-dependent local-density approximation (TDLDA). (The formal aspects of these theories are presented in Appendix B.) In addition to discussing jellium model results, we shall also review some *ab initio* and pseudopotential model calculations.

In Sec. IV.B we review the recent literature and discuss agreements and discrepancies between the theoretical and experimental results for the static polarizabilities and the resonances in the photoabsorption cross sections. Section IV.C is devoted to a presentation of RPA sum-rule relations and the classical limits of the RPA, leading to the well-known results of the Mie theory (1908) for surface plasmons in metallic spheres, and of a transparent physical picture of the coupling of surface and volume plasmons.

The two observables of metallic clusters that so far have been investigated by these methods and compared to experiment are the static electric dipole polarizability and the photoabsorption cross section. The static dipole polarizability of a microscopic system is defined as in classical physics: one applies an external, static electric field $\mathbf{E}_0$ and expands the total energy up to second order in $\mathbf{E}_0$. The coefficient of the quadratic term is then the polarizability. Formally this is achieved by including the electric dipole operator $\vec{D}$

$$\vec{D} = e \sum_{i=1}^{Z} \vec{r}(i) \tag{4.1}$$

in the variational equation via the Lagrange multipliers $\vec{\lambda} = (\lambda_x, \lambda_y, \lambda_z)$:

$$\delta \langle \Psi_\lambda | \hat{H} - \vec{\lambda} \cdot \vec{D} | \Psi_\lambda \rangle = 0 \ . \tag{4.2}$$

In Eq. (4.1), i runs over the number Z of "active" electrons: in *ab initio* approaches these would be all electrons; in pseudopotential or jellium models, $Z = wN$ is the number of valence electrons. By solving Eq. (4.2), one obtains the "constrained" ground state Ψ_λ from which the polarizability tensor $\vec{\alpha}$ (made diagonal by choosing a suitable coordinate system) is found either from the term linear in $\vec{\lambda}$ of the induced dipole moment (hence "linear response") or from the quadratic term in the total energy[10]:

$$\alpha_{x_i} = \frac{d}{d\lambda_{x_i}} \langle \Psi_\lambda | D_{x_i} | \Psi_\lambda \rangle |_{\vec{\lambda}=0} = \frac{d^2}{d\lambda_{x_i}^2} \langle \Psi_\lambda | \hat{H} | \Psi_\lambda \rangle |_{\vec{\lambda}=0} \ . \tag{4.3}$$

If one is dealing with a spherical system, the above definition has the formal inconvenience that the external field breaks the spherical symmetry, which complicates the solution of the variational equation (4.2). However, since only the linear response at $\vec{\lambda}=0$ is required, this difficulty can be circumvented by a multipole expansion of the wave function. The linear response, i.e., the lowest-order change in the ground-state wave function (or density), will always have the same multipolarity as the external field, and therefore it is sufficient to consider only the corresponding multipole (here: the dipole) component of the wave function or density, for which the variational equation still can be written in the spherical variable r. For the calculation of atomic dipole polarizabilities, this technique was used by Mahan (1980), who modified the equations originally derived from the RPA by Sternheimer (1957; see also earlier references quoted therein).

Alternatively, α_{x_i} can be obtained from the moment $m_{-1}(D_{x_i})$ of the RPA dipole strength function [see Sec. IV.C below and Eq. (B13) in Appendix B.2]. This is the most convenient way if one starts from a microscopic RPA calculation. (Both ways may be combined to obtain a rather sensitive numerical test of the numerical methods; similarly, other sum rules discussed in Sec. IV.C may be used for this purpose.)

In the long-wavelength limit, which is well fulfilled for small- and medium-sized clusters, the photoabsorption cross section $\sigma(\omega)$ is dominated by dipole absorption. It can thus be obtained directly from the RPA dipole strength function $S_Q(E)$ given in Appendix B.2, Eq. (B6), evaluated for $\hat{Q} = \vec{D}$ and averaged over the spatial directions:

[10] We assume here that the unperturbed ground state has no permanent dipole moment. Furthermore, we treat only the electronic response; in structural models, the ionic contributions must be added separately.

$$\sigma(\omega)=\frac{4\pi\omega}{3c}\sum_{x_i} S_{D_{x_i}}(E=\hbar\omega) \ . \tag{4.4}$$

This can also be expressed in terms of the imaginary part of the dynamic polarizability $\alpha(\omega)$:

$$\sigma(\omega)=\frac{4\pi\omega}{c}\mathrm{Im}[\alpha(\omega)] \ . \tag{4.5}$$

In the usual formulation of the TDLDA (see, for example, Ekardt, 1984a), one calculates the dynamic polarizability $\alpha(\omega)$ directly.

In principle, one encounters a fundamental problem in the calculation of photoabsorption cross sections within the framework of density-functional theory. As is well known, the density-functional theory gives *a priori* no access to excited states. Nevertheless, the TDLDA has been quite successful for the calculation of the dipole response of atoms (see, for example, Stott and Zaremba, 1980; Zangwill and Soven, 1980). As discussed at the end of Appendix B.1, the time-dependent formulation of density-functional theory is a highly nontrivial problem; the TDLDA should therefore be used with some caution. Gross and Kohn (1990) have proposed an explicitly frequency-dependent exchange-correlation energy functional that can be used for TDLDA calculations. To our knowledge, this functional has not been used for finite systems so far.

B. Linear-response calculations

Before discussing the dynamic response predicted by RPA or TDLDA calculations, we examine the static dipole response. This already shows some of the inherent limitations of the jellium model.

1. Static dipole polarizabilities

It is convenient to compare the dipole polarizability calculated from the quantum theory with the classical polarizability of a conducting sphere. This is given by

$$\alpha_{\mathrm{cl}}=R^3 \ . \tag{4.6}$$

The static response in the jellium model is predicted to be larger. The main reason for the increase is the so-called electronic spillout, as observed by Snider and Sorbello (1983a, 1983b) and by Beck (1984b). Snider and Sorbello (1983b) showed in Thomas-Fermi-Weizsäcker density-variational calculations (cf. Sec. V.B.1) that the dipole polarizability of a spherical metal cluster is given by

$$\alpha=(R_I+\delta)^3 \ , \tag{4.7}$$

where δ in the limit $R_I\to\infty$ goes to a constant δ_p that is the position of the image plane relative to the jellium edge for an infinite plane metal surface in an external electric dipole field (Lang and Kohn, 1973). Therefore α approaches its classical value (4.6) like $\alpha/\alpha_{\mathrm{cl}}\to 1+3\delta_p/R_I$. Beck (1984b) showed in Kohn-Sham-LDA calculations that δ in Eq. (4.7) is proportional to the electronic spillout ΔZ, defined as the number of electrons outside the jellium edge:

$$\Delta Z=4\pi\int_{R_I}^{\infty} r^2\rho(r)dr \ . \tag{4.8}$$

As discussed by de Heer (1993), the experimental polarizability of alkali clusters is much larger than the classical formula (4.6) and is not quantitatively reproduced by the jellium response.[11] In fact, the polarizabilities obtained in the jellium model are systematically too small by $\sim 15-20\,\%$ for Na and K clusters in the region $2<N<40$. For Al clusters the situation is less clear: here the jellium model tends to overestimate the polarizabilities for $N\lesssim 40$, whereas for $40\lesssim N\leq 60$ there seems to be a reasonable agreement (see Fig. 23 of de Heer, 1993).

The lack of polarizability of alkali clusters found in the microscopic jellium-Kohn-Sham-LDA calculations has often been attributed to the LDA treatment of the exchange energy: the noncancellation of self-interactions (see Appendix A.1) leads to too much screening and thus a too fast falloff of the self-consistent Kohn-Sham potential, which in turn gives rise to an underestimation of the density tail and thus of the electronic spillout. Indeed, the self-interaction correction (see Sec. III.C.3), which was introduced in order to correct this shortcoming of the LDA, was found by Stampfli and Bennemann (1987) to increase the polarizabilities of small Na clusters considerably, thus removing a good part of the discrepancy with experiment. This has recently been confirmed by Pacheco and Ekardt (1992).

The weighted-density approximation (WDA), which is tailored to yield the correct asymptotic $\sim 1/r$ falloff of the Kohn-Sham potential (see Sec. III.C.4), has also been reported by Rubio *et al.* (1991a) and by Balbás and Rubio (1990) to increase the polarizabilities.

The relevance of the above self-interaction correction and WDA results can be explicitly tested in Hartree-Fock (HF) calculations, in which there is no problem of spurious self-interaction contributions or of a wrong falloff of the average potential, since the exchange is treated exactly here.

Guet and Johnson (1992) have performed HF+RPA calculations in the spherical jellium model for closed-shell Na clusters with N up to 92. They used the uncorrelated HF ground state and solved the RPA equations (including approximately the continuum contributions). They found that the static polarizabilities were in-

[11] Kresin (1989–1992) obtained a very good agreement of calculated polarizabilities with experimental values. His method makes use of approximate Thomas-Fermi solutions for the electronic densities and thus is an approximation to the microscopic Kohn-Sham-LDA-RPA approach, which fails as described above. The good agreement must therefore be considered as a coincidence.

creased over the Kohn-Sham-TDLDA results towards the experimental values, but by a much lesser amount than through the self-interaction correction. However, the increase with respect to the LDA results is due only to neglect of correlations (other than exchange) in the ground state: the correlations lead to an increased binding of the electrons and therefore to a reduction of their polarizability. This had been shown explicitly in earlier results by Hansen (1989), who did HF calculations for Na_8 and Na_{20} with and without explicit inclusion of an LDA functional for the correlation energy. In fact, it is more correct to compare the HF results to Kohn-Sham-LDA calculations without correlations.

Hansen and Nishioka (1993) fully confirmed these results. They performed HF calculations in the spherical jellium model for Na clusters with N up to 58 and compared their results to Kohn-Sham-LDA calculations with exchange only. They showed that the HF treatment, due to the nonlocal and strongly state-dependent mean field, leads to a considerably stronger binding of the single-particle states, particularly the lowest ones, but at the same time suppresses the inner part of their wave functions. The two effects have a tendency to cancel, and the resulting densities are close to the Kohn-Sham-LDA densities.

This is shown in Fig. 7, where we display the densities obtained by Hansen and Nishioka (1993), in the HF, the Hartree (no exchange), and the Kohn-Sham-LDA (exchange only) approximations. It is very interesting to note that, in spite of the correct asymptotic $1/r$ falloff of the state-dependent HF potentials, the HF density tails cannot be distinguished from the Kohn-Sham-LDA tails—at least in the region shown in the figure. Thus the exact treatment of the exchange does not increase the spillout of the electrons, contrary to general expectations. Consequently the static dipole polarizability also stays the same. Indeed, applying a static external dipole field, Hansen and Nishioka (1993) found the polarizability of Na_8 in HF to be only marginally larger than in the Kohn-Sham-LDA approach without correlations.

In summary, it appears from these HF results that the local-density approximation for the exchange is surprisingly good, even for small Na clusters. A similar conclusion could also be drawn by Reinhard (1992) and Guet *et al.* (1993) for the correlation contributions, especially of RPA type, to binding and ionization energies (see Sec. III.C.2). This contradicts the above findings with the self-interaction correlation and WDA, and rather suggests the conclusion that the failure of the jellium model to yield the correct polarizabilities (and redshifts of the photoabsorption resonances; see below) is due to the neglect of the ionic structure.

Unfortunately, no *ab initio* quantum-molecular calculations have been done so far for the static polarizabilities of metal clusters. However, density-functional results with pseudopotentials including the ionic structure are available. Moullet *et al.* (1990a, 1990b), who optimized the ionic structure of Na_2–Na_9 in a local-spin-density (LSDA) treatment using nonlocal pseudopotentials, obtained very good values for the dipole polarizabilities, including the fine structure of the experimentally observed values (e.g., the dip at $N=4$; see Fig. 22, Sec. V.C.1, of de Heer, 1993). They showed that the comparison of experimental and calculated values of α can be used to decide which isomeric form of the ionic geometry is present in the ground state, which is not always possible on grounds

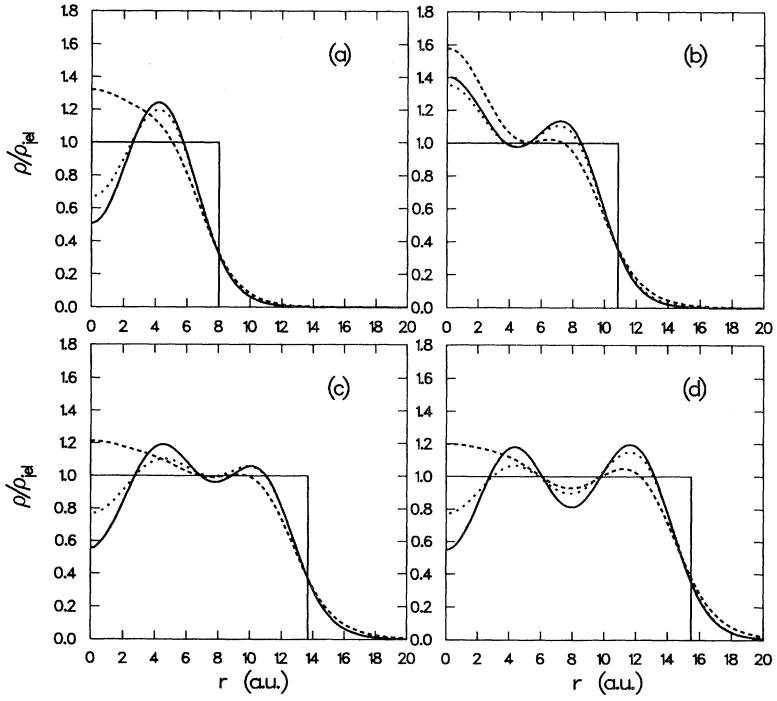

FIG. 7. Electronic densities (in units of the jellium density ρ_{J0}) of spherical Na clusters: (a) $N=8$; (b) $N=20$; (c) $N=40$; (d) $N=58$. Solid lines, Hartree-Fock results; dotted lines, Kohn-Sham results in LDA with exchange only; dashed lines, Hartree results (no exchange at all). The square profiles show the jellium densities. From Hansen and Nishioka, 1992.

of a minimization of the total energy alone. The results of Moullet *et al.* (1990a, 1990b) depend to some extent on the choice of the pseudopotential, but clearly show that the inclusion of ionic structure improves the agreement with experiment appreciably. It should be noted that no self-interaction correction was included in their calculation.

These results seem to suggest that a non-negligible part of the observed polarizabilities comes from the nonlocal effects associated with the pseudopotentials. Note that the ionic core polarizability will also contribute and is not included in any of these treatments.

Earlier results with structural models using pseudopotentials had already indicated the above improvement. Manninen (1986b), using a local pseudopotential, found reasonably good agreement of the average polarizabilities α of Na_2–Na_8 with the experimental values. He used, however, only an approximate expression for the energy, derived perturbatively by minimizing the classical Madelung energy. Furthermore, the absolute values of α were improved by the choice of an unusually large pseudopotential parameter $r_c = 4.0$ a.u. He did not reproduce the dip for Na_4. Similarly, Rubio *et al.* (1990) found the spherically averaged pseudopotential model to improve the polarizabilities of Al clusters with $N < 40$ over the jellium model results.

The simple extensions of the jellium model that simulate a part of the ionic structure (see Sec. III.D) also indicate this trend: Rubio *et al.* (1991b) (see also Balbás and Rubio, 1990) and Lauritsch *et al.* (1991) noticed that the introduction of a diffuse surface of the jellium background density helps to increase the static polarizabilities obtained in jellium-LDA calculations. In fact, by a variational determination of the diffuseness of the jellium surface, Rubio *et al.* (1991b) obtained good agreement with the experimental polarizabilities of Na clusters. Finally, recent Kohn-Sham-LDA-RPA calculations by Genzken *et al.* (1993) with a pseudopotential-folded diffuse jellium density (cf. Sec. III.D.2) also yielded the same results.

2. Dipole resonances and the dynamic response

The classical theory of dynamic polarizability predicts a single dipole resonance at a frequency given by (Mie, 1908)

$$\omega_{\rm Mie} = \left[\frac{Z\hbar^2 e^2}{mR^3} \right]^{1/2}, \tag{4.9}$$

which, with $R = r_s Z^{1/3}$, is equal to $1/\sqrt{3}$ times the bulk plasma frequency.

The linear response obtained in the jellium model follows the Mie result, but only in a qualitative way. This was shown in self-consistent Kohn-Sham-TDLDA calculations by Ekardt (1984a, 1985a, 1985b) and Penzar *et al.* (1990), in LDA+RPA calculations using semiclassical potentials (cf. Sec. V.B.2) by Yannouleas *et al.* (1989, 1990, 1993), and in full HF+RPA calculations by Guet and Johnson (1992).[12]

The dipole absorption cross sections of spherical alkali clusters obtained in all these jellium calculations usually exhibit a dominant peak that exhausts some 75–90 % of the dipole sum rule and is redshifted by 10–20 % with respect to the Mie formula (4.9). As will be discussed in Sec. IV.C below, the centroid of the RPA strength distribution tends towards the Mie resonance in the limit of a macroscopic metal sphere. Its redshift in finite clusters is a quantum-mechanical finite-size effect that is closely related to the electronic spillout.

Some 10–25 % of the dipole strength is typically found at higher energies and can be interpreted as a reminiscence of a strongly fragmented volume plasmon (see Sec. IV.C below). Often, the dominant peak is also fragmented into two (e.g., Na_{20}) or more lines (e.g., Na_{40}). The fragmentation of collective strength in spherical clusters can be attributed to an interference of specific particle-hole (or more complicated) excitations with the predominant collective mode (Yannouleas *et al.*, 1989, 1993; Yannouleas and Broglia, 1991a). This fragmentation may be compared to Landau damping in the solid, although there it refers to a collective state lying in a single-particle continuum.[13]

When compared to experiment, all jellium calculations yield an insufficient redshift of the Mie resonance. This is directly connected to the lack of polarizability via the sum-rule estimate E_1 (see Sec. IV.C below). Therefore a finite surface diffuseness of the jellium density (cf. Sec. III.D), or other corrections found to improve the polarizability, will also improve the position of the dipole resonance.

There are other deviations from the single-resonance Mie formula that are reproduced by the jellium model calculations. In open-shell clusters one finds a further splitting of the dipole resonance, which is a consequence of their static deformation and can easily be described in the phenomenological Clemenger-Nilsson model (Selby *et al.*, 1991; Bernath *et al.* (1991); see also Sec. VIII of de Heer, 1993). It has also been obtained self-consistently in the spheroidal jellium model with TDLDA calculations by Ekardt and Penzar (1991). Very recently, the double-peak feature in the photoabsorption cross section of positively charged clusters has been observed for K_{11}^+ by Bréchignac *et al.* (1992a), for Ag clusters in the region $10 \le N \le 16$ by Tiggesbäumker *et al.* (1992), and for Na clusters with $14 < N < 48$ (except $N = 21$ and 41) by Lützenkirchen *et al.* (1992) and Borggreen *et al.* (1993).

[12] A self-consistent spherical jellium-Kohn-Sham-LDA+RPA code was made available by Bertsch (1990).

[13] The same kind of fragmentation also occurs for the nuclear giant resonances. It is much stronger there due to the spin-orbit interaction. For a comparison of the situations in nuclei and atomic clusters, we refer the reader to Reinhard *et al.* (1992).

The latter results confirm the transition of oblate to prolate ground-state deformations obtained in the deformed jellium model when filling the $1d$ shell for $8 < N \leq 18$ (see also the discussion in Sec. III.B.2). In larger clusters, however, it is not easy to disentangle the effects coming from static deformations and those from the fragmentation mechanism discussed above.

It can thus be said that the microscopic jellium model with TDLDA or RPA calculations is able to describe the correct qualitative trends of the observed resonances in the photoabsorption cross sections of small clusters, including effects of fragmentation and deformation splitting. The interpretation of the resonances as surface plasmons, weakly coupled to volume plasmons, will be discussed in Sec. IV.C below.

Some differences from experiment have been explained by phenomenological corrections to the jellium model: Blanc *et al.* (1991) showed that the use of an "effective mass" of the electron, taken to be the known value for bulk lithium, can fit the unusually large red shift of the dipole resonance of Li_8 in terms of a corrected Mie frequency. Similarly, an *ad hoc* "core-polarizability" correction in the jellium-RPA calculation can explain the deviation of the resonances observed in large potassium clusters by Bréchignac *et al.* (1992b; see de Heer, 1993, Sec. VIII). Such corrections introducing empirical bulk parameters into finite systems have not, however, been microscopically justified so far and therefore have little predictive power.

The observed widths of the resonance peaks are even more difficult to explain microscopically than their positions. Several processes can in principle contribute to the width of the plasmon peak:

(i) Emission of an electron, i.e., autoionization ("escape width"). This is only possible if the plasmon energy lies above the ionization threshold.

(ii) Evaporation of a single neutral atom.

(iii) Interference of the collective state with specific particle-hole states that lie close in energy (fragmentation; cf. "Landau damping" in the solid).

(iv) Coupling of the dipole oscillation to other collective electronic modes (for nuclear giant resonances called "spreading width").

(v) Coupling of the collective electronic vibration to collective ionic vibrations (cf. phonons in a lattice).

Of these processes, only (i) and (iii) can be described in the usual RPA, which includes one-particle/one-hole ($1p$-$1h$) configurations only. The coupling to other collective electronic modes (iv) would require at least a $2p$-$2h$, and more generally an np-nh, treatment which becomes numerically very involved. Coupling to ionic motion [(ii) and (v)] is strictly not possible within the jellium model. The fragmentation (iii) has already been discussed above; in small clusters like Na_{20}, where a corresponding splitting has been experimentally resolved, it cannot be made responsible for the linewidth. Rather little is known so far about the coupling to other electronic vibrations (iv). To the extent that all higher-multipole collective electronic vibrations are expected at considerably higher energies (see Brack, 1989; Serra *et al.*, 1989a, 1989b) and that their coupling to the dipole mode would require multi-particle-hole excitations, this mechanism is not expected to give an important contribution to the observed width (Bertsch and Tomanek, 1989).

The only processes that would give a true coherent width due to decay into a continuum are the processes (i) and (ii). However, electron emission (i) is not possible in most (small) clusters, where the ionization threshold is typically 1–2 eV higher than the observed plasmon peak. (This is different from the case of nuclear giant resonances, which lie high up in the nucleon continuum, so that their widths include a large contribution from the evaporation of a nucleon.) Evaporation of a monomer (i), with a typical dissociation energy of about 1 eV, is energetically possible and, in fact, believed to be the actual decay channel of the observed surface plasmons. However, its contribution to their width is expected to be on the order of, at most, a few millielectron volts, if standard estimates of evaporation times are used (see, for example, Selby *et al.*, 1991), which are of the order of the inverse Debye frequency and therefore cannot explain the observed plasmon widths of about ~ 0.3–0.5 eV.

An appreciable contribution to the width can be expected from the coupling to collective ionic vibrations (v), although the energy scale of the latter is of the order of meV only. As we have discussed above, static deformations of a cluster split the dipole peak into two or three subpeaks. Therefore an incoherent superposition of thermal (or quantum-mechanical zero-point) vibrations of the ions will lead to an effective broadening of an otherwise sharp dipole plasmon. A fully microscopic description of this mechanism is outside the scope of an RPA calculation, and one must therefore resort to simple phenomenological models in order to estimate this effect. To this end Bertsch and Tomanek (1989) proposed a method that has been successfully used to estimate spreading widths of nuclear collective vibrations (Gallardo *et al.*, 1985; Bertsch and Broglia, 1986; see also Bertsch, Bortignon, and Broglia, 1983). The ionic vibration was assumed here to be of (axially symmetric) quadrupole type. The coupling to the electronic motion was described by parametrizing the static deformation energy in terms of the empirical surface energy of the bulk metal. The thermal fluctuations of the cluster surface, which led to a broadening of the electronic dipole plasmon through deformational splitting, were estimated adibatically via statistical Boltzmann factors. The resulting width was found to be of the order of ~ 0.4 eV for small sodium clusters at room temperature, in reasonable agreement with the observed linewidths of dipole plasmons (see Sec. VIII.L of de Heer, 1993).

This model was taken up by Pacheco and Broglia (1989) and further refined in a series of papers, taking the zero-point shape vibrations into account as well (see Pacheco *et al.*, 1991, and references quoted therein). The quadrupole motion was extended to include nonaxial de-

formations, and the β,γ deformation energy surfaces (cf. Sec. III.B.2) of the deformed clusters were calculated within the Clemenger-Nilsson model. Penzar, Ekardt, and Rubio (1990) treated the same effects self-consistently in the spheroidal jellium model (see also Ekardt and Penzar, 1991).

The mechanism of thermal line broadening due to shape vibrations of the whole cluster predicts a temperature (T) dependence of the width of the form $\Gamma \propto \sqrt{T}$. Experimentally, the temperature dependence of the linewidth is, however, too poorly known to test this prediction. Similarly, the form of the resonance would be predicted to have a Gaussian falloff. Some experimental dipole resonances, particularly for charged clusters, can be fitted rather well with a Lorentzian shape; in other cases the falloff seems to be steeper (see Sec. VIII.L of de Heer, 1993). In general, however, the experimental information from photoabsorption measurements is too limited to decide on the precise line form of the resonances.

In large matrix-supported clusters the experimental widths Γ of the dipole absorption lines are nearly temperature independent and can be fitted by an inverse-radius law (see, for example, Kreibig and Genzel, 1985):

$$\Gamma = A\frac{v_F}{R} , \tag{4.10}$$

where R is the radius of the cluster and v_F the Fermi velocity of the valence electrons. This fit does not, however, extrapolate to the observed widths in free clusters with $N \lesssim 50$, which are considerably smaller.

Equation (4.10) had been predicted by Kawabata and Kubo (1966) from semiclassical response theory. Their coefficient A, however, does not fit the experimental one, which seems to depend on the embedding matrix (Kreibig and Genzel, 1985). Recently Yannouleas and Broglia (1992) have rederived Eq. (4.10) with a larger coefficient A. They used the so-called wall-dissipation mechanism (Blocki *et al.*, 1978), which has been studied in nuclear physics in connection with fission and heavy-ion dynamics; it is equivalent to Landau damping in the solid and corresponds in large clusters to the fragmentation mechanism (iii) above.

In summary, it must be said that the decay mechanisms of the collective dipole resonances in metal clusters are, both theoretically and experimentally, still rather poorly understood. More experimental information on their temperature dependence and the detailed line form is required to shed light on this problem and to test the simple theoretical models developed so far.

3. General discussion

On a quantitative level, calculations including ionic structure have achieved greater accuracy than jellium calculations in reproducing the experimental dipole response. Unfortunately, *ab initio* calculations of the dynamic dipole response are only available so far for Na and Li clusters with $Z \leq 8$ (see Bonačić-Koutecký *et al.*, 1990, 1991). These calculations typically predict more fragmentation of the strength function than the jellium model,[14] although in the "magic" 8-electron system the results are similar, with a single dominant peak. It is also found for this system that the RPA treatment essentially reproduces the response obtained with more accurate configuration-mixed wave functions.

The systematic lack of dipole polarizability and the corresponding absence of redshift in the dipole resonances, found in all jellium-LDA calculations for alkali clusters, are closely related to each other by general sum-rule arguments (see Sec. IV.C below). The origin of this failure is not easy to pin down quantitatively, although it is clear from the quantum-chemical calculations that the ionic core needs to be better treated. The wrong asymptotic falloff of the Kohn-Sham potential due to the LDA treatment of the exchange is another possible error source. The self-interaction-corrected LDA results and the WDA calculations discussed in Sec. IV.B.1 above ought to give a partial answer to the problem of the LDA exchange, but they seem to be contradicted by Hartree-Fock results on the one hand and by the pseudopotential model results, which include the ionic structure, on the other hand. It is therefore very important to pursue these theoretical investigations, both testing the LDA and studying the role of the ionic structure more systematically.

Clearly, the experimental details of the electric response of metal clusters serve as a crucial testing ground for the theory. The calculated dipole strength and its fragmentation depend rather sensitively, however, on details of the models, such as the self-consistency of the potential, the exchange-correlation-energy density functional, or the pseudopotential used. A numerical source of uncertainty stems from the fact that the space of particle-hole configurations included in the calculation must be restricted for practical reasons. This concerns, in particular, the electronic states lying in the continuum, which are often treated only approximately. Moreover, the use of a restricted Gaussian basis set in *ab initio* and pseudopotential calculations might easily lead to a numerical underestimation of the electronic density tail and thus of the polarizability.[15] Therefore more systematic and rigorous investigations of all these approximations are definitely called for.

Finally, a few words concerning the terminology used in the predominant jellium model literature might be appropriate here. Terms like "surface plasmon," "volume plasmon," "effective mass," or "Landau damping" are strictly defined for infinite systems only, and their usage

[14]For the "nonmagic" clusters, the character of the fragmentation depends on the assumed ionic configuration to a degree that allows one to determine the configuration from the empirical dipole strength function.

[15]One numerical test of possible truncation errors is to check the fulfillment of the energy-weighted sum rule; see Eq. (4.13) below and Eq. (B7) in Appendix B.2.

for small clusters may raise objections. However, the qualitative behavior of the electric response of small alkali clusters, even with $N<20$, is dominated by the same physics as the condensed-matter phenomena denoted by these names, even if significant quantitative differences exist (such as the relative positions of the unperturbed particle-hole excitations, the plasmon peaks, and the continuum threshold). Clearly, the use of these terms for small systems underscores the similarity of the physical phenomena, but it should not cover the differences.

In purely microscopic language, the electronic response is made up by (multi-) particle-hole excitations. However, to the extent that individual particle-hole transitions often have little physical meaning, the use of macroscopic or semiclassical pictures can help one gain a better physical understanding. We hope to illustrate this point of view in the following section.

C. Sum-rule approach

The results of microscopic RPA and TDLDA calculations are obtained in rather involved numerical codes and are not always easy to interpret. Many of the global response properties can, however, be analyzed and understood in a transparent way in terms of sum rules that apply to the RPA response.

1. Sum-rule relations and classical limits

The sum-rule approach (Bohigas *et al.*, 1979) allows one to estimate the global features of an RPA spectrum, such as its centroid and variance, in terms of simple—in some cases even analytical—expressions (see Appendix B.2 for the formal details). This approach has been widely used in nuclear physics, particularly in connection with giant nuclear resonances (see, for example, Bohigas *et al.*, 1979; Gleissl *et al.*, 1990). It has also been applied to metal clusters by Bertsch and Ekardt (1985) and later by many others (Brack, 1989; Serra *et al.*, 1989a, 1989b, 1990; Reinhard *et al.*, 1990; Lipparini and Stringari, 1991), Reinhard and Gambhir (1992). Sorbello (1983) discussed a "dipole force sum rule" that is closely related to the RPA sum rules discussed here.

We define the RPA moment m_k as

$$m_k=\frac{1}{\pi}\int dE\, E^k \mathrm{Im}[\alpha(E)]\ , \tag{4.11}$$

where $\mathrm{Im}[\alpha(E)]$ is the imaginary part of the dynamic polarizability function as calculated in RPA. Physically, these moments can be related to energy-weighted moments of the photoabsorption cross section $\sigma(E)$ by

$$m_k=\frac{\hbar c}{4\pi^2}\int_0^\infty E^{k-1}\sigma(E)dE\ . \tag{4.12}$$

However, one should bear in mind that some of the moments may physically diverge, even though they are finite in RPA.

We discuss in the following the most important moments m_k obtained for the electric dipole operator (4.1). The linear moment m_1 is the simplest case; it is model independent, and the RPA value is exact. It is proportional to Z:

$$m_1=\frac{\hbar^2e^2}{2m}Z\ , \tag{4.13}$$

so that one obtains the famous Thomas-Reiche-Kuhn or "f-sum" rule:

$$\int\sigma(E)dE=2\pi^2\frac{e^2\hbar c}{mc^2}Z\ . \tag{4.14}$$

Thus, theoretically, the integrated photoabsorption cross section just measures the total number of electrons taking part in the collective motion. Hence the experimental determination of this integral helps to identify the collective nature of a resonance. The observed resonances in alkali clusters typically account for at least 60% of the total dipole strength (see Sec. VIII of de Heer, 1993).

The moment m_3 of the RPA response can be shown (see Appendix B.2) to be the restoring force parameter for translational oscillations of the electrons against the ionic background. For the electronic Hamiltonian (2.4), the only contribution to the restoring force of dipole oscillations can come from the external ionic potential V_I, since both the kinetic energy and the Coulomb interaction between the electrons are translationally invariant. The corresponding expression for m_3 can easily be derived using the techniques discussed in Appendix B.2 and reads

$$m_3(D_{x_i})=\frac{e^2}{2}\left[\frac{\hbar^2}{m}\right]^2\int V_I(\mathbf{r})\frac{d^2}{dx_i^2}\rho(\mathbf{r})d^3r\ , \tag{4.15}$$

where $\rho(\mathbf{r})$ is the density of valence electrons. For a spherical density $\rho(r)$, Eq. (4.15) can easily be transformed using the Poisson equation for V_I to yield a simple overlap integral of the electron density with the ionic density ρ_I (Brack, 1989):

$$m_3=\frac{e^4}{2}\left[\frac{\hbar^2}{m}\right]^2\frac{4\pi}{3}\int\rho_I(r)\rho(r)d^3r\ . \tag{4.16}$$

Note that this formula holds for any form of ionic density distribution, as long as the electron density is spherical, and is therefore not limited to the jellium model. For the latter, using Eqs. (3.6) and (3.12), one can rewrite Eq. (4.16) further as

$$m_3=\left[\frac{\hbar^2}{m}\right]^2\frac{e^2Z}{2r_s^3}\left[1-\frac{\Delta Z}{Z}\right]\ , \tag{4.17}$$

where ΔZ is the electronic spillout defined in Eq. (4.8) above.

To our knowledge, the experimental photoabsorption cross sections have not been analyzed so far in terms of their quadratic-energy weighted moments which are proportional to m_3. Such an analysis by means of the above

equations might give some information about the overlap of the electrons with the ionic charge distribution.

However, these results for m_3 and m_1 can also be exploited in a different way. An estimate of the peak energy can be constructed from the ratio m_3/m_1,

$$E_3=\sqrt{m_3/m_1}\ . \tag{4.18}$$

As is known from general sum-rule relations (Bohigas, *et al.*, 1979), this gives an upper limit of the centroid $\bar{E}$ of any strength function, which for a narrow collective resonance is close to its peak energy (see Appendix B.2). From Eqs. (4.13) and (4.17) one gets for the spherical jellium the spillout formula

$$\begin{aligned} E_3&=\left[\frac{\hbar^2}{m}\frac{e^2}{r_s^3}\left[1-\frac{\Delta Z}{Z}\right]\right]^{1/2} \\ &=\frac{1}{\sqrt{3}}\hbar\omega_{\rm pl}\left[1-\frac{\Delta Z}{Z}\right]^{1/2}\ ; \end{aligned} \tag{4.19}$$

here $\hbar\omega_{\rm pl}$ is the bulk plasma frequency. Note that in the limit $\Delta Z=0$, E_3 becomes exactly equal to the classical Mie frequency (4.9) of the dipole surface plasmon, as discussed further below for the general multipole case.

Within the jellium model one thus obtains, through the identification of E_3 with the energy of a surface dipole plasmon, a simple and transparent explanation of its redshift with respect to the Mie frequency: it is due to the quantum-mechanical spillout of the electrons over the jellium surface. A more refined picture, in which couplings of surface and volume plasmons are included, will be discussed further below. Note, however, that the direct connection of the redshift with the electronic spillout is justified only in the simple jellium model in which the positive charge distribution has a sharp edge.

The energy E_3 has been widely used for estimating the energies of giant resonances in nuclei. The physical meaning of this upper estimate E_3 of $\bar{E}$, as discussed also in Appendix B.2, is that of a rapid, diabatic oscillation of the valence electrons against the ions. The oscillation is so fast that the self-consistent mean field of the electrons remains that of the ground state; one therefore also speaks of the "sudden approximation" for the collective electronic motion. The numerical evaluation of E_3 leads one to values that are only marginally higher than the dominant peak energies of TDLDA or RPA results (Bertsch and Ekardt, 1985; Yannouleas *et al.*, 1989; Reinhard *et al.*, 1990; Lipparini and Stringari, 1991).

Another very useful moment is m_{-1}. Unlike m_1 and m_3, there is no closed formula for m_{-1}, but since it is just one-half of the static polarizability [see Eq. (B13) in Appendix B.2] it is easy to calculate in the RPA. We use m_1 and m_{-1} to construct another estimate of the resonance, E_1:

$$E_1=\sqrt{m_1/m_{-1}}\ . \tag{4.20}$$

Using Eq. (4.13), we can express E_1 for the dipole response as

$$E_1(D_{x_i})=\sqrt{\hbar^2e^2Z/m\alpha_{x_i}}\ . \tag{4.21}$$

One can say rigorously that a lower limit for the centroid $\bar{E}$ of the strength function is given by the inequality $\bar{E}\geq E_1$.

The physical significance of this lower limit of $\bar{E}$ is that of a slow, adiabatic motion of the electrons, which adjust their density (and with it their mean field) at any moment to the external dipole field. It is important to note that the terms "diabatic" and "adiabatic" here concern the motion of the electrons only and are independent of the adiabaticity of the ionic motion in the Born-Oppenheimer sense.

If E_1 is identified with the peak position of the dipole resonances, Eq. (4.21) is surprisingly well fulfilled by the experimental results. It is therefore often used to predict dipole resonance peak energies in terms of measured polarizabilities (see Sec. VIII of de Heer, 1993). Note that Eq. (4.21) is exact for the peak energy of a Lorentzian form of the cross section, for which E_1 coincides with the mean value $\bar{E}$.

The apparent difference between the two physical pictures, leading to the rapid diabatic limit E_3 and the slow adiabatic limit E_1, seems to be in contradiction with the fact that both energies are close to the measured peak energies of the plasmon resonances (apart from splittings and the overall absence of redshift). However, as has been noticed in the theoretical calculations (Bertsch and Ekardt, 1985; Brack, 1989; Yannouleas *et al.*, 1989, Reinhard *et al.*, 1990), these two energies are surprisingly close for the dipole plasmons of alkali clusters; in fact, their difference is smaller than the difference of either of them from the measured peak energies. This shows us that when the strength function is strongly concentrated in a single resonance there is no distinction between adiabatic and diabatic motion of the electrons with respect to the ionic background.

For collective modes of higher multipolarity, the situation may become quite different. In the case of nuclear collective quadrupole vibrations, for example, there is a difference of almost an order of magnitude between E_1, which can be approximately identified with the low-lying shape vibrations, and E_3, which is known to yield an excellent description of the high-lying quadrupole giant resonances (see, for example, Lipparini and Stringari, 1989; Gleissl *et al.*, 1990).

An interesting result is obtained if one takes the classical limit of the energy E_3 for a macroscopic metal sphere, i.e., the limit $Z\rightarrow\infty$ of a spherical cluster. In this limit, the jellium model is certainly a good approximation for the ionic density, and the electrons will have a step-function-like density with the same radius. Therefore their spillout (which is a purely quantum-mechanical phenomenon) will be zero, and from the result (4.19) above one finds that E_3 goes over into the classical Mie frequency for the surface plasmon. Brack (1989) has shown that the same limit holds for all electric multipole vibrations described by the operators $\hat{Q}_L=er^LP_L(\cos\theta)$:

$$E_3(\hat{Q}_L)\rightarrow\hbar\omega_L^{\rm Mie}=\left[\frac{L}{2L+1}\right]^{1/2}\hbar\omega_{\rm pl}\quad\text{for } Z\rightarrow\infty\ , \tag{4.22}$$

in agreement with the expression derived by Mie (1908) for surface plasmons of multipolarity L.

Similar considerations can be made for the energy E_1 in Eq. (4.21), which involves the static polarizability. If we assume that the polarizability for all multipolarities L in the limit of large radii reaches its classical value

$$\alpha_{\rm class}^{(L)}=R_I^{2L+1} \tag{4.23}$$

and combine this with the expression (see, for example, Brack, 1989)

$$m_1(\hat{Q}_L)=\frac{\hbar^2e^2}{2m}L\int r^{2L-2}\rho(r)d^3r\ , \tag{4.24}$$

we obtain the same limit as in (4.22) for the energy E_1:

$$E_1(\hat{Q}_L)\rightarrow\hbar\omega_L^{\rm Mie}=\left[\frac{L}{2L+1}\right]^{1/2}\hbar\omega_{\rm pl}\quad\text{for } Z\rightarrow\infty\ . \tag{4.25}$$

We thus find that the two estimates E_3 and E_1 become identical in the large-Z limit for spherical clusters. Since their difference gives an upper bound of the variance σ through the inequality given in Eq. (B9) of Appendix B.2, we learn from this result that the variance of the dipole strength should go to zero in the macroscopic limit. We shall further elucidate this point below in connection with a discussion of the coupling between surface and dipole plasmons.

A warning must be given here. The limit "$Z\rightarrow\infty$" in Eqs. (4.22) and (4.25) should not be taken too literally, since for macroscopic clusters or metal spheres the long-wavelength limit and thus the use of a static dipole operator is no longer justified. The above discussion applies, therefore, only up to the limit in which clusters are still smaller than the wavelength corresponding to the observed surface plasmon frequency, which is typically about 500 nanometers for Na, corresponding to $Z\simeq10^{10}$.

In this respect we note that Serra *et al.* (1990) have studied the electronic multipole response of spherical metal clusters in jellium-Kohn-Sham calculations using operators of the type $j_L(qr)Y_{L0}(\theta)$ and the simple sum-rule approach. For small values of the momentum transfer q they recovered the surface mode systematics discussed above, whereas for large q the response was found to be mainly determined by particle-hole excitations. For intermediate q values, bulk oscillations were found and their connection with the hydrodynamical model predictions were established. In the limit of a big sphere, they obtained an improved bulk-plasmon pole approximation for the dispersion relation, which includes non-negligible exchange and correlation effects.

2. Coupling of surface and volume plasmons

The simple sum-rule model using the two estimates E_3 and E_1 is not quite satisfactory, in spite of many qualitative successes and the limits discussed above, since it works well only in the idealized case of a narrow resonance that exhausts the m_1 sum rule for a given excitation operator (cf. the so-called plasmon-pole approximation). As the experimental results and the fully microscopic RPA and TDLDA calculations show, the reality is often more complicated and presents one with fragmented collective strength (see Sec. IV.B.2). One can, however, go one step further in the exploitation of sum-rule relations and thereby come closer to the microscopic RPA.

An approximate RPA treatment, which makes the assumption of local currents (or velocity fields) and leads to a secular equation for coupled harmonic vibrations described in terms of local trial operators $Q_i(\mathbf{r})$, has recently been proposed by Brack (1989) and Reinhard *et al.* (1990) and used for the calculation of dipole plasmons and polarizabilities of alkali clusters. The ground-state densities obtained in the self-consistent jellium-Kohn-Sham method are the only ingredients; this approach does not require any adjustable parameters. It is, in fact, an extension of the fluid dynamics approach that has been successfully used to describe nuclear giant resonances (Bertsch, 1975; da Providência and Holzwarth, 1985; see also Lipparini and Stringari, 1989, for a recent review. Both approaches and their relation to classical hydrodynamics are briefly discussed in Appendix B.2.)

The static dipole polarizabilities obtained for sodium clusters in the local-current RPA by Reinhard *et al.* (1990) are in perfect quantitative agreement with those resulting from the much more time consuming microscopic linear-response calculations by Beck (1984b), Ekardt (1985a, 1985b), and Manninen *et al.* (1986). In a semiclassical version of the local-current RPA, the correct average values of the polarizabilities have been obtained in terms of extended Thomas-Fermi variational densities (Brack, 1989; cf. also Sec. V.B).

In the following, we shall use the local-current RPA picture to discuss some aspects of the physics of surface and volume plasmons in metal clusters. (We refer the reader to Appendix B.2 for the relevant formalism.) For a given (electric) multipolarity L, the coupled intrinsic modes of the cluster may be described by the following trial set of local operators:

$$Q_i(\mathbf{r})=r^{p_i}Y_{L0}(\theta)\ , \tag{4.26}$$

where p_i is an arbitrary real number ≥1. By constructing the restoring force and inertial tensors (B28), (B27) corresponding to these modes and solving the secular equation (B26), one obtains a spectrum of eigenmodes from which the various sum rules can be evaluated. Since the gradients of Q_i are proportional to the velocity fields, $p_i=L$ is the mode corresponding to incompressible flow, with $\Delta Q_L=\Delta(r^LY_{L0})=0$. Thus the operator Q_L

describes pure surface oscillations without compression. In the large-N classical limit, this leads to the pure Mie surface plasmon, as we see from the limits of $E_3(Q_L)$ and $E_1(Q_L)$ in Eqs. (4.22) and (4.25) above. Modes with $p_i \neq L$, on the other hand, lead to local compression of the electron density. As shown by Brack (1989), the coupling of any number of modes with $p_i \neq L$ gives in the classical limit a degenerate set of eigenmodes, all having the volume-plasmon energy $\hbar\omega_{\rm pl}$; the energy $E_3(Q_i)$ consequently has the same limit:

$$E_3(Q_i) \to \hbar\omega_{\rm pl} \quad \text{for } Z \to \infty \quad (p_i \neq L) \; . \tag{4.27}$$

(As in the previous section, the symbol ∞ should in reality be a number not larger than about 10^{10}.) Note that the surface and the volume modes are completely decoupled in this limit: the volume modes cannot be excited by the electric multipole operator (4.26) with $p_i = L$. This result is a generalization (to $L \neq 1$) of that obtained by Jensen (1937), who investigated the dipole eigenmodes of a metal sphere using classical hydrodynamics in a variational local-density scheme.

In finite clusters, these two types of modes are coupled due to finite-size and quantum-mechanical effects (spill-out of the electron density; kinetic, exchange, and correlation energies). This coupling leads to the following changes from the above classical result:

(i) The compressional volume-type modes are no longer degenerate; the volume plasmon is fragmented into a bunch of scattered eigenfrequencies. That part of the volume plasmon which lies in the electron ionization continuum can, in fact, be found as a strongly Landau-damped resonance, as shown by Ekardt (1985a, 1985b), but it carries a negligible fraction ($< 10^{-3}$) of the total dipole strength.

(ii) The surface plasmon and parts of the fragmented volume plasmon are shifted away from their respective classical Mie frequencies. In the case of the dipole modes, both are redshifted. The same redshift is found for higher multipolarities in large clusters; for small clusters, however, the kinetic-energy contribution to the restoring forces can lead to a substantial blueshift (Brack, 1989; Serra *et al.*, 1989a, 1989b). This is exactly the mechanism that shifts the nuclear quadrupole giant resonance to higher energies and leads to a fundamental difference between normal hydrodynamics and fluid dynamics (see Appendix B.2.c).

In the microscopic particle-hole excitation (RPA) picture, this coupling leads to fragmentation of the dipole strength, discussed in Sec. IV.B above. The fragmentation of the surface-plasmon peak cannot always be correctly described in the local-current RPA picture; obviously, the strong coupling effects between particular particle-hole excitations must be connected with nonlocal currents. But the remaining strength of ~ 10–25 % lying above the surface peak can be interpreted as the remainder of a strongly fragmented volume plasmon.

Let us illustrate the picture of coupled surface and volume modes for the dipole case $L = 1$. For $p_i = 1$ one gets the dipole operator Q_1 (in the z direction); the scaling transformation (B21) then is a simple translation: the dipole Mie plasmon is a pure translational oscillation of all the electrons against the ionic background.

In Fig. 8 we show the dipole spectra obtained in the local-current RPA approach from self-consistent Kohn-Sham ground-state densities for spherical sodium clusters of increasing sizes. The energies of the eigenmodes are given as histograms; the height of the lines corresponds to the percentage of the dipole m_1 sum rule carried by each state. At the top of the figure we see Na_8; the experimental position of the surface plasmon (de Heer, Selby *et al.*, 1987) is indicated by an arrow. The dominant peak of the theoretical spectrum is at ~ 2.75 eV and carries 84% of the dipole strength; it is redshifted with respect to the classical Mie surface plasmon, which lies at 3.4 eV and is indicated by a vertical dashed line in the figure. (The fact that the redshift is not strong enough to reach the experimental position has already been discussed in Sec. IV.B above.) The remaining strength of 16% is scattered over several states in the region ~ 3.5–5 eV; only two of them carry more than one percent. These states contain the remaining strength of the fragmented volume plasmon; their centroid is also sub-

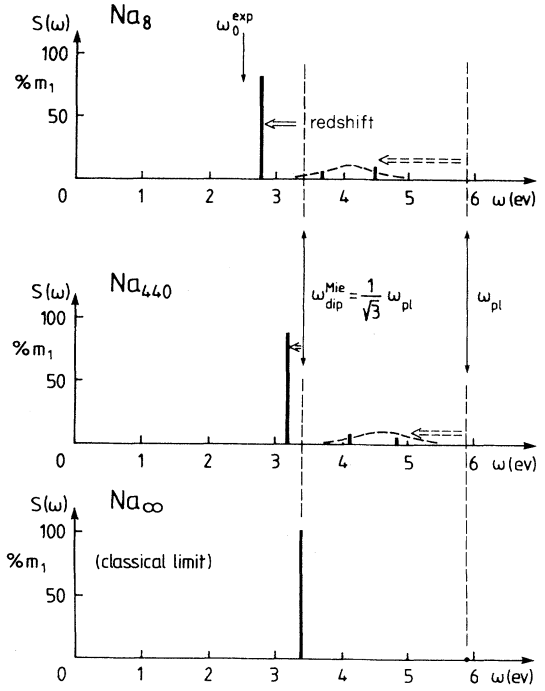

FIG. 8. Collective dipole spectra for sodium clusters, obtained in spherical jellium Kohn-Sham plus local-RPA calculations (Brack, 1989; Reinhard *et al.*, 1990). Shown is the strength in percents of the total dipole m_1 strength (normalized to 100%). The lowest spectrum (Na_∞) represents the classical limit, where 100% of the strength lies in the surface-plasmon (frequency $\omega_{\rm dip}^{Mie}$) and the volume-plasmon (frequency $\omega_{\rm pl}$) has zero strength. For the finite clusters, the surface plasmon is redshifted and its missing strength is distributed over the remainder of the strongly fragmented volume plasmon.

stantially redshifted with respect to the volume-plasmon energy of 5.85 eV. [Note that in a microscopic RPA calculation (Yannouleas *et al.*, 1989) almost identical spectra are obtained. The distribution of the fragmented volume-plasmon states is somewhat different, and the surface mode can be fragmented too, but the moments m_3, m_1, m_{-1} and the variance σ agree to within less than 5% for the two calculations (Reinhard *et al.*, 1990).] At the bottom of Fig. 8, the limit $N \to \infty$ is shown, representing a macroscopic metal sphere with a sharp surface: One surface plasmon at the Mie frequency $\hbar\omega_{\rm pl}/\sqrt{3}$ that carries 100% of the dipole strength, and one (infinitely degenerate) volume plasmon at $\hbar\omega_{\rm pl}$ that is fully decoupled and therefore has no dipole strength. For clusters in between, the tendency is to reduce the coupling between surface and volume modes and to increase the dipole strength of the surface mode with increasing N.

The distinction between volume and surface plasmons is strictly possible only in the large-particle limit. For smaller particles, their coupling and the increasingly dominant role of the surface mix the two types of modes. However, a look at the transition densities $\delta\rho(\mathbf{r})$ corresponding to some of the eigenmodes shown in Fig. 8 will reveal why it is still meaningful to speak of surface and volume modes even in relatively small clusters. The transition density $\delta\rho_i(r)$ of the ith eigenmode defined by

$$\delta\rho_i(r) = -\nabla\cdot(\rho\mathbf{u}_i) \tag{4.28}$$

in terms of its velocity field $\mathbf{u}_i$ (see Appendix B.2.b) tells us where the essential changes occur during the collective vibration in each eigenmode.

Figure 9 shows the transition densities $\delta\rho_i$ along the z axis obtained by Genzken (1992) for various cluster sizes and for two typical eigenmodes: the lowest, most collective mode (shown by solid lines), and one of the fragmented volume modes lying around 5 eV (shown by dashed lines). These results were obtained both in semiclassical calculations, using the model of Brack (1989) and shown in the left parts (a), (b), (e), (f) of the figure, labeled ETF (extended Thomas-Fermi), and microscopically as by Reinhard *et al.* (1990), shown in the right parts (c), (d), (g), (h) of the figure, labeled KS (Kohn-Sham). In the semiclassical results, where the densities $\rho(r)$ are constrained to be constant in the interior part of the cluster, the separation can be clearly observed even in the smallest cluster Na_8: the lowest mode has all its transition density peaked in the narrow surface region near the jellium edge, whereas the higher mode has an appreciable nonzero transition density in the inner volume region. In the microscopic Kohn-Sham results, the shell oscillations of the electronic densities partially blur the situation, but the same trends can be observed at least in the larger clusters. For microclusters like Na_{20} and Na_8, it is no longer possible to divide the electronic density distribution into a volume and a surface part due to the large shell oscillations. Correspondingly, the two types of modes are much more strongly mixed in these small systems. Nevertheless, the notion of the two most predominant physical types of collective oscillations, namely, translational surface modes and compressional volume modes, remains a useful concept.[16]

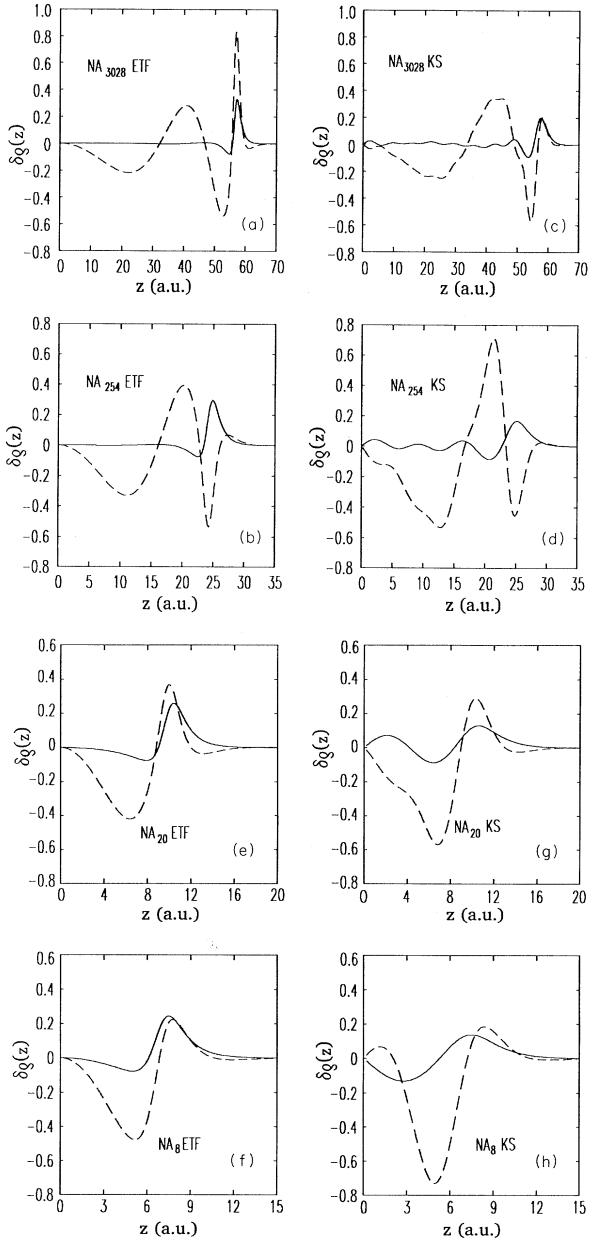

FIG. 9. Dipole transition densities (4.28) along the z axis for spherical sodium clusters: left parts (ETF): semiclassical local-RPA results (Brack, 1989); right parts (KS): Kohn-Sham results in local RPA (Reinhard *et al.*, 1990); solid curves, lowest eigenstate (dipole plasmon); dashed curves, state lying around 5 eV (belonging to the fragmented volume plasmon). From Genzken, 1992.

[16]Kresin (1991) has also used the picture of coupled surface and volume plasmons, with the somewhat oversimplifying assumption of a single volume-plasmon frequency.

It is again instructive to compare the analogous situation in nuclear physics. The famous nuclear giant isovector dipole resonance, a strongly collective vibration of protons against neutrons, can be interpreted in very similar terms. The two leading mechanisms are a compressional mode (corresponding to the volume plasmon) proposed by Migdal (1944) and by von Steinwedel and Jensen (1950), and a purely translational mode (corresponding to the surface plasmon) proposed by Goldhaber and Teller (1948). In a hydrodynamic description one obtains a good fit to the average energies of the experimental giant dipole resonances by taking a suitable combination of the two modes (Myers *et al.*, 1977). After explicit diagonalization of the two coupled modes, the lower of the two eigenfrequencies fits the experimental resonances, whereas the higher is larger by roughly a factor of two and escapes experimental detection (Gleissl *et al.*, 1990). The microscopic HF+RPA theory has difficulty explaining the finer details and the proper widths of these resonances (see, for example, Liu and Van Giai, 1976), but an analysis of transition densities supports the picture of the above two classical modes.

Another measure for the coupling between surface and volume plasmons is given by the variance σ of the dipole strength distribution. As discussed in Appendix B.2, an upper limit of σ can be given in terms of $E_3(Q_1)$ and $E_1(Q_1)$; see Eq. (B9). Since both these energies go to the same limit, $\hbar\omega_{\rm pl}/\sqrt{3}$ for large N, σ has to go to zero. Note, however, that this variance should not be directly identified with the experimentally measured linewidth Γ of the surface plasmon that we discussed at the end of Sec. IV.B.2.

The theoretical RPA prediction of some 10–15 % of the dipole strength, lying well above the surface plasmon and containing part of the fragmented volume plasmon, cannot be verified in the case of sodium due to a lack of experimental data in that energy range. However, recent photoabsorption measurements in small Ag clusters with $N=8-40$ (Tiggesbäumker *et al.*, 1992) systematically reveal some dipole strength lying clearly above the dominant surface-plasmon peak, in qualitative agreement with the RPA prediction. To the extent that the jellium model can be trusted for small Ag clusters, this may confirm the above picture at least qualitatively.

We finally point out that Barberán and Bausells (1985) have discussed the coupling of surface and bulk plasmons in connection with the inelastic scattering of electrons from small metal spheres. Ekardt (1987) discussed in this context wave-vector dispersion versus angular momentum dispersion of the volume plasmons in small metal clusters using spherical jellium-TDLDA-Kohn-Sham calculations.

V. LARGE CLUSTERS: A STEP TOWARDS THE BULK?

In this section we deal with very large metal clusters containing up to many thousands of atoms. We discuss them from two complementary points of view: in Sec. V.A we focus on their shell structure and in Sec. V.B on their average properties. In both contexts, we use the self-consistent jellium model as a basis and semiclassical methods as important tools: on the one hand, the quantization of classical trajectories helps one to understand the so-called supershell structure, and on the other hand, the semiclassical density-variational method allows one to obtain average cluster properties regardless of their size and thus to study them in the asymptotic limit $N\rightarrow\infty$.

A. Shells and supershells

1. Shell effects in finite fermion systems

Quantization of a system of particles in a finite spatial domain leads to discrete energy eigenvalues, which are usually grouped into bunches of degenerate or close-lying levels, called shells. The amount of bunching depends on the symmetries and the integrability of the confining potential. For fermion systems obeying the Pauli principle, this leads to shell effects which are well-known in atoms and nuclei: local minima in the total binding energy per particle versus particle number or deformation, sawtooth-like behavior of the particle separation energy (ionization potential, electron affinity), or oscillations in the radial density distribution. These effects can be described theoretically in terms of independent (or weakly interacting) fermions moving in a common potential. Inversely, the experimental observation of shell effects suggests the existence of a mean field in which fermions (more generally, some quasiparticles with fermionic nature) move more or less independently. In the case of metal clusters, the observation of shell effects has been very suggestive, indeed, of the single-particle motion of the loosely bound valence electrons and has stimulated the development and refinement of the mean-field-type models described earlier in this review.

Shells of single-particle levels are a global phenomenon in the sense that they depend more on the overall form of the mean field (e.g., symmetry, steepness of the surface, deformation) than on the finer local details of its radial dependence (e.g., oscillations which themselves can be connected to shell effects). For large alkali clusters, this means that the inclusion of the ionic structure on top of a jellium model calculation need not modify appreciably the shell situation, provided that the (spherical or deformed) jellium density comes close to the averaged ionic distribution and that the single-particle nature of the electronic orbits is predominant. This may explain the success of the jellium model in correctly explaining most of the observed "magic numbers" corresponding to spherical-shell closings, in particular of the very large alkali clusters, which we discuss in the following subsection.

That shells are not only peculiar to spherical systems has most clearly been formulated by Strutinsky (1968), who pointed out the close connection between the oscil-

lating part of the single-particle level density, $\delta g(E)$, and the oscillating part of the total energy, i.e., the "shell correction" δE [see Eq. (5.1) below], both as functions of particle number and of *deformation*. In fact, the mere existence of static nuclear deformations is due to shell effects and could be accounted for theoretically by the famous Nilsson model (Nilsson, 1955; Mottelson and Nilsson, 1955)—which has been revived by Clemenger (1985a, 1985b) in a simplified form (namely, leaving out the spin-orbit interaction). The mechanism, which leads to a spontaneous deformation of the mean field—even if the basic two-body interaction is a central one—is just another example of the Jahn-Teller effect (Jahn and Teller, 1937): when a spherical l shell is only partially filled, the system lifts the degeneracy of its ground state by allowing the mean field to give up spherical symmetry, resulting in an energy gain. However, the shell effects in deformed systems are usually less pronounced than in spherical ones. (See, for example, the smaller subpeaks in the cluster abundances of Knight *et al.*, 1985, which correspond to deformed subshells, compared to the dominant spherical-shell peaks.)

A very effective and successful method for investigating the shell structure in the total energy of a finite fermion system, as a function of both deformation and particle number, has been introduced by Strutinsky (1968). According to his basic theorem, the energy of an interacting fermion system can be divided into a smooth part $\tilde{E}$ and an oscillating part, the energy shell correction δE:

$$E=\tilde{E}+\delta E \ . \tag{5.1}$$

Whereas $\tilde{E}$ varies slowly with particle number and with the deformation of the system, the shell correction δE contains all the oscillations coming from the shell bunching of energy levels. To a very good approximation, δE can be extracted from the sum of occupied single-particle energies (or quasiparticle energies, see Bunatian *et al.*, 1972) ε_i of the averaged mean field, i.e., from $E_{\rm sp}=\sum_{i=1}^{N}\varepsilon_i$, by subtracting its suitably defined averaged part (Strutinsky, 1968). Brack and Quentin (1981) have numerically tested this approximation using Hartree-Fock calculations with effective nuclear interactions, and also investigated its extension to finite temperatures. In practice, the average energy $\tilde{E}$ can be taken from a phenomenological liquid-drop model, whereas δE can be found from the single-particle energies ε_i of phenomenological shell-model potentials. [For an extensive review on the Strutinsky method and its application to nuclear fission barrier calculations, see Brack *et al.* (1972).] A modified form of the Strutinsky renormalization idea was discussed by Brack *et al.* (1991b) in their calculation of thermal electronic properties of metal clusters.

The regular oscillatory behavior of both the single-particle level density and the shell-correction energy leads, in general, to shape isomerism: several local minima can exist in the multidimensional energy surface. A famous example in nuclear physics are the fission isomers, which were correctly interpreted for the first time by Strutinsky (1968) using the shell-correction formalism. That shape isomers in metal clusters are found not only in quantum-chemical and molecular-dynamics calculations, but also within the deformed jellium model, has been discussed already in Sec. III.B.2.

One should therefore use the term "magic number" with some care: it may not be taken as a synonym for sphericity. This was justified in the first years after the discovery of the nuclear shell model (Goeppert-Mayer, 1949; Haxel, Jensen, and Suess, 1949), when "magic numbers" like 82 and 126 had been recognized as the numbers of nucleons corresponding to filled major spherical shells (where the strong spin-orbit coupling was an essential ingredient). Since enhanced stability also occurs in deformed systems, the corresponding numbers of particles can also have "magic" character, e.g., the neutron number $N=146$, which is characteristic of the most stable fission isomers in actinide nuclei having large deformations corresponding to an axis ratio of $\sim$2:1 (see, for example, Bjørnholm and Lynn, 1980).

Just recently, the Strutinsky shell-correction method has been applied to large deformed sodium clusters by two independent groups. Frauendorf and Pashkevich (1993) used a deformed version of the Woods-Saxon potential parametrized by Nishioka *et al.* (1990) to calculate the ground-state deformations of Na clusters with $N \leq 300$, including axial quadrupole, octupole, and hexadecupole shapes. Reimann *et al.* (1993) improved the Clemenger-Nilsson model by fitting the l^2 term to self-consistent Kohn-Sham levels of spherical clusters. They calculated the equilibrium deformations of spheriodal Na clusters with $50 \leq N \leq 850$ and reanalyzed the experimental mass abundance spectra of Bjørnholm *et al.* (1990,1991), finding good agreement between the calculated and observed "deformed magic" numbers.

Many aspects of shell structure can be qualitatively, and sometimes even quantitatively, described by semiclassical methods. A very powerful tool for investigating the gross shell structure in the single-particle level density of a given potential in terms of classical trajectories has been developed by Gutzwiller (1971) and by Balian and Bloch (1972; see also earlier papers cited in these two articles). Strutinsky *et al.* (1977) generalized this method successfully for realistic nuclear potentials and explained the behavior of the various isomeric valleys in contour plots of the level density and the energy as functions of particle numbers and deformation (see also Strutinsky, 1975). Nishioka *et al.* (1990) applied the same kind of analysis to metal clusters, using Woods-Saxon-type potentials, and discussed the "supershell" structure, which will be the subject of the following subsection.

We shall not present here the details of the Gutzwiller-Balian-Bloch theory and its applications to metal clusters, but refer the interested reader to a forthcoming review article by Bjørnholm *et al.* (1993). Some of the simplest aspects and results of this approach will be referred to below in order to explain the observed shell

structure in large alkali clusters. Reimann and Brack (1993) have observed that the calculated ground-state deformations of spheroidal sodium clusters with $50 \lesssim N \leq 850$ (Reimann *et al.*, 1993) can be explained in terms of a family of classical rhomboidal planar orbits of a particle in a spheroidal cavity, exactly as it was proposed by Strutinsky *et al.* (1977) in the context of nuclear deformations on the basis of the Balian-Bloch theory.

2. Electronic supershell structure in large alkali clusters

One of the salient features of the level density in a steep confining potential is a beating pattern: the regular oscillations reflecting the main shells are modulated by an oscillating amplitude of lower frequency. Such a pattern was found by Balian and Bloch (1972) to be a very general feature of quantal eigenmodes in a cavity with reflecting walls. For the case of a spherical cavity, they showed that this beating is the result of an interference of the two most important classical trajectories responsible for the oscillating part of the level density, namely, triangles and squares. (Other orbits contribute, too, but with smaller amplitudes; they are important only near the interference minima.) Their contribution to the level density $g(k)$ as a function of the wave number $k=\sqrt{2mE}/\hbar^2$ equals (see also Strutinsky, 1975)

$$\delta g_{(3+4)}(k)=\frac{1}{2}(kR/\pi)^{1/2}\frac{2mR^2}{\hbar^2}\left\{A_3\sin\left[kL_3+\frac{\pi}{4}\right]+A_4\sin\left[kL_4+\frac{3\pi}{4}\right]\right\}, \tag{5.2}$$

where R is the radius of the cavity. This superposition of two sin functions with comparable amplitudes $A_3=(\sqrt{3}/2)^{1/2}$, $A_4=(1/\sqrt{2})^{1/2}$, and wavelengths $L_3=3\sqrt{3}R$, $L_4=4\sqrt{2}R$ leads to a beating of the level density; up to a small term contributing less than 5%, one obtains

$$\delta g_{(3+4)}(k)\simeq(kR/\pi)^{1/2}\frac{2mR^2}{\hbar^2}A_3\cos(k\bar{L})\cos\left[k\Delta L-\frac{\pi}{4}\right] \tag{5.3}$$

with

$$\bar{L}=\frac{1}{2}(L_3+L_4)\,,\quad \Delta L=\frac{1}{2}(L_3-L_4)\,. \tag{5.4}$$

Here the factor $\cos(k\bar{L})$ gives the fast oscillations in energy, representing the main-shell oscillations, and the second cos factor gives the beating amplitude.

The same pattern is also found for the density of energy eigenvalues in smooth potentials, provided their surface is steep enough. (The pure spherical harmonic oscillator and Coulomb potentials have no well defined surface region; correspondingly, their level densities do not show any beating pattern.) In Fig. 10 we show the electronic level density obtained by Nishioka *et al.* (1990) for a spherical Na cluster. They used a phenomenological Woods-Saxon potential fitted to the self-consistent jellium-Kohn-Sham results of Ekardt (1984b) and extrapolated it to a size of $N=3000$. To emphasize the gross shell structure, the discrete eigenvalue spectrum was folded with a Lorentzian having a width of about a fifth of the main-shell spacing. The shell oscillations around the average level density and the beating pattern are evident in this figure. Nishioka *et al.* (1990) termed the groups of main shells, separated by the interference minima, "supershells" and discussed their stability against variations in the radial dependence of the potential. Clemenger (1991) has also used Woods-Saxon potentials, related by simple scaling considerations in order to describe different metals, to discuss the supershell structure.

This supershell beating is also present in the total energy of the system. In Fig. 11 we show the energy shell correction for spherical sodium clusters with N up to 3000 obtained in self-consistent Kohn-Sham calculations by Genzken and Brack (1991) and Genzken *et al.* (1992) at various temperatures T, plotted versus $N^{1/3}$. The shell correction $\delta F(N)$ is defined here as the difference between the total free energy $F(N)$ of a cluster with N atoms and its average part $\bar{F}(N)$:

$$\delta F(N)=F(N)-\bar{F}(N)\,. \tag{5.5}$$

Strutinsky (1968) introduced a numerical energy-averaging procedure to calculate $\bar{E}(N)$ at $T=0$ from the single-particle energies ε_i, which can be extended to finite temperatures (Brack and Quentin, 1981). A simple alternative way is to use a liquid-drop model expansion of the total free energy of the type discussed in Sec. V.B.2:

$$\bar{F}(N)=F_{\rm LDM}(N)=e_bN+a_sN^{2/3}+a_cN^{1/3}\,. \tag{5.6}$$

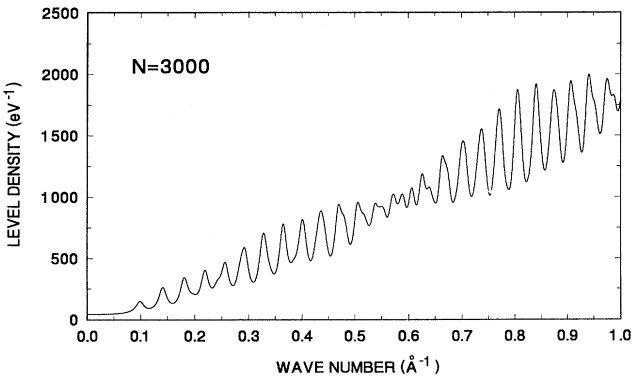

FIG. 10. Electronic single-particle level density $g(k)$ as a function of wave number k, evaluated in a spherical Woods-Saxon potential corresponding to a Na cluster with $N=3000$, by Nishioka *et al.* (1990).

[In obtaining Fig. 11, a_s and a_c were determined at each temperature by a simple fit such that $\delta F(N)$ is oscillating around zero; the bulk energy was fixed at its theoretical value $e_b=-2.2567$ eV obtained for $r_s=3.96$ a.u. (Genzken and Brack, 1991).] The supershell beating is clearly visible in $\delta F(N)$. Note, however, that the amplitude of the shell oscillations is reduced with increasing temperature, and the minima become less sharp than at $T=0$. The "magic numbers" corresponding to filled spherical main shells are given in the curve for $T=0$ at the corresponding minima.

Neither the level density nor the shell-correction energy $\delta F(N)$ are directly observable. As discussed by Bjørnholm *et al.* (1990, 1991), the mass abundances in expansion beams depend rather on the differences $\Delta_1 F(N)=F(N-1)-F(N)$ and $\Delta_2 F(N)=F(N+1)+F(N-1)-2F(N)$, which are very sensitive to temperature-smoothing effects for the larger cluster sizes. In fact, these latter quantities were shown by Brack *et al.* (1991a, 1991b) to vanish almost completely for $N\gtrsim 600$ at temperatures $T\simeq 600$ K or above, putting in doubt the observability of the supershell structure, which only starts at $N\gtrsim 900$, in supersonic expansion experiments. Nevertheless, Pedersen *et al.* (1991) and Martin, Bjørnholm *et al.* (1991) have experimentally put the existence of supershells in Na clusters into evidence, and Bréchignac *et al.* (1992c) observed them in Li clusters.

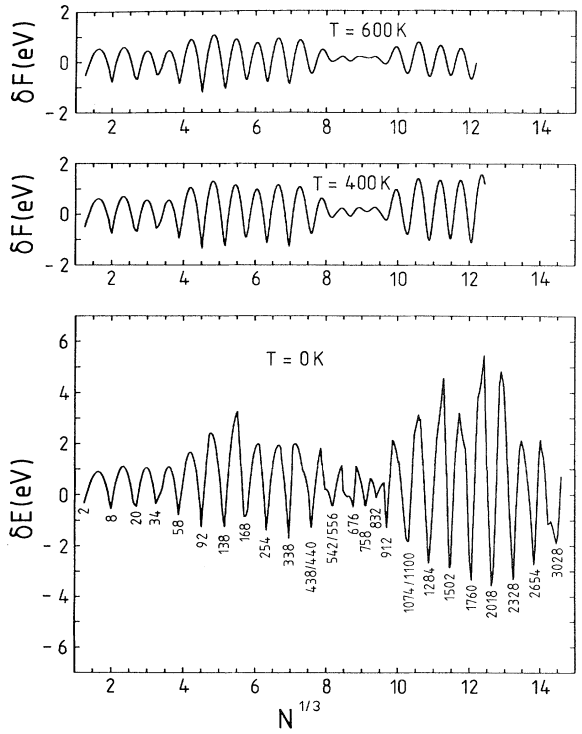

FIG. 11. (Free) energy shell correction (5.5) vs $N^{1/3}$ at three temperatures, obtained in spherical jellium-Kohn-Sham-LDA calculations by Genzken and Brack (1991). In the lowest part, the "magic numbers" corresponding to filled major spherical shells are indicated.

In order to make the beating pattern of the shell oscillations visible in very large clusters, where thermal suppression of the shell structure becomes important, Pedersen *et al.* (1991) multiplied the logarithmic derivatives of the mass yields by a factor depending exponentially on $N^{1/3}$. This is justified by the following argument. The temperature dependence of $\delta F(N)$ for a spherical closed-shell system can be schematically estimated from the harmonic-oscillator model (Bohr and Mottelson, 1975) to vary as

$$\delta F(T)=\delta F(0)\frac{t}{\sinh t}\ ,\quad t=T\frac{2\pi^2}{\hbar\omega}\ . \tag{5.7}$$

Expanding for large temperatures and using $\hbar\omega\propto N^{-1/3}$ this gives, indeed, a temperature suppression factor $\propto\exp(-N^{1/3})$. Therefore, scaling up the experimentally observed mass yields by the inverse factor just compensates for this thermal compression.

In the upper part of Fig. 12 we have reproduced the relevant figure of Pedersen *et al.* (1991), which shows the first differences of the logarithmic experimental yields, $\Delta_1 \ln I_N$, averaged over a range $N\pm K_0$ with $K_0=0.03N$ in order to eliminate statistical fluctuations and multiplied by $\sqrt{N}\exp(cN^{1/3})$. Here c is an adjusted constant containing the effective temperature, and the extra factor $\sqrt{N}$ compensates for the decrease of the shell correction at $T=0$ with increasing N (Bohr and Mottelson, 1975). Note that in taking the differences $\Delta_1 \ln I_N$, one focuses on the oscillating part of the mass yields, which is dominated by electronic effects, whereas the smooth ionic contributions, as well as possible systematic experimental errors, are canceled.

In the lower part of Fig. 12 we show the theoretical jellium model results by Genzken and Brack (1991) for the negative second difference of the total free energies, $-\Delta_2 F(N)$, multiplied by the same enhancement factor (with the value of c readjusted by $\sim 10\%$). In this quantity, too, the ionic contributions, which are only crudely represented in the jellium model anyhow, are practically canceled. The similarity of the two curves shown in this figure is striking. In comparing them, one makes the implicit assumption

$$I_N\sim\exp\{-\Delta_1 F(N)/kT\}\ . \tag{5.8}$$

Since $\Delta_1 F(N)$ is the free dissociation energy of one neutral atom [up to the constant $F(1)$, which cancels when taking the second difference $\Delta_2 F$], the Boltzmann factor on the right-hand side of Eq. (5.8) is a measure of the relative stability of the cluster N against evaporation of a monomer,

$$\mathrm{Na}_N\rightarrow\mathrm{Na}_{N-1}+\mathrm{Na}_1\ , \tag{5.9}$$

in an evaporative ensemble at thermodynamic equilibrium. Although this is certainly a rather simplifying assumption, which neglects dynamic and nonequilibrium effects of the evaporation process (see Bjørnholm *et al.*, 1991, 1993, for a discussion of this point), it seems to be

supported by the qualitative agreement of the two curves in Fig. 12. In any case, this result demonstrates that the finite temperature of the valence electrons can play an essential role in the mass yields.

Rather direct evidence of the electronic nature of the observed supershells is also found from the radius increment $\Delta R = r_s \Delta N_0^{1/3}$ between two clusters with neighboring magic numbers N_0. As can be seen from Figs. 11 and 12, $\Delta N_0^{1/3}$ is almost constant within each supershell. This becomes even more evident if one plots the quantity $N_0^{1/3}$ versus the number of the magic shell, the "shell index" i, as done in Fig. 13 below: all points lie on portions of straight lines with a slope of $s = \Delta N_0^{1/3} = 0.61 \pm 0.01$. This can be easily understood from the results of Balian and Bloch (1972) cited above, which lead to the form (5.3) of the level-density oscillations. For a classical orbit (with length L) that is planar, a simple one-dimensional quantization can be used,

$$\oint p\, dq = \hbar k L = nh \quad (n \gg 1) \tag{5.10}$$

which, after division by $\hbar k$, is equivalent to demanding

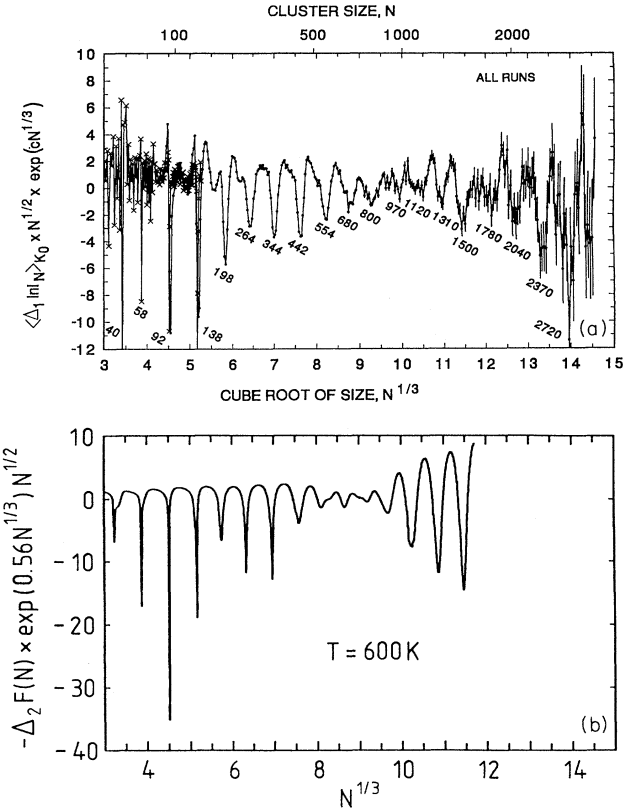

FIG. 12. Supershell beats in large sodium clusters: (a) Logarithmic derivative of the experimental mass yield of sodium clusters from an adiabatic expansion source, by Pedersen *et al.* (1991) (see this reference and the text for details); (b) second differences of total free energy obtained in self-consistent spherical jellium-Kohn-Sham-LDA calculations by Genzken and Brack (1991). See the text for an explanation of the exponential scaling factors.

that L be a multiple n of the de Broglie wavelength $\lambda = 2\pi/k$ of the electron. Inserting in Eq. (5.10) the Thomas-Fermi expression for the Fermi momentum of the valence electrons, $2\pi/k_F = (32\pi^2/9)^{1/3} r_s = 3.27 r_s$, and the average length responsible for the main-shell oscillations from Eq. (5.4), $\bar{L} = 5.42R = 5.42 r_s N^{1/3}$, one finds that the Wigner-Seitz radius r_s cancels, and one obtains immediately the increment of the magic "shell radius" $N_0^{1/3}$,

$$s = \Delta N_0^{1/3} = \frac{3.27}{5.42} = 0.603\ . \tag{5.11}$$

This value agrees well with the experimental data. Actually, the result (5.11) is valid only for an infinitely steep spherical potential well; in a realistic potential with a diffuse surface, the "corners" of the classical trajectories will be rounded off and $\Delta N_0^{1/3}$ will be somewhat larger than 0.603. This demonstrates that, indeed, the observed main shells are the result of a quantization of the valence electrons in their mean field. [Finer details of the shell oscillations depend also on the quantization of the motion perpendicular to the classical orbits, which is far less trivial; see Gutzwiller (1971), Balian and Bloch (1972), and Strutinsky *et al.* (1977).]

In Fig. 13, we have made a compilation of the "shell radius" $N_0^{1/3}$ versus shell index i for various experimental

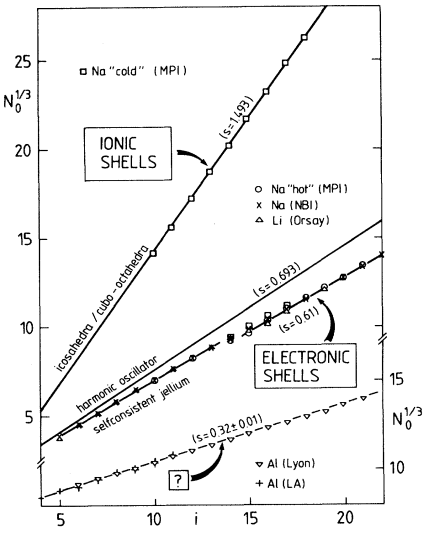

FIG. 13. "Shell radius" $N_0^{1/3}$ vs "shell index" i for spherical clusters with "magic numbers" N_0. IONIC SHELLS correspond to complete ionic icosahedral or cubo-octahedral configurations. ELECTRONIC SHELLS correspond to filled major spherical shells of the valence electrons. "?", see text for the interpretation of the Al data. The solid lines are theoretical curves with their slopes s indicated in parentheses. The various symbols correspond to the experimentally observed most abundant species: □ (Na "cold," MPI), Martin *et al.* (1990, 1991b); O (Na "hot," MPI), Martin, Bjørnholm, *et al.*, 1991); × (Na, NBI), Pedersen *et al.* (1991); △ (Li, Orsay), Bréchignac *et al.* (1992c); ∇ (Al, Lyon), Lermé *et al.* (1992); + (Al, LA), Persson *et al.* (1991).

and theoretical situations. The solid lines with slope $s=0.61$ represent both the results of Nishioka *et al.* (1990), using a Woods-Saxon potential with constant surface diffuseness, and the self-consistent jellium model results of Genzken and Brack (1991) for Na clusters. Exactly the same slope is also found for Li clusters (Genzken *et al.*, 1992), demonstrating its independence of the Wigner-Seitz radius r_s according to the above reasoning. The rupture of the lines around $i=14-15$, corresponding to $N\sim 800-900$, reflects a phase shift of the main-shell oscillations by 180° when passing from one supershell to the next, in accordance with Eq. (5.3) above. For Li, this phase change occurs just above $i=14$ and for Na just below $i=14$; this is due to the slightly increased surface diffuseness for Li clusters compared to that of the Na clusters.

The same phase shifts and slopes, within experimental uncertainties, have been measured by three independent groups. In Fig. 13 the experimental shell radii, found by Martin, Bjørnholm, *et al.* (1991) and Pedersen *et al.* (1991) for Na clusters and by Bréchignac *et al.* (1992c) for Li clusters, are shown by different symbols. (Not all symbols are indicated on those points where they all coincide.) They nicely confirm the theoretical predictions, particularly for the Li clusters.

At first glance, it appears that self-consistency is not very important for the global effect shown in Fig. 13: the slopes s found for Na clusters with the phenomenological Woods-Saxon and the self-consistent Kohn-Sham potentials are identical. [This is not very surprising, since the Woods-Saxon potential of Nishioka *et al.* (1990) was explicitly fitted to self-consistent Kohn-Sham potentials, though only for smaller clusters.] However, the details of the phase change around $i=14-15$ do depend on the potential and most sensitively on its surface steepness, which is not independent of N in the self-consistent Kohn-Sham results (Genzken and Brack, 1991). Indeed, in the latter the phase change occurs at lower cluster sizes than for the Woods-Saxon potential, namely around $N\sim 800$, which compares favorably with the experimental results of Martin, Bjørnholm, *et al.* (1991) and Bréchignac *et al.* (1992c).

It should be stressed that the counting of main shells, i.e., the attribution of the shell index i to the major minima of the oscillations, is not quite unique in the region of interference minima, since the oscillations there are less regular than in the middle of the supershells and exhibit minor subshells that are not easily distinguished from what one should call main shells. (As mentioned above, this is due to the contributions of more complicated classical trajectories.) Therefore, in establishing plots of the type shown in Fig. 13, both from experimental and theoretical results, a certain bias cannot be excluded. The least one can say is that the experimental results are compatible with the above interpretation of an interference between triangular and squared orbits with comparable amplitudes, and that a phase shift does occur in the region where the amplitude of the shell oscillations is smallest.

As we have seen above, the average slope, $s=0.61$, is very close to that found in an infinitely steep spherical potential well, Eq. (5.11); it is slightly larger (although inside the theoretical and experimental uncertainties) due to the diffuseness of the realistic potential. We show in Fig. 13 the line corresponding to a pure spherical harmonic-oscillator potential; its magic numbers vary as

$$N_0(i)=\frac{1}{3}i(i+1)(i+2)\quad (i=1,2,3,\ldots)\,, \tag{5.12}$$

giving a slope $s=0.693$. This is clearly outside the experimental error bars and also quite different from the self-consistent jellium model results.

A completely different slope of $s=1.493$ was found for a series of magic numbers $N_0>1500$ observed by Martin *et al.* (1990, 1991b); it can be attributed to the ionic structure, as will be discussed in the following subsection.

One might also want to compare the spherical "magic" shell-closure numbers N_0 found in the Kohn-Sham calculations directly with those observed in experiment. The latter are typically given with an uncertainty of $\sim 1-2\,\%$, depending somewhat on the kind of analysis done to the mass abundance data. Within these limits, there is a rather good agreement found between experiment and the jellium model predictions. There are a few systematic differences, however. One example is that the jellium model predicts a strong shell closure for $N=186$, whereas the experiments point towards $N=196$ or 198; similarly, $N=254$ is predicted and $N=264$ is seen experimentally. These shifts of the shell closures can partially be removed by the introduction of minor modifications to the jellium density distribution (see Sec. III.D.1).

In some recent experiments on Al clusters, Lermé *et al.* (1992) found a very regular shell structure in a size region of $600<Z<2700$ valence electrons; however, no supershell beating could be observed in this region. Moreover, the slope s for these shells is smaller by about a factor of 2 than that found for Na and Li clusters: $s\simeq 0.318\pm 0.004$. Earlier, Persson *et al.* (1991) had observed similar shells for Al clusters with $400<Z<1300$ electrons; they fall on a slope $s=0.315\pm 0.006$. Both sets of data are included in the lower part of Fig. 13. If these shells are to be attributed to quantized electronic orbits, these cannot be single-turn trajectories but rather ones that make two turns around the center before closing. Lermé *et al.* (1992) have proposed five-cornered starlike orbits that would lead to a calculated slope of $s=0.33$. Indeed, these authors point out that, for a sufficiently diffuse surface of the potential, the triangular and squared orbits cannot close any more—as was also observed by Nishioka *et al.* (1990). However, the surface diffuseness needed to obtain the desired star orbits is much larger than that of the fitted Woods-Saxon potential for Na clusters. Moreover, the potential of Lermé *et al.* (1992), when used in a fully quantum-mechanical calculation, does not give a shell structure that corresponds either to the star orbits or to experiment (Genzk-

en *et al.*, 1992). The jellium model does predict an increase in the surface diffuseness with decreasing r_s, but the effect is much smaller (see also Lang and Kohn, 1970). On the other hand, Persson *et al.* (1991) found a reasonable agreement of their observed magic numbers $400 < Z < 1300$ with jellium model predictions. The situation is therefore not quite clear. More investigations on Al clusters, for which the jellium model is definitely less justified than for the alkalis, will be necessary to understand these very interesting results. Very recently, Martin *et al.* (1992) have also observed a similar structure in the mass spectrum of cold Al clusters with $250 < N < 10\,000$ and interpreted them in terms of ionic shells. We shall discuss this in the next section.

3. From electronic to ionic shells

It is easy to show that magic numbers for $\Delta_1 F$ in very large cold clusters must be determined by crystal structure rather than electronic shells. When an atom is added to a crystalline cluster, it may complete a layer or start a new layer, and this gives a contribution to $\Delta_1 F$ independent of the size of the cluster. On the other hand, according to Strutinsky theory the fluctuation in the electronic energy contribution obeys the proportionality

$$\delta\Delta_1 F \sim \delta\epsilon_F \sim \epsilon_F \frac{\delta g}{g_0} \ . \tag{5.13}$$

From Eq. (5.2) and the relation $g_0 \sim R^3$ it follows that this contribution decreases as $R^{-1/2}$ or $N^{-1/6}$ and is thus small for very large clusters.

Indeed, some of the data on magic numbers in very large clusters favor an interpretation as crystal faceting effects. Martin *et al.* (1990, 1991b) found an interesting transition of the shell spacings above $N \simeq 1500$, using photoionization time-of-flight mass spectroscopy for relatively cold Na clusters. Up to this size, they observed magic numbers falling exactly on the lower part of the line with slope $s = 0.61$ in Fig. 13, extrapolated up to $i = 17$ corresponding to $N_0 = 1430 \pm 20$. (These results are indicated by square boxes in the figure, but shown only for $i \geq 14$ in order not to overload the lower part of that line.) These magic numbers up to $i = 13$ were later confirmed in experiments in which the clusters were laser warmed before ionization (Martin, Bjørnholm, *et al.*, 1991). However, in the region $1980 \lesssim N \lesssim 21\,300$, a totally different spacing between the magic-shell radii was found, corresponding to a slope $s = 1.49$, as shown in the upper left of Fig. 13. These shells were identified by Martin *et al.* (1990, 1991b) as atomic shells corresponding to icosahedral or cubo-octahedral close-packed ionic configurations, as they are well known for van der Waals clusters. Indeed, both these configurations lead to the magic numbers

$$N_0(i) = \frac{1}{3}(10i^3 - 15i^2 + 11i - 3) \quad (i = 1,2,3,\ldots) \ , \tag{5.14}$$

giving the slope $s = 1.493$. This atomic shell structure has also been observed by the same authors for K and Ca clusters with $1980 \lesssim N \lesssim 8170$ and in Mg clusters with $146 < N < 2870$ (Martin *et al.*, 1991a, 1991b; Martin, Näher *et al.*, 1991).

The interpretation is that, at lower temperatures, there might be a transition around $N \sim 1500$–1800 from liquid to crystalline clusters. This is consistent with the results on "warm" clusters (Martin, Bjørnholm *et al.*, 1991), where the average initial temperature of the cluster beam is estimated to be ~ 500 K.

It constitutes a considerable challenge to verify the above interpretation of a phase transition by theoretical calculations. Of course, the ionic shell structures cannot be described by the jellium model. On the other hand, the large clusters discussed here are far beyond the reach of purely microscopic treatments such as quantum-chemical or molecular-dynamics theories. There is therefore a definite need to develop simplified models that are able to describe the interplay between ionic geometry and electronic shell effects in large clusters. Some interesting steps in this direction have been taken recently by Maiti and Falicov (1991, 1992) using perturbative pseudopotential calculations. The spherically averaged pseudopotential (SAPS) model (see the end of Sec. II.C) might also be a promising tool for such studies.

The regular shell structure in large Al clusters discussed above in connection with Fig. 13 has recently been observed by Martin *et al.* (1992). They interpreted it in terms of subshells of close-packed octahedral ionic shapes, correlating the maxima in the mass spectra with the filling numbers corresponding to the addition of successive triangular facets.

B. Semiclassical theory and large-N expansions: links to the macroscopic world

The present section is devoted to a discussion of density-variational calculations in the strict sense, i.e., where the density $\rho(\mathbf{r})$ of the valence electrons is the direct variational quantity in contrast to the single-particle wave functions $\varphi_i(\mathbf{r})$ varied in the Kohn-Sham or Hartree-Fock methods. This becomes possible through the use of explicit semiclassical approximations to the kinetic-energy functional $T_s[\rho]$ in terms of $\rho(\mathbf{r})$ and its gradients, instead of Eq. (3.5), which involves the $\varphi_i(\mathbf{r})$. The attribute "semiclassical" is used to indicate that expansions in powers of $\hbar$ are involved in deriving the explicit functionals used for $T_s[\rho(\mathbf{r})]$. The two most common functionals, that of the Thomas-Fermi (TF) theory and its extensions, are presented in Appendix A.2.a.

With such an explicit functional $T_s[\rho(\mathbf{r})]$ for the kinetic energy, the variation principle for the total energy can be applied, according to the Hohenberg-Kohn theorem (cf. Appendix A.2.a), by a direct variation of the density $\rho(\mathbf{r})$:

$$\frac{\delta}{\delta\rho(\mathbf{r})}\left[E_{\rm tot}[\rho(\mathbf{r})]-\mu\int\rho(\mathbf{r})d^3r\right]=0\ , \qquad (5.15)$$

where the Lagrange multiplier μ fixes the number of electrons and physically is understood as the chemical potential. This leads to a Euler-Lagrange-type differential equation for the density which is nonlinear and whose order depends on the number of gradient terms included.

The main advantage of this method is that one only has to vary one density function $\rho(\mathbf{r})$ (or, if spin degrees of freedom play a role, two spin densities) instead of many single-particle wave functions. This often gives more physical insight than microscopic methods, since the observables can be connected directly to the density $\rho(\mathbf{r})$ and other local functions and many mechanisms may become more transparent.

The price one pays is that the functional $T_s[\rho]$ forbids the inclusion of shell effects. One can thus obtain only average properties (total energy, density and its moments, ionization potential, electron affinity, polarizability, plasmon energies, etc.) but in a parameter-free and self-consistent way even for very large systems.

Due to the missing shell effects, the semiclassical results cannot usually be directly compared with experiment. However, it is possible to treat shell effects perturbatively at relatively low cost, using the ideas developed by Strutinsky (1968) in nuclear physics and sketched in Sec. V.A.1 above. In fact, the semiclassical variational results for the average energy $\tilde{E}$ and for the average potentials, from which the shell-corrections δE can be extracted, represent the ideal input into a Strutinsky calculation in which the total energy is written in the form of Eq. (5.1). Alternatively, the shell effects may be added at the end of a semiclassical density-variational calculation simply by solving once the Kohn-Sham equations using the variational average potential $\tilde{V}$. With the latter method one obtains not only the total energy, but also a good approximation to the self-consistent Kohn-Sham orbitals from which other observables can be calculated. Both methods have proven useful in nuclear physics as economical substitutes for fully microscopic Hartree-Fock calculations (see, for example, Brack *et al.*, 1985). They have not been used in cluster physics so far, but might prove useful for systematic calculations of very large clusters in which the fully self-consistent microscopic Kohn-Sham method becomes too time consuming.

Finally, the semiclassical density-variational method gives access to a self-consistent determination of the coefficients in liquid-drop-type asymptotic expansions of the average energy and other variables in powers of $N^{-1/3}$. This provides links between the finite system and properties of the semi-infinite system (i.e., an infinite plane surface), such as the surface energy and the bulk work function.[17] We refer the reader to Perdew (1988, 1989), who demonstrated how the expressions for ionization energies and electron affinities obtained by such methods (cf. Sec. V.B.3 below) could be used to interpolate from the bulk all the way to single atoms.

1. Semiclassical density-variational calculations

The solution of the variational equation (5.15) for the density $\rho(\mathbf{r})$ can, in principle, be obtained directly in coordinate space. This may, however, be numerically very difficult due to the high degree of nonlinearity, in particular if higher gradient corrections are included in the energy functional. Reasonable approximations are often obtained in a restricted basis of trial density functions by minimizing the total energy with respect to some variational parameters.

In the remainder of this section, we shall briefly mention density-variational calculations of metal cluster properties using the Thomas-Fermi (TF) functional $T_{\rm TF}[\rho]$ and its extensions (TFW, TFWD, ETF, etc.; see Appendix A.2.a). Some of their results have already been quoted in the earlier chapters of this review; some of the papers are mentioned merely for historical reasons. Results of large-N expansions and liquid-drop parameters will be discussed in the following two sections. In all these calculations, exchange and correlation energies were included in the local-density approximation. Only spherical clusters have been treated so far.

The first jellium model calculations for metal clusters altogether, of which we are aware, were done in 1975 by Cini. He used the Thomas-Fermi-Weizsäcker kinetic-energy density and a variational space of spherical double-exponential trial densities. He discussed ionization potentials (IP) and electron affinities (EA) and their N dependence. Snider and Sorbello (1983a) used a very similar model, varying the Weizsäcker coefficient (discussed in Appendix A.2.a), obtained IPs and EAs, and found the slope parameter α in the IP to be different from 3/8 (see Sec. V.B.3 below for discussion). They then applied the same model to the calculation of static dipole polarizabilities by applying an external electrical field (Snider and Sorbello, 1983b; Sorbello, 1983) and discussed a dipole force sum rule (see Sec. IV). Snider and Sorbello (1984) extended their earlier model to the spin-density formalism in order to study odd-even effects in the IPs of microclusters.

Iñiguez *et al.* (1986) did variational Thomas-Fermi-Weizsäcker-Dirac (TFWD) calculations both for the jellium model and using pseudopotentials and obtained IPs, EAs, and cohesive energies of small sodium clusters.

Kresin (1988–1991) used the Thomas-Fermi theory for small metal clusters and developed an approximate analytical solution of the Thomas-Fermi equation. He discussed diamagnetism and later applied his model to surface plasmons and static dipole polarizabilities of spherical clusters (cf. Sec. IV).

Brack (1989) used the full extended Thomas-Fermi (4) kinetic-energy functional, Eq. (A21), with three-

[17]The inclusion of ionic structure effects can here be rather crucial; see Sec. V.B.2 below.

parameter variational densities and found a rather accurate reproduction of the average Kohn-Sham densities and potentials by Ekardt (1984b), particularly in the surface region. He studied dipole polarizabilities and multipole vibrations via sum rules and the "local RPA" approach discussed in Sec. IV.C.2 and Appendix B.2.c. Spina *et al.* (1990) showed that these variational densities reproduce very accurately the bulk work functions and surface energies found by Tarazona and Chacón (1989), who solved the full extended Thomas-Fermi (4) Euler equation (see Appendix A.2.a) in the semi-infinite geometry.

Spina and Brack (1990) used the same parametrized trial densities in a semiclassical jellium model that includes schematic ionic structure through spherically averaged pseudopotentials, with results similar to the microscopic spherically averaged pseudopotential model by Iñigues *et al.* (1989, 1990; see Sec. II.C).

Serra *et al.* (1989a, 1989b, 1990) and Balbás and Rubio (1990) also studied the multipole response of spherical clusters in density variational calculations with an approximate TFWD functional (see Sec. IV).

Engel and Perdew (1991) were the first to solve the full extended Thomas-Fermi (4) Euler equation for spherical clusters directly in r space. They discussed the asymptotic behavior of ionization potentials and electron affinities (see Sec. V.B.3 below).

2. Liquid-drop model expansion of the energy

Density-variational calculations give a natural starting point for the self-consistent determination of liquid-drop parameters by means of a "leptodermous" expansion of the total binding energy of a saturated fermion system. This idea lies behind the famous mass formula for nuclear binding energies developed by von Weizsäcker (1935) and Bethe (1937); it was successfully further developed from the basis of Thomas-Fermi theory by Strutinsky and Tyapin (1964) and by Myers and Swiatecki (1969). We shall only sketch here the principal ideas and refer the reader to the literature for details. As an application, we discuss the asymptotic behavior of ionization potentials and electron affinities of metal clusters in Sec. V.B.3 below.

Assume that the density is going to a constant value ρ_0 in the interior of the system and that there exists a well-defined surface region where $\rho(\mathbf{r})$ drops from ρ_0 to zero. Introduce α as a measure for the surface thickness and a reference radius R (e.g., the average location of the surface, measured from the center). When $\alpha \ll R$, the system is "thin-skinned" or "leptodermous." The basic idea then is to perform a so-called leptodermous expansion in powers of the small variable $x=\alpha/R$ around the leading volume term, which is given in terms of a steplike density profile. This expansion is asymptotic in nature and *a priori* valid only for large enough systems.

That the electronic densities of large metal clusters fulfill the assumption of leptodermicity very well is illustrated in Fig. 14. It shows the density profile of Na_{2654} obtained in self-consistent jellium model Kohn-Sham calculations by Genzken and Brack (1991), overlayed with the profile of an infinite plane surface taken from Lang and Kohn (1970). The oscillations near the surface of the spherical cluster reproduce rather accurately the Friedel oscillations of the semi-infinite profile that will be reached asymptotically for $N\to\infty$. The oscillations near the interior of the finite cluster are due to the filled spherical shells near the Fermi energy.[18]

For a neutral spherical system with N particles and a reference radius $R=r_0N^{1/3}$, the above technique leads to the liquid-drop model expansion of the total binding energy:

$$E(N)=a_vN+a_sN^{2/3}+a_cN^{1/3}+a_0+\cdots . \tag{5.16}$$

Here a_v is the volume or bulk energy, which is defined as the energy per particle of the infinite system with constant density ρ_0:

$$a_v=e_b=\mathcal{E}[\rho_0]/\rho_0 . \tag{5.17}$$

The surface energy a_s in Eq. (5.16) is given by

$$a_s=4\pi r_0^2\sigma \tag{5.18}$$

in terms of the surface tension σ, i.e., the energy per unit area of an infinite plane surface. Not only a_s but also the curvature energy a_c, and the higher-order coefficients in Eq. (5.16) can be obtained uniquely in terms of the density profile perpendicular to the surface of the semi-infinite system (see Myers and Swiatecki, 1969; Brack *et al.*, 1985).[19]

Although extended Thomas-Fermi variational densities serve as a natural starting point, the leptodermous expansion is not restricted to semiclassical theory and can also be applied to microscopic densities obtained within the LDA-Kohn-Sham approach. The Friedel oscillations in the semi-infinite density profile (Lang and Kohn, 1970, see Fig. 14) do not disturb the principle of the leptodermous expansion discussed here. Numerically, however, they lead to convergence problems in the evaluation of the curvature energy a_c (Stocker and Farine, 1985). Their relative contribution to the surface energy a_s of metals is found to be only a few percent (Seidl, Spina, and Brack, 1991; Engel and Perdew, 1991; Fiolhais and Perdew, 1992).

---

[18]Only oscillations due to shells with low angular momenta l can be distinguished near the center. See also Thorpe and Thouless (1970), who have discussed both types of density oscillations in the nuclear physics context.

[19]Note that the direct determination of the coefficients a_s, a_c, etc. by a least-squares fit of Eq. (5.16) to microscopically calculated energies is hampered by shell effects (see, for example, Utreras-Diaz and Shore, 1989). This may be done with semiclassically obtained average energies, if sufficiently large particle numbers are used (up to $N\gtrsim 10^5$; see Seidl, Spina, and Brack, 1991, and Fiolhais and Perdew, 1992).

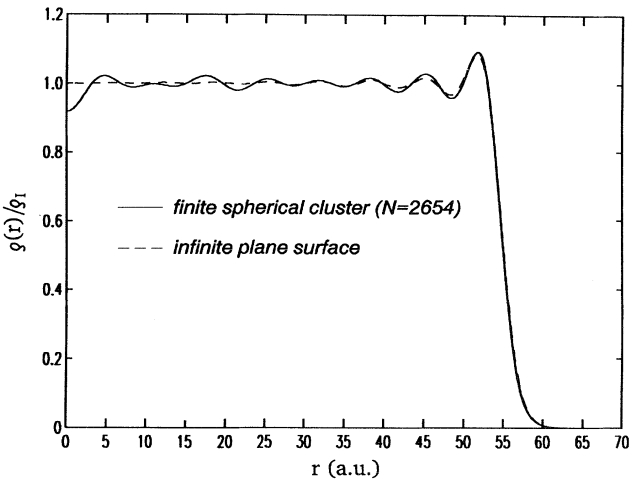

FIG. 14. Asymptotic behavior of electronic density: solid line, electron density of a spherical sodium cluster with $N=2654$ atoms, from spherical jellium-Kohn-Sham-LDA calculations by Genzken and Brack (1991). Dashed line, electron density profile perpendicular to an infinite plane surface of sodium metal, obtained in jellium-Kohn-Sham-LDA calculations by Lang and Kohn (1970). The two curves are adjusted so that the jellium edge is at the same location along the r axis.

For metal clusters, the leptodermous expansion of the total energy has been studied by Seidl, Spina, and Brack, (1991) with extended Thomas-Fermi (4) results using the jellium model, and by Fiolhais and Perdew (1992), who used both semiclassical and Kohn-Sham calculations for the jellium and the stabilized jellium model (see Sec. III.D.2). Pseudopotential corrections to the surface energy have also been studied in extended Thomas-Fermi (4) calculations by Spina *et al.* (1990).

The agreement of the calculated liquid-drop model parameters with experimental quantities depends on the quality of the model used. The simple jellium model cannot yield the correct cohesive energy of the bulk metal; the volume energy e_b here is just the energy per electron of a structureless infinite gas with the r_s value of the bulk metal. Surface energies a_s obtained in the jellium model for metals with $r_s > 4$ a.u. (i.e., K, Rb, and Cs) agree within 10–20 % with experimental values, as shown by Lang and Kohn (1970) in Kohn-Sham calculations with semi-infinite geometry. For metals with smaller r_s the agreement becomes worse; for $r_s < 2.3$ a.u. (e.g., for aluminum), one even obtains unphysical negative values of a_s. This is greatly improved when the ionic structure is accounted for. Lang and Kohn (1970, 1971) showed that a perturbative inclusion of pseudopotentials allows one to reproduce the experimental surface energies within 10–30 % for most metals. (See Monnier *et al.*, 1978, for a nonperturbative inclusion of pseudopotentials.) The stabilized jellium model, which yields the correct cohesive and bulk energies (cf. Sec. III.D.2), reproduces these results more or less (Fiolhais and Perdew, 1992), although the ionic correction to a_s has the wrong sign for $r_s > 4$ a.u. (i.e., where the simple jellium model works best). Curvature energies a_c have been extracted recently from experimental vacancy formation energies by Perdew *et al.* (1991) and agree with the values calculated by Fiolhais and Perdew (1992) within a factor of less than two for $r_s \leq 5$ a.u. and three for $r_s < 5$ a.u.; no difference was found here between jellium and stabilized jellium.

3. Asymptotic behavior of ionization potentials and electron affinities

Since much experimental information is available on ionization potentials IP and electron affinities EA of metal clusters, and their large-N behavior has received considerable attention in the literature, we shall discuss here their asymptotic expressions derived by the techniques discussed above. They are defined by

$$\mathrm{IP}=E(N,-1)-E(N,0)\ , \quad \mathrm{EA}=E(N,0)-E(N,+1) \tag{5.19}$$

in terms of the total energy $E(N,q)$ of a cluster with N atoms and q excess electrons. When the above leptodermous expansion was generalized for a charged system the following expansion of $E(N,q)$ was derived by Seidl, Meiwes-Broer, and Brack (1991) and Seidl, Spina, and Brack (1991) within the spherical jellium model, to the leading orders in $q \ll N$:

$$E(N,q)=-q\Delta\varphi^{\mathrm{out}}+\frac{(qe)^2}{2R_I} +(N+q)e_b+a_sN^{2/3}+\cdots\ . \tag{5.20}$$

Here $\Delta\varphi^{\mathrm{out}}$ is the outer part of the Coulomb barrier of an infinite plane metal surface, i.e., the work required to bring a test charge from the jellium edge to infinity:

$$\Delta\varphi^{\mathrm{out}}=\varphi(\infty)-\varphi(0) =4\pi e^2\int_0^\infty z[\rho(z)-\rho_0\Theta(-z)]dz\ . \tag{5.21}$$

The second term in Eq. (5.20) is just the classical electrostatic energy of a surface-charged metal sphere with radius R_I.

With $q=\pm 1$ one finds from Eq. (5.20) the following asymptotic expressions for IP and EA which are valid for large N:

$$\mathrm{IP}(N)=W_b+\alpha\frac{e^2}{R_I}+O(R_I^{-2})\ , \tag{5.22}$$

$$\mathrm{EA}(N)=W_b-\beta\frac{e^2}{R_I}+O(R_I^{-2})\ , \tag{5.23}$$

where W_b is the bulk work function given by

$$W_b=\Delta\varphi^{\mathrm{out}}-e_b\ . \tag{5.24}$$

The "slope parameters" α and β in Eqs. (5.22) and (5.23), which dominate the size dependence in large clusters, re-

ceive their leading contribution $\frac{1}{2}$ from the classical charging energy, i.e., the second term in Eq. (5.20). Quantum-mechanical corrections due to the diffuseness of ρ and to explicit kinetic, exchange, and correlation energy contributions, which are all contained in the higher-order terms (indicated by dots) in the expansion (5.20), lead to deviations of α and β from their common classical value $\frac{1}{2}$.

Perdew (1989) and Engel and Perdew (1991) derived Eqs. (5.22) and (5.23) starting from the variational equation (5.15) and expanding the chemical potential μ as a function of the cluster radius R_I, leading to the same $1/R_I$ corrections for IP and EA (see also Balbás and Rubio, 1990).[20] The numerical values obtained for α and β by Seidl, Meiwes-Broer, and Brack (1991) and Seidl, Spina, and Brack (1991) in variational extended Thomas-Fermi calculations with parametrized trial densities were well confirmed by Engel and Perdew (1991) with fully variational solutions of the extended Thomas-Fermi (4) Euler-Lagrange equation.

The calculated values of α and β for various simple metals are close to, but not exactly equal to, $\frac{3}{8}$ and $\frac{5}{8}$, respectively; they depend slightly, but systematically, on the Wigner-Seitz radius r_s. In the analysis of experimental results on IP and EA, similar values have been found, although their correct values often cannot be extracted from small clusters (see Secs. VI and VII of de Heer, 1993, and the discussion further below). Their approximate agreement with the values $\alpha=\frac{3}{8}$ and $\beta=\frac{5}{8}$, obtained from a classical image-charge argument (Smith, 1965; Wood, 1981), has unfortunately led to a great deal of confusion in the literature (see, for example, Haberland, 1992). As pointed out by Makov *et al.* (1988), Perdew (1989), and de Heer and Milani (1990), this argument is not physically justified: the classical image potential cannot be applied to a point charge at distances of atomic dimensions from a metal surface. Therefore the approximate equality of the correct slope parameters with the values $\frac{3}{8}$ and $\frac{5}{8}$, respectively, must be taken to be accidental. As clearly shown within density-functional theory, the correct classical limit for a charge continuously distributed over a sphere leads to their common value $\frac{1}{2}$ (Perdew, 1989; Seidl, Meiwes-Broer, and Brack, 1991). The deviations from this value can be accounted for by quantum-mechanical corrections, as mentioned above (see also Makov and Nitzan, 1991). Actually, this should not be so surprising, since the leading term of IP and EA, namely the bulk work function W_b, is also a purely quantum-mechanical entity. There is no reason why the next-order corrections to IP and EA should be explicable by purely classical arguments.

Another confusion in the literature concerns the application of the expansions (5.22) and (5.23) to measured values of IP and EA of small clusters. Many experimentalists parametrized their data by truncating these asymptotic expressions after the terms linear in $N^{-1/3}$, fitting their results by straight lines in a plot versus $1/R_I$ going through the measured bulk work function W_b at $1/R_I=0$. This is dangerous, and the resulting slope parameters cannot be trusted for the following reasons: (i) many experimental data for small clusters fall into a region where the higher-order terms in $1/R_I$ cannot be neglected, so that the curves are no longer straight lines, particularly for EA; (ii) the shell oscillations are rather strong and make the fits ambiguous; and (iii) there is sometimes a rather large uncertainty in the measured values of W_b, which affects the values of the slope parameters. Furthermore, a spillout correction has often been included in the definition of the radius by setting $R_I=r_sN^{1/3}+a$ in the denominators of the $1/R_I$ terms of Eqs. (5.22) and (5.23), using a more or less *ad hoc* chosen value for a. This effectively includes higher-order terms in $N^{-1/3}$, albeit with a biased coefficient; it may improve the local fits in a limited size range, but it also affects the apparent values of the slope parameters.

The work of Engel and Perdew (1991) and Seidl, Spina, and Brack (1991) shows that very large particle numbers $N\gtrsim 10^5$ are needed in order to determine the asymptotic slopes α and β uniquely. This can only be done, of course, in semiclassical calculations. This also shows that their determination from experimental data is not easy, particularly in view of the shell effects.

Seidl, Meiwes-Broer, and Brack (1991) have shown that the variational semiclassical results for IP and EA fit the size dependence of the experimental data of simple metal clusters surprisingly well on the average, although the bulk limit W_b is off by some 5–10 %, which is a well-known defect of the jellium model without pseudopotential corrections (Lang and Kohn, 1971). It is also clear from their results that the quadratic and higher-order terms in $N^{-1/3}$ of the asymptotic expansions (5.22) and (5.23) cannot be neglected when fitting data of clusters with $N<100$, in particular for the electron affinities.

In view of these results and in order to avoid the ambiguities outlined above, we strongly advocate the use of the particular forms (5.22) and (5.23) in fitting the N dependence of IP and EA data (cf. also the analysis of the experimental data in Secs. VI and VII of de Heer, 1993).

Equation (5.24) for the bulk work function is not very frequently used in the literature; it was derived by Mahan and Schaich (1974) employing a theorem by Budd and Vannimenus (1973) (see also Monnier *et al.* 1978). For densities $\rho(z)$ which solve the variational Euler equation for the semi-infinite problem exactly, W_b (5.24) is identical to the more widely used expression introduced by Lang and Kohn (1970):

$$W_b'=\Delta\varphi-\mu_b \ . \tag{5.25}$$

Here $\Delta\varphi$ is the full Coulomb barrier of the plane metal surface

$$\Delta\varphi=\varphi(\infty)-\varphi(-\infty) \ , \tag{5.26}$$

[20] In this derivation, the bulk work function W_b is given by the equivalent expression (5.25) discussed below.

which can be given in terms of simple integrals over the density profile $\rho(z)$, and μ_b is the bulk chemical potential defined by

$$\mu_b = \frac{d}{d\rho_0}\mathcal{E}[\rho_0] \ . \tag{5.27}$$

For approximate density profiles (e.g., parametrized trial densities used in restricted variational calculations), it turns out that the expression W_b (5.24) is much less sensitive to numerical errors or approximations than the standard expression W_b' (5.25); this has been investigated in detail by Monnier *et al.* (1978) and by Perdew and Sahni (1979).

In Fig. 15, taken from Spina *et al.* (1990), we illustrate the asymptotic behavior of IP and EA. The crosses connected by the solid lines represent the variational semiclassical results obtained in the extended Thomas-Fermi (4) approximation for spherical Na clusters with $8 < N < 125\,000$. The nonlinearity of EA in $N^{-1/3}$ is clearly visible. Note also the correct limiting value of the theoretical bulk work function W_b, which is different here from W_b' due to the use of a restricted set of trial density functions.

A surprising result is the curve labeled W^* in Fig. 15. The quantity W^* is calculated with the same expressions (5.21) and (5.24) which defined W_b, but using the finite-cluster density profile $\rho(r)$ of the actual cluster with electron number N, extrapolated to $r = -\infty$. The curve W^* is practically constant with the value W_b. This means that we can obtain the correct theoretical bulk work function, to within a few percent, from a simple semiclassical variational calculation (which, by the way, can be done on a simple personal computer) for a microcluster with as few as eight atoms.

In Fig. 16, taken from Seidl, Meiwes-Broer, and Brack (1991), we show the difference between the ionization potential and the electron affinity of Al clusters as a function of the inverse cluster radius. The dots are experimental results and the solid line is the result of a semiclassical density-variational calculation with the full extended Thomas-Fermi (4) kinetic-energy functional in the spherical jellium model. Note that in the difference IP-EA, the bulk work function (which is not correctly rendered in the jellium model) cancels. This difference thus focuses on the finite-size effects. The good agreement is another example of the fact that the jellium model can correctly reproduce average trends of finite-size effects—in the present case even down to the dimer.

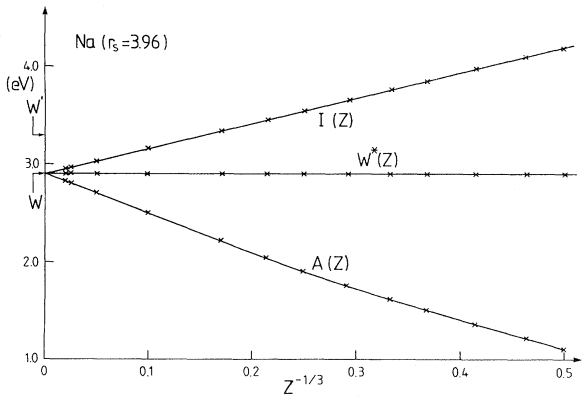

FIG. 15. Ionization potentials $I(Z)$ and electron affinities $A(Z)$ of sodium clusters with Z atoms, obtained in semiclassical ETF(4) density-variational calculations by Spina *et al.* (1990), vs $Z^{-1/3}$. The quantity $W^*(Z)$ and the two theoretical values W and W' for the bulk work function are defined and explained in the text. From Spina *et al.* (1990).

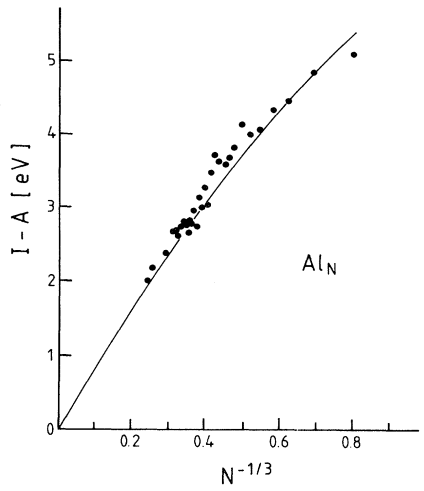

FIG. 16. Difference between ionization potential (I) and electron affinity (A) of Al clusters vs $N^{-1/3}$; ●, experimental results; solid line, results of variational extended Thomas-Fermi(4) calculations in the spherical jellium model. (From Seidl, Meiwes-Broer, and Brack, 1991; see this reference for the experimental data.)

VI. SUMMARY AND CONCLUSIONS

In this review article we have given a survey of theoretical approaches for the description of simple metal clusters. We have focused on mean-field theory appropriate to finite fermion systems using the Hartree-Fock (HF) and the density-functional methods, the latter mainly in the local-density approximation (LDA). We have extensively discussed the electric response properties and their description in the time-dependent LDA and the random-phase approximation (RPA).

In many respects, the metal clusters appear as droplets of a quantum Fermi liquid in which the valence electrons are the dominant degrees of freedom and the ionic structure seems to have little influence. This is particularly so for the observed magic numbers in alkali clusters with up to $N = 3000$ atoms, in which the picture of valence electrons confined in a smooth—self-consistent or suitably parametrized—potential also can account for the supershell structure.

In theoretical investigations of electronic shell structure, the jellium model is playing an important role due

to its computational simplicity, which permits us to connect small and very large cluster sizes in a unified picture. It is very hard, if not impossible, to assess its limitations in a quantitative manner from within the model itself. For microclusters with up to $N \sim 20$ atoms, where *ab initio* quantum-chemistry or molecular-dynamics calculations are technically feasible, it has become evident that details of the experimental ionization potentials, electron affinities, polarizabilities, and fine structure of the photoabsorption cross section do depend on the ionic geometry and that such calculations give a better quantitative description than the jellium model. But still, the average trends of these observables can often be described surprisingly well by the jellium model even for small clusters. If deformations of the positive charge distribution are included, the jellium model can also account for the averaged ionic geometry, leading, for example, to a shape isomerism similar to that found in the structural models.

For the static electric dipole polarizabilities and the positions of the collective electronic dipole resonances, the jellium model with LDA misses some 10–20 % of the average experimental results. Two competing explanations for this failure have been given. One of them invokes the missing ionic contributions, the other points to the failure of the LDA in yielding the correct $1/r$ falloff of the total potential, which can be partially overcome by self-interaction corrections or extensions of the LDA (the so-called weighted density approximation, WDA). The LDA, which has been used with considerable success in many branches of physics, faces a rather crucial test in calculations for metal clusters—as well as for plane metal surfaces—due to the steep surface of the electronic density. We have discussed some recent calculations, performed within the jellium model, using a HF basis plus perturbation expansion and explicit evaluations of RPA correlations. The results for ionization potentials and polarizabilities are very close to Kohn-Sham-LDA results and thus seem to confirm the validity of the local-density approximation even in small alkali clusters. We therefore tend to believe that the missing electronic response is due to the missing ionic structure. Indeed, explicit structural pseudopotential calculations for clusters up to $N \sim 10$ tend to give significantly improved results, even within the LDA. When the ionic structure effects are partially simulated in the jellium model by introducing a diffuse surface of the positive charge distribution, the discrepancy is also removed. In any case further theoretical investigations, both extending the LDA and including ionic structure, will be necessary to settle this question.

The interplay of electronic and ionic binding effects contributes in an essential way to the richness of the structural forms of matter, in both the inorganic and the organic worlds. It dominates the smallest micromolecules, where a distinction between metals and nonmetals is hardly possible. But it is also important in very large metal clusters with up to $N = 20\,000$ and more atoms, in which ionic shells corresponding to a dense packing of the atoms can be observed if the clusters are sufficiently cold. These ionic structures have, however, a different symmetry from that of the ionic lattice in the bulk metal. Therefore the old question: " How many atoms are needed to make a piece of bulk material?" is still not answered. Apparently 20 000 alkali atoms are not enough.

The relative importance of electronic and ionic shell effects in these large metal clusters depends crucially on their temperature. This subject deserves more experimental and theoretical attention in future research. A description by first-principles *ab initio* methods is impossible for such sizes. Approximate models, such as the tight-binding or the Hueckel model, perturbative or spherically averaged pseudopotential calculations, or the effective-medium theory, must be applied and further developed.

We have given some emphasis to semiclassical variational methods and a local-current approximation to the RPA built on sum-rule relations, which allow one to evaluate average static and dynamic response properties for very large systems in which fully microscopic calculations are no longer possible. We think that these methods might be helpful in future investigations, particularly in the mesoscopic domain. The large-N expansion of the semiclassical results also yields direct contact to volume and surface properties of the bulk metal. In this connection, we have found that the jellium model is a useful mediator between the microcosm and the macrocosm.

ACKNOWLEDGMENTS

This review would not have been initiated without the stimulation of Walt de Heer, and it would never have been completed without the continuous support and encouragement of Sven Bjørnholm. I am deeply indebted to them, as well, for their careful reading of the manuscript and many valuable suggestions for improvements. I am grateful to P. Ballone, G. F. Bertsch, O. Genzken, C. Guet, H. Nishioka, and P.-G. Reinhard for clarifying discussions and for their reading parts of the manuscript, and to V. Bonačić-Koutecký, J. Borggreen, W. Ekardt, K. Hansen, M. S. Hansen, B. Mottelson, J. Pacheco, and J. Pedersen for further stimulating discussions. Thanks are due to O. Genzken, M. S. Hansen, G. Lauritsch, H. Nishioka, and T. Hirschmann for the communication of unpublished results, which have been used in some figures. Last but not least, I want to express my gratitude to my family for their patience and their indulgence.

This work was partially supported by the Danish Natural Science Foundation, the Deutsche Forschungsgemeinschaft, and the Commission of the European Communities. The hospitality extended to me during several visits to the Niels Bohr Institute, Copenhagen, is gratefully acknowledged.

APPENDIX A: MEAN-FIELD THEORIES

We start from the Hamiltonian of a system of N electrons moving in an external potential $V_{\rm ext}(\mathbf{r})$ and interacting through the Coulomb two-body potential:

$$\hat{H}=\sum_{i=1}^{N}\left\{\frac{\mathbf{p}_i^2}{2m}+V_{\rm ext}(\mathbf{r}_i)+\frac{1}{2}\sum_{j(\neq i)=1}^{N}\frac{e^2}{|\mathbf{r}_i-\mathbf{r}_j|}\right\}. \tag{A1}$$

The exact wave function $\Psi(\mathbf{r}_1,\mathbf{r}_2,\ldots,\mathbf{r}_N)$ belonging to this Hamiltonian generally cannot be calculated. From it we define the one-body density matrix[21] $\rho_1(\mathbf{r}',\mathbf{r})$:

$$\rho_1(\mathbf{r}',\mathbf{r})=\int d^3r_2\int d^3r_3\cdots\int d^3r_N\Psi^*(\mathbf{r}',\mathbf{r}_2,\ldots,\mathbf{r}_N)\Psi(\mathbf{r},\mathbf{r}_2,\ldots,\mathbf{r}_N)\,. \tag{A2}$$

Its diagonal part is the density $\rho(\mathbf{r})$ which will be normalized to the number N of electrons:

$$\rho(\mathbf{r})=\rho_1(\mathbf{r},\mathbf{r})\,,\quad \int\rho(\mathbf{r})d^3r=N\,. \tag{A3}$$

In both Hartree-Fock (HF) theory and density-functional theory, to be sketched in the next two subsections, the density $\rho(\mathbf{r})$ is written in terms of single-particle wave functions $\varphi_i(\mathbf{r})$:

$$\rho(\mathbf{r})=\sum_{i=1}^{N}|\varphi_i(\mathbf{r})|^2\,. \tag{A4}$$

1. Hartree-Fock theory

In HF theory the ground-state wave function of an N-body system is approximated by a Slater determinant Φ built from a complete orthogonal set $\{\varphi_\alpha(\mathbf{r})\}$ of single-particle wave functions:

$$\Phi(\mathbf{r}_1,\mathbf{r}_2,\ldots,\mathbf{r}_N)=\det|\varphi_i(\mathbf{r}_j)|_{i,j=1,2,\ldots,N}\,. \tag{A5}$$

The density matrix (A2) then takes the form

$$\rho_1^{\rm HF}(\mathbf{r}',\mathbf{r})=\sum_{i=1}^{N}\varphi_i^*(\mathbf{r}')\varphi_i(\mathbf{r})\,, \tag{A6}$$

from which Eq. (A4) follows. The choice of the single-particle wave functions φ_i is made by a variational principle: One makes the expectation value of the total Hamiltonian (A1) between the Slater determinants (A5) stationary with respect to the wave functions φ_i, subject to the condition of their orthogonalization by means of Lagrange multipliers ε_i:

$$\frac{\delta}{\delta\varphi_i^*(\mathbf{r})}\left[\langle\Phi|\hat{H}|\Phi\rangle-\varepsilon_i\int|\varphi_i(\mathbf{r})|^2d^3r\right]=0\,. \tag{A7}$$

The variation (A7) leads to a set of coupled integro-differential equations of Schrödinger form:

$$\{\hat{T}+V_{\rm ext}(\mathbf{r})+V_H(\mathbf{r})\}\varphi_i(\mathbf{r})+\hat{V}_F\varphi_i(\mathbf{r})=\varepsilon_i\varphi_i(\mathbf{r})\,, \tag{A8}$$

the so-called HF equations. Here $V_H(\mathbf{r})$ is the Hartree (or direct, or classical) Coulomb potential

$$V_H(\mathbf{r})=e^2\int\frac{\rho(\mathbf{r}')}{|\mathbf{r}-\mathbf{r}'|}d^3r' \tag{A9}$$

and $\hat{V}_F$ is the nonlocal Fock (or exchange) potential, which is an integral operator and originates from the antisymmetrization of the wave function Φ. It is defined (apart from spin complications) by

$$\hat{V}_F\varphi_i(\mathbf{r})=-\frac{1}{2}e^2\int\frac{\rho_1^{\rm HF}(\mathbf{r}',\mathbf{r})}{|\mathbf{r}-\mathbf{r}'|}\varphi_i(\mathbf{r}')d^3r'\,. \tag{A10}$$

Since both V_H and $\hat{V}_F$ depend on the wave functions, the HF equations (A8) are nonlinear and must be solved self-consistently; this is usually done iteratively. The biggest complication in this procedure is the integral operator $\hat{V}_F$ for the exchange.

The lowest energy obtained after convergence is usually called the HF energy $E_{\rm HF}$, and the corresponding Slater determinant is denoted by $|{\rm HF}\rangle$:

$$E_{\rm HF}=\min_{\{\Phi\}}\langle\Phi|\hat{H}|\Phi\rangle=\langle{\rm HF}|\hat{H}|{\rm HF}\rangle\,. \tag{A11}$$

The sum of Hartree and Fock potentials in Eq. (A8) is usually referred to as the "HF potential," $V_{\rm HF}=V_H+\hat{V}_F$. Naturally, the HF energy may be broken up into its different contributions by writing

$$E_{\rm HF}=\int\{\tau(\mathbf{r})+V_{\rm ext}(\mathbf{r})\rho(\mathbf{r})+\tfrac{1}{2}V_H(\mathbf{r})\rho(\mathbf{r})\}+E_x\,, \tag{A12}$$

where the kinetic-energy density $\tau(\mathbf{r})$ is given by

$$\tau(\mathbf{r})=\frac{\hbar^2}{2m}\sum_{i=1}^{N}|\nabla\varphi_i(\mathbf{r})|^2 \tag{A13}$$

and E_x is the exchange Coulomb energy corresponding to Eq. (A10):

$$E_x=-\frac{1}{4}e^2\int\int\frac{\rho_1^{\rm HF}(\mathbf{r}',\mathbf{r})\rho_1^{\rm HF}(\mathbf{r},\mathbf{r}')}{|\mathbf{r}-\mathbf{r}'|}d^3r'd^3r\,. \tag{A14}$$

It is a well-known feature of the self-consistent mean-field theory that the total energy is not equal to the sum of occupied single-particle energies ε_i. Indeed, from Eqs. (A8) and (A12) one easily verifies that

[21] For the sake of simplicity, and since they will not really be needed here, we do not exhibit the spin degrees of freedom. They would, in fact, render the expressions for the exchange (Fock) terms given in Appendix A.1 below somewhat more complicated; for that we refer the reader to any standard textbook on many-body theory.

$$E_{\rm HF}=\sum_i^N \varepsilon_i-\frac{1}{2}\langle {\rm HF}|V_{\rm H}+\hat{V}_{\rm F}|{\rm HF}\rangle \ . \tag{A15}$$

Strictly speaking, the above expressions for $V_{\rm H}$, $\hat{V}_{\rm F}$, and E_x contain unphysical contributions due to the interaction of the electron in the ith state with itself, which should have been omitted [see the condition $i\neq j$ in Eq. (A1) above]. However, when one takes the sum of direct and exchange terms in $E_{\rm HF}$, these contributions cancel exactly. Leaving them out of both potentials would make the latter state dependent—as in simple Hartree theory— and render the HF equations still more complicated to solve. It is therefore standard praxis to keep them in both potentials. [As is known from classical physics, the inclusion of the self-interaction in the Hartree potential (or the corresponding classical Coulomb energy) does not cause any harm for a continuous density distribution $\rho(\mathbf{r})$.] This point, however, becomes of crucial importance as soon as different approximations are made for the direct and the exchange terms of the Coulomb energy, as is the case in most applications of the density-functional theory.

2. Density-functional theory

Density-functional theory goes beyond the HF approach in that correlations are taken into account which are not contained in the HF energy (A12). In principle, this theory maps the full many-body problem for the ground state of a correlated fermion system onto simple mean-field equations. Practically, however, the exchange and correlation contributions can only be evaluated approximately. Still, density-functional theory has had considerable success in many branches of physics. For recent reviews on density-functional theory and its applications in atomic, molecular, and solid-state physics, we refer the reader to Jones and Gunnarsson (1989) and to Dreizler and Gross (1990).

a. Hohenberg-Kohn theorem and density-variational equations

The basic idea of density-functional theory is almost as old as quantum mechanics and was used by Thomas (1927) and Fermi (1928) in their famous work: to calculate the total energy of a system by an integral over an expression depending only on the local ground-state density $\rho(\mathbf{r})$:

$$E_{\rm tot}=\int \mathcal{E}[\rho(\mathbf{r})]d^3r=E[\rho] \ . \tag{A16}$$

Mathematically speaking, the energy is assumed to be a functional of $\rho(\mathbf{r})$, denoted by $E[\rho]$. The formal basis of the ensuing theory was laid by Hohenberg and Kohn (1964) in their famous theorem, which they proved for a nondegenerate electronic system. A more general proof, independent of ground-state degeneracy and of the so-called V representability assumed by Hohenberg and Kohn, was given by Levy (1979). The Hohenberg-Kohn theorem states that the exact ground-state energy of a correlated electron system is a functional of the density $\rho(\mathbf{r})$ and that this functional has its variational minimum when evaluated for the exact ground-state density. This means that, ideally, the variational equation

$$\frac{\delta}{\delta\rho(\mathbf{r})}\left[E[\rho(\mathbf{r})]-\lambda\int\rho(\mathbf{r})d^3r\right]=0 \ , \tag{A17}$$

using the Lagrange multiplier λ to fix the number of particles according to (A3), would lead to a knowledge of the exact ground-state energy and density—if the exact functional $E[\rho]$ were known (which, alas, it is not).

We do not need to go into further details about this basic theorem and the general formalism of density-functional theory, since this is the subject of many excellent reviews. For further reference, let us just sketch the main steps and give the most important formulae needed in the main text. The usual way to break up the energy functional (A16) for the Hamiltonian given by Eq. (A1) is

$$E[\rho]=T_s[\rho]+\int\{V_{\rm ext}(\mathbf{r})\rho(\mathbf{r})+\tfrac{1}{2}V_H[\rho(\mathbf{r})]\rho(\mathbf{r})\}d^3r +E_{\rm xc}[\rho] \ . \tag{A18}$$

Here $T_s[\rho]$ contains that part of the kinetic energy that corresponds to a system of independent particles with density ρ; the external potential energy and the Hartree-Coulomb energy are clear from the above. The last term in Eq. (A18) is the so-called exchange-correlation energy; it contains the exchange part of the Coulomb energy, i.e., E_x in Eq. (A14) above, plus all the contributions due to other correlations related to the fact that the exact wave function is not a Slater determinant, including the correlation part of the kinetic energy.

$E_{\rm xc}[\rho]$ is not known exactly for any finite interacting fermion system, and it is a matter of state-of-the-art density-functional theory to use more or less fancy approximations to it. The simplest but very successful approximation is the local-density approximation (LDA) to be discussed in the Sec. A.2.c below. The same holds for the kinetic-energy functional $T_s[\rho]$, which is not known explicitly for many-fermion systems.

The famous Thomas-Fermi (TF) model of the atom (Thomas, 1927; Fermi, 1928) represents a textbook example of density-functional theory, in which the density is varied directly according to Eq. (A17). Here one exploits the fact that for a Fermi gas with constant density ρ, the kinetic-energy density is proportional to $\rho^{5/3}$; in the local-density approximation one therefore has the kinetic-energy functional

$$T_{\rm TF}[\rho]=\frac{\hbar^2}{2m}\kappa\int\rho^{5/3}(\mathbf{r})d^3r \ , \quad \kappa=\frac{3}{5}(3\pi^2)^{2/3} \ . \tag{A19}$$

Using this functional for $T_s[\rho]$ in Eq. (A18), omitting the exchange-correlation energy, and performing the varia-

tion (A17), one arrives at the following equation for the density:

$$\frac{5}{3}\frac{\hbar^2}{2m}\kappa\rho^{2/3}(\mathbf{r})+V_{\rm ext}(\mathbf{r})+V_H(\mathbf{r})=\lambda\ , \tag{A20}$$

which is equivalent to the well-known Thomas-Fermi equation. [The latter is usually derived for the total potential with $V_{\rm ext}(\mathbf{r})=-Ne^2/r$, after eliminating the density $\rho(\mathbf{r})$ with the help of the Poisson equation.]

Many improvements to the Thomas-Fermi theory have been proposed over the time. Dirac (1930) introduced the exchange-energy correction (A31) in the local-density approximation discussed below. Von Weizsäcker (1935) derived an inhomogeneity correction to the kinetic-energy functional leading to an additional term $(\nabla\rho)^2/(4\rho)$ in the integrand of Eq. (A19). The corresponding approaches are usually denoted by the letters TFD, TFW, and TFWD, depending on the number of terms included. In the so-called extended Thomas-Fermi model (see, for example, Kirzhnits, 1957), a systematic expansion of the kinetic-energy functional in terms of gradients and higher derivatives of the density is derived with semiclassical methods. Either by an expansion of the density matrix in powers of $\hbar$ (Wigner, 1932; Kirkwood, 1933), or by a commutator algebra (Kirzhnits, 1957) which is fully equivalent, one arrives at the following functional (Hodges, 1973):

$$T_{\rm ETF}[\rho]=\frac{\hbar^2}{2m}\int\left\{\kappa\rho^{5/3}+\frac{1}{36}\frac{(\nabla\rho)^2}{\rho}+\frac{1}{6480}(3\pi^2)^{-2/3}\rho^{1/3}\left[8\left[\frac{\nabla\rho}{\rho}\right]^4-27\left[\frac{\nabla\rho}{\rho}\right]^2\frac{\Delta\rho}{\rho}+24\left[\frac{\Delta\rho}{\rho}\right]^2\right]+\cdots\right\}d^3r\ . \tag{A21}$$

The coefficient of the second term is nine times smaller than that of the original Weizsäcker term. Equation (A21) has the correct coefficient in the limit of slowly varying densities, whereas the Weizsäcker coefficient ($\frac{1}{4}$ instead of $\frac{1}{36}$) is correct in the limit of rapid density oscillations with small amplitude (see Jones and Gunnarson, 1989, for a detailed discussion). The terms in square brackets in Eq. (A21) come from the $\hbar^4$ terms of the semiclassical expansion, and the dots stand for contributions from the higher orders (6,8, . . .) in $\hbar$. (Note that up to nth derivatives of the density appear originally under the integral when expanding to order $\hbar^n$; the two highest ones can, however, be removed by partial integration if the density is assumed to be analytical and to vanish at infinity.) Some of the gradient terms in Eq. (A21) have also been derived in linear-response theory (Kohn and Sham, 1965). Similar gradient corrections leading beyond the local-density approximation have also been derived for the exchange-correlation energy functional $E_{\rm xc}[\rho]$ (see Sec. III.C.5 for a brief discussion).

The series (A21) represents an asymptotic expansion of the noninteracting kinetic-energy functional $T_s[\rho]$. It is semiclassical in the sense that it does not correctly reproduce shell effects but converges towards an average part of the kinetic energy, which varies smoothly with the number of particles and with the deformation of the system, if a correspondingly averaged density is used. Guet and Brack (1980) analyzed the convergence of Eq. (A21) using smoothed densities obtained by the Strutinsky averaging method (Strutinsky, 1968; Brack *et al.*, 1972) and found that including terms up to order $\hbar^4$ [i.e., the terms shown in (A21)] it reproduces very accurately the average kinetic energy of a system of fermions in harmonic-oscillator or Woods-Saxon potentials, independently of particle number and deformation. The same functional has also been tested for atoms in terms of HF densities (see Murphy and Wang, 1980, and references quoted therein). The finite-temperature extension of the functional $T_{\rm ETF}[\rho]$ up to fourth order has been derived by Bartel *et al.* (1985); from its $T\to 0$ limit one obtains a rigorous proof (see also Brack, 1984) of the correctness of the functional (A21) in the classically forbidden region, for which the above-mentioned $\hbar$ expansions are mathematically not well founded at $T=0$.

Using the extended Thomas-Fermi kinetic-energy functional (A21), one can still perform the variation (A17) directly. This leads to a nonlinear fourth-order differential equation for the density. In the main text, we refer to it as the extended Thomas-Fermi (4) equation, if all explicitly shown gradient terms are included. The asymptotic decrease of the solution for $\rho(\mathbf{r})$ at large distances depends solely on the highest derivative term included in $T_{\rm ETF}[\rho]$. In Thomas-Fermi theory, the density of an atom is well known to fall off as r^{-6}. Including the second-order Weizsäcker term (i.e., in the TFW or TFWD approximation), one finds an exponential decrease, which, however, is too fast if the coefficient $\frac{1}{36}$ is used. Therefore in many Thomas-Fermi-Weizsäcker (or TFWD) calculations the coefficient of the Weizsäcker term has been treated as a fit parameter. Going up to order $2m$ with $m\geq 2$ in the expansion (A21), one finds asymptotically [Guet and Brack, 1980 (note added in proof)]

$$\rho(r)\sim r^{-3m/(m-1)}\quad (m\geq 2) \tag{A22}$$

for a spherical system. The highest derivative terms in the integrand of Eq. (A21), which have the slowest falloff, vary as the density (A22) and therefore lead to finite contributions to the kinetic energy at all orders $2m$, contrary to a rather widespread belief. Even though the asymptotic decrease (A22) of $\rho(r)$ is not realistic, the extended

Thomas-Fermi density-variational method has been quite successful at obtaining average energies, densities, and other properties of finite fermion systems. [Obviously, the asymptotic behavior (A22) of $\rho(r)$ is only reached far outside the physically important surface region, so that, in practice, it affects the interesting observables very little if at all (see also Engel and Perdew, 1991).] We refer the reader to Jones and Gunnarsson (1989) and to Dreizler and Gross (1990) for applications to electronic systems, and to Brack *et al.* (1985) and Treiner and Krivine (1986) for applications to nuclei.

b. Kohn-Sham equations

In order to avoid the difficulty of finding an explicit density functional for the kinetic energy, Kohn and Sham (1965) proposed to write the density $\rho(\mathbf{r})$ in the form of Eq. (A4) in terms of some trial single-particle wave functions $\varphi_i(\mathbf{r})$. This is, in fact, possible for any non-negative normalizable density (Gilbert, 1975). The noninteracting part of the kinetic-energy density can then be given in the form $\tau(\mathbf{r})$ (A13) in terms of the same $\varphi_i(\mathbf{r})$. The variation (A17) of the energy functional can now be done through a variation of the trial functions $\varphi_i(\mathbf{r})$ with a constraint on their norms, as in the HF variation (A7), except that $\langle\Phi|\hat{H}|\Phi\rangle$ here is replaced by $E[\rho]$ (A16). This leads to the widely used Kohn-Sham equations,

$$\{\hat{T}+V_{\rm KS}(\mathbf{r})\}\varphi_i(\mathbf{r})=\varepsilon_i\varphi_i(\mathbf{r}) , \tag{A23}$$

in which the local potential $V_{\rm KS}(\mathbf{r})$ is a sum of three terms:

$$V_{\rm KS}(\mathbf{r})=V_{\rm KS}[\rho(\mathbf{r})]=V_{\rm ext}(\mathbf{r})+V_{\rm H}[\rho(\mathbf{r})]+V_{\rm xc}[\rho(\mathbf{r})] . \tag{A24}$$

The first two terms are the same as above, and the third term is just the variational derivative of the exchange-correlation energy:

$$V_{\rm xc}[\rho(\mathbf{r})]=\frac{\delta}{\delta\rho(\mathbf{r})}E_{\rm xc}[\rho] . \tag{A25}$$

Like the HF equations, the Kohn-Sham equations (A23) are nonlinear due to the density dependence of $V_{\rm KS}$ (A24). The important difference, however, is that the potential $V_{\rm KS}(\mathbf{r})$ is local and the Kohn-Sham equations therefore are much easier to solve.

A remark is necessary concerning the interpretation of the wave functions $\varphi_i(\mathbf{r})$ and the energies ε_i obtained from the Kohn-Sham equations: they do not have the same physical meaning as in HF theory. The ansatz (A4) for the density does not imply that the total wave function of the system here is taken to be a Slater determinant. In fact, one does not know the total wave function in density-functional theory; the functions $\varphi_i(\mathbf{r})$ are just a variational tool to obtain the approximate ground-state density. Likewise, the ε_i do not, in general, have the meaning of single-particle energies. An exception is made for the energies of the highest occupied Kohn-Sham level ($\varepsilon_{\rm HO}$) and the lowest unoccupied Kohn-Sham level ($\varepsilon_{\rm LU}$) on either side of the Fermi energy. They can be used to estimate ionization potentials and electron affinities, respectively (see, for example, Levy and Perdew, 1985, and references quoted therein). The physics of this is very similar to that of the so-called Koopmans theorem, which is usually derived within HF theory but applies also in density-functional theory. Apart from some small rearrangement corrections due to the self-consistent change of the mean field upon taking out the last electron of an atom, the ionization potential is given by

$$\mathrm{IP}=E(N-1)-E(N)\simeq-\varepsilon_{\rm HO}=-\varepsilon_N . \tag{A26}$$

Similarly, the electron affinity is approximately found as

$$\mathrm{EA}=E(N)-E(N+1)\simeq-\varepsilon_{\rm LU}=-\varepsilon_{N+1} . \tag{A27}$$

[In exact density-functional theory, $-\varepsilon_{\rm HO}$ can be shown to be identical to the ionization potential for atoms, or the work function for bulk metal (see, for example, Almbladh and von Barth, 1985). These "ideal" statements are, however, violated in practice by the use of approximate energy functionals using, e.g., the LDA (see the next subsection) or the generalized gradient approximation (see Sec. III.C.5). If these approaches are combined with the jellium model, a correction $e^2/2R_I$ must be added to $-\varepsilon_{\rm HO}$ in order to obtain the IP of metal clusters (Perdew, 1989). We refer the interested reader to an extensive discussion of the Koopmans theorem for solids and atoms by Perdew (1985).]

The density-functional theory can easily be extended to take the electron spin explicitly into account by introducing a spin-up density and a spin-down density. This leads, instead of Eq. (A23), to two coupled equations for the two spin densities. In metal clusters, there is so far no evidence for any spin-orbit splitting effects. Therefore the only place where the spin densities are needed here is the case of an odd number of valence electrons, in which one orbit is only occupied by a single electron. Since we shall only discuss clusters with even N in this article, we do not go into the details of the spin-dependent density-functional theory and instead refer the reader to the literature (Jones and Gunnarsson, 1989; Dreizler and Gross, 1990).

Another extension of the density-functional theory concerns the inclusion of a finite temperature $T>0$ of the electrons. Mermin (1965) derived the Hohenberg-Kohn theorem and the Kohn-Sham formalism at $T>0$ for a grand canonical system of electrons. Later Evans (1979) showed that the density-functional theory also applies to canonical systems. In essence, one goes over from the (internal) energy $E[\rho]$ (A18) of the system to the free energy $F[\rho]$,

$$F[\rho]=E[\rho]-TS_s[\rho] , \tag{A28}$$

where S_s is the noninteracting part of the entropy. The exchange-correlation energy $E_{\rm xc}[\rho]$ will, in general, de-

pend on T explicitly (i.e., not only through the density). The Kohn-Sham formalism then is obtained by including in the definition of the densities (A4) and (A13) the finite-temperature occupation numbers n_i,

$$\rho(\mathbf{r})=\sum_i |\varphi_i(\mathbf{r})|^2 n_i \ , \quad \tau(\mathbf{r})=\frac{\hbar^2}{2m}\sum_i |\nabla\varphi_i(\mathbf{r})|^2 n_i \ , \quad \sum_i n_i = N \ , \tag{A29}$$

and by minimizing $F[\rho]$ with respect to both the φ_i and the n_i. Since S_s does not depend explicitly on the wave functions φ_i, the variation of the latter gives exactly the same form (A23) of the Kohn-Sham equations, the only difference being that the potential $V_{\rm KS}$ becomes temperature dependent. Variation of the n_i gives their explicit form in terms of the ε_i; the result depends on whether one treats the system as a canonical or a grand canonical ensemble. (In the latter case, in which the chemical potential μ is used to constrain the average particle number N, one obtains the familiar Fermi occupation numbers.) For an extensive discussion of the finite-temperature density-functional theory and calculations for $T>0$, see the review article by Gupta and Rajagopal (1982). Its application to metallic clusters is discussed in Secs. III.B.3 and V.A.2.

c. Local-density approximation

The Kohn-Sham approach is very appealing since, ideally, it allows one to reduce the correlated many-body problem to the solution of a self-consistent one-body problem of Hartree type. The reality is that only approximate functionals for the exchange-correlation part of the energy are at hand. The simplest and most frequently applied functionals for $E_{\rm xc}[\rho]$ make use of the *local-density approximation* (LDA). One performs more or less sophisticated many-body calculations for a hypothetical infinite system of electrons with constant density ρ, whereby the diverging Hartree energy is canceled by embedding the electrons in a jelliumlike background of opposite charge density. The resulting energy per electron is used to extract the corresponding exchange-correlation part $e_{\rm xc}(\rho)$, which is a function of the variable ρ. The LDA for a finite system with variable density $\rho(\mathbf{r})$ then consists in assuming the local exchange-correlation energy density to be that of the corresponding system with density $\rho=\rho(\mathbf{r})$:

$$E_{\rm xc}^{\rm LDA}[\rho]=\int \rho(\mathbf{r}) e_{\rm xc}(\rho(\mathbf{r}))d^3r \ . \tag{A30}$$

The extension to the spin-density formalism is straightforward; it is usually termed "local-spin-density" (LSD or LSDA) formalism.

The exchange energy part of the local-density approximation was derived by Dirac (1930),

$$E_x^{\rm LDA}[\rho]=-\frac{3}{4}\left[\frac{3}{\pi}\right]^{1/3} e^2 \int [\rho(\mathbf{r})]^{4/3} d^3r \ , \tag{A31}$$

and is also often referred to as the Slater approximation.

The most commonly used correlation energy functionals in cluster physics are those of Wigner (1934), with

$$e_c^W(\rho)=-\frac{0.88}{r_s(\rho)+7.8} \ , \tag{A32}$$

and of Gunnarsson and Lundqvist (1976), with

$$e_c^{\rm GL}(\rho)=-0.0666\left[(1+x^3)\log\left[1+\frac{1}{x}\right]+\frac{1}{2}x-x^2-\frac{1}{3}\right] \ , \quad x=\frac{r_s(\rho)}{11.4} \ ; \tag{A33}$$

both are in atomic energy units (Ry) and are written in terms of the electronic Wigner-Seitz radius $r_s(\rho)=(3/4\pi\rho)^{1/3}$.

A lot of research has been done in going beyond the LDA and LSDA schemes. Both density gradient expansions and explicitly nonlocal forms of $E_{\rm xc}[\rho]$ have been developed and extensively studied (see, for example, Dreizler and Gross, 1990, Chap. 7). Some of them are briefly reviewed in Sec. III.C, although not much work has been done with them for metal clusters so far. Ballone *et al.* (1992) have performed variational quantum Monte Carlo calculations for energies, densities, and pair-correlation functions of electrons confined by a spherical jellium potential, in order to test the LDA.

d. Pseudopotentials

The application of the Kohn-Sham method to complex atomic molecules or clusters becomes very time consuming with increasing number of atoms. The variation of the positions of all atoms and a simultaneous, fully self-consistent treatment of all electrons in systems with more than 10–20 atoms exceeds the capacities even of modern computers. To restrict the number of degrees of freedom, one often exploits the approximate separability of an atom into one or a few valence electrons and an ionic core. The idea is to treat only the valence electrons explicitly by density-functional theory as interacting particles in the field created by the ions. The effects of the core electrons (screening and the Pauli exclusion principle) are taken into account for each atom by introducing a so-called effective core potential or pseudopotential seen by the valence electron(s). Pseudopotential theory thus makes the assumption "atom=ion+valence electron(s)," which generally works very well; it has been successfully used in atomic and molecular physics (see, for example, Szasz, 1985, for an extensive review). For metals like K and Cs, the assumption of a single valence

electron and a structureless ion is less justified, since the ionic cores of these atoms are highly polarizable.

There exist various pseudopotentials of different degrees of phenomenology in the literature—the most sophisticated ones, built on *ab initio* quantum-chemical calculations, being nonlocal or semirelativistic and free of adjustable parameters but also difficult to use in complex molecules or clusters. At short distances from the atomic nucleus, they are repulsive due to the Pauli principle, which excludes the valence electrons from the states occupied by the core electrons. At large distances, they fall off like the spherical Coulomb potential of the unscreened effective charge of the ion. A peculiarity of the pseudopotentials for simple metals like the alkalis is that they are rather weak; this gives a qualitative understanding of the relative success of the jellium model for these metals.

An extremely simple but effective pseudopotential has been introduced by Ashcroft (1966). It simulates the main requirements by a simple Coulomb potential that is cut off at the so-called empty-core radius r_c and is set equal to zero inside:[22]

$$V_{\rm ps}(r)=-\frac{we^2}{r} \quad \text{for } r>r_c$$
$$=0 \quad \text{for } r<r_c \ . \tag{A34}$$

Here w is the number of valence electrons of the atom. With an empirical parameter r_c for each atom, the Ashcroft pseudopotential has successfully been applied to bulk and surface properties of many solids (see, for example, Ashcroft and Mermin, 1976) and it is therefore very popular in cluster calculations.

Another simple local pseudopotential has been proposed and used for metal clusters by Manninen (1986b). However, it should be mentioned that the pseudopotentials used in quantum chemistry and in condensed-matter physics are considerably more sophisticated. When intended for self-consistent mean-field calculations, an important criterion for a pseudopotential is that of "transferability," i.e., the requirement that the valence electron charge in the vicinity of the ionic core agree with what would be calculated in an *ab initio* approach (see, for example, Hamann, Schlüter, and Chiang, 1979).

e. Car-Parrinello equations

We shall finally sketch the equations derived by Car and Parrinello (1985) for the so-called molecular-dynamics (MD) method. One starts from the fact that, in density-functional theory, the total energy of a cluster is a functional $E[\rho,\mathbf{R}_\alpha]$ of both the electronic density ρ, and thus the Kohn-Sham orbital functions φ_i, and the positions $\mathbf{R}_\alpha$ of the ions (the latter entering the Kohn-Sham equations through the pseudopotentials). Treating both φ_i and $\mathbf{R}_\alpha$ as independent degrees of freedom, one finds that the variational principle applied to the total Lagrangian of the system leads to the following coupled equations of motion (Car and Parrinello, 1985):

$$\mu\ddot{\varphi}_i(\mathbf{r},t)=-\frac{\delta}{\delta\varphi_i^*(r,t)}E[\rho,\mathbf{R}_\alpha]+\sum_k \Lambda_{ik}\varphi_k(\mathbf{r},t) \ ,$$
$$M_\alpha\ddot{\mathbf{R}}_\alpha=-\nabla R_\alpha E[\rho,\mathbf{R}_\alpha] \ , \tag{A35}$$

where M_α are the masses of the ions, μ is a fictitious "mass" of the electronic degrees of freedom (but not the electron mass!), and the Lagrange multipliers Λ_{ik} ensures the orthonormalization of the Kohn-Sham orbits. In the limit $\mu \ll M_\alpha$ no energy will be transferred from the electronic to the ionic degrees of freedom, in consistency with the Born-Oppenheimer approximation. Solving Eqs. (A35) allows one to follow the time evolution of the ionic coordinates and thus to describe their dynamics (or thermodynamics); the valence electrons hereby follow self-consistently and adiabatically the time-dependent mean field. For $\mu=0$, the upper equation in (A35) reduces with $\Lambda_{ik}=\delta_{ik}\varepsilon_i$ to the stationary Kohn-Sham equation (A23).

APPENDIX B: LINEAR-RESPONSE THEORY

1. RPA and TDLDA

The random-phase approximation (RPA) formulated by Bohm and Pines (1953) can be derived as the small-amplitude limit of the time-dependent Hartree-Fock (HF) theory by linearizing the quantal equations of motion. It is most successfully used to describe collective small-amplitude excitations in many-body systems. The essence of the RPA is to construct excited states as superpositions of particle-hole excitations. We shall first present it in the framework of HF theory (Appendix A.1) and then discuss its application to density-functional theory (Appendix A.2). We give only a few basic formulae here; for a detailed presentation of the RPA formalism, see, for example, Thouless (1961) or Rowe (1968),

Let $|\mathrm{HF}\rangle$ be a Slater determinant that describes the ground state (A5) of the system in the HF approximation, where all "hole" states below the Fermi energy ($\varepsilon_h<E_F$) are filled and the "particle" states above the Fermi energy ($\varepsilon_p>E_F$) are empty. To define a correlated RPA ground state $|\mathrm{RPA}\rangle$, one adds to $|\mathrm{HF}\rangle$ a superposition of $2p$-$2h$ excitations:

$$|\mathrm{RPA}\rangle=\left[1+\sum_{pp'hh'}\gamma^{pp'hh'}a_p^\dagger a_{p'}^\dagger a_h a_{h'}\right]|\mathrm{HF}\rangle \ . \tag{B1}$$

Excited RPA states $|n\rangle$ are defined as linear combinations of $1p$-$1h$ excitations from the ground state $|\mathrm{RPA}\rangle$:

$$|n\rangle=\sum_{ph}(x_n^{ph}a_p^\dagger a_h-y_n^{ph}a_h^\dagger a_p)|\mathrm{RPA}\rangle \ . \tag{B2}$$

In the above definitions, $a^\dagger$ and a are creation and annihi-

[22] In some applications, the pseudopotential is put to a nonzero constant value for $r<r_c$ (see, for example, Maiti and Falicov, 1991).

lation operators, respectively, for particle and hole states. In principle, the sum in Eq. (B2) runs over all possible $1p$-$1h$ excitations; practically, one limits oneself to a configuration space that must be large enough to give convergence of the final results. The RPA amplitudes x_n^{ph} and y_n^{ph}, from which the coefficients $\gamma^{pp'hh'}$ in (B1) can be computed, are found from diagonalization of the total Hamiltonian (including the two-body interaction V) in the restricted space of $1p$-$1h$ states. Retaining only the terms of first order in the x_n^{ph} and y_n^{ph}, which is tantamount to linearizing the equations of motion, one arrives at the RPA equation that determines the excitation energy spectrum $\hbar\omega_n$:

$$\begin{bmatrix} A & B \\ B^* & A^* \end{bmatrix} \begin{bmatrix} X_n \\ Y_n \end{bmatrix} = \hbar\omega_n \begin{bmatrix} X_n \\ -Y_n \end{bmatrix} . \tag{B3}$$

Here $X_n = x_n^{ph}$ and $Y_n = y_n^{ph}$ are the RPA amplitudes appearing in Eq. (B2), and A and B are the following combinations of antisymmetrized two-body matrix elements of the interaction V:

$$\begin{aligned} A &= A^{ph,p'h'} = \delta_{pp'}\delta_{hh'}(\varepsilon_p - \varepsilon_h) + \langle h'p | V | \widetilde{p'h} \rangle , \\ B &= B^{ph,p'h'} = \langle pp' | V | \widetilde{hh'} \rangle . \end{aligned} \tag{B4}$$

(If one starts from a fully self-consistent HF basis for the p and h states, the mean-field part of the interaction V does not contribute, and only the residual interaction is needed in the above matrix elements.)

Once one has solved the above RPA equations, the spectrum $\{\hbar\omega_n, |n\rangle\}$ can be used to calculate the response to an external excitation operator, as discussed in Appendix B.2 below and in Sec. IV.

The use of the RPA within the framework of density-functional theory is straightforward. Although the ground-state wave function here is not explicitly taken as a Slater determinant, it is still possible to use the Kohn-Sham orbitals to create particle-hole excitations. This method, usually called the time-dependent local-density approximation (TDLDA), was developed for the calculation of atomic polarizabilities by Zangwill and Soven (1980) and by Stott and Zaremba (1980). The TDLDA is equivalent to the RPA if the residual interaction used in the matrix elements (B4) is obtained from the energy density functional $E[\rho]$ (A16) by a double variational derivative:

$$V_{\rm res}[\rho(\mathbf{r})] = \frac{\delta^2}{\delta\rho(\mathbf{r})^2} E[\rho] . \tag{B5}$$

Two *caveats* must be given here. First, there is a formal difficulty in using the LDA in a time-dependent theory. The Hohenberg-Kohn theorem and the density-functional theory built upon it, as we have presented it in Appendix A.2, is strictly limited to the static ground state. The general formulation of a time-dependent density-functional theory is a problem fraught with difficulties, and in general the static functional $E[\rho]$ cannot be used by just inserting the time variable as a parameter of the density, $\rho(\mathbf{r},t)$, except in the adiabatic limit of slow collective motion (Kohl and Dreizler, 1986). We refer the reader to Gross and Kohn (1990) for a recent review on time-dependent density-functional theory, in which an explicitly frequency-dependent exchange-correlation energy functional is also discussed.

Second, there is a danger of double-counting correlations when using the standard exchange-correlation LDA functionals in an RPA or TDLDA calculation, since RPA correlations are usually already built into the ground-state energy $E[\rho]$ via these functionals. Strictly, one should take these contributions out of the functional $E_{\rm xc}[\rho]$ before using it via Eqs. (B3)–(B5) to obtain the RPA excitation energies $\hbar\omega_n$. This, however, is not easy, since they are usually lumped together with other correlations in a parametrized way. Numerically, their contribution to the calculated RPA excitation energies $\hbar\omega_n$ is not very large, so that this problem is not a very serious one. But it would be definitely wrong to use the correlated RPA ground state (B1) to evaluate the ground-state energy. A partial remedy to this problem consists in making use only of certain moments of the RPA strength function whose values do not depend on the inclusion of the RPA correlations in the ground state (see the following subsection).

2. Sum rules and relations to classical hydrodynamics

a. Sum-rule expressions

It is often useful to discuss the global properties of a spectral distribution in terms of its moments. Starting from an RPA spectrum $\{\hbar\omega_n, |n\rangle\}$, one defines the strength function $S_Q(E)$ for the linear response of a system to an external excitation operator $\hat{Q}$:

$$S_Q(E) = \sum_{n\neq 0} |\langle n|\hat{Q}|\mathrm{RPA}\rangle|^2 \delta(E - \hbar\omega_n) , \tag{B6}$$

where we have put the energy of the RPA ground state $|\mathrm{RPA}\rangle$ (B1) equal to zero. The kth energy-weighted moment of the strength function is given by

$$m_k(\hat{Q}) = \int_0^\infty E^k S_Q(E) dE = \sum_{n\neq 0} (\hbar\omega_n)^k |\langle n|\hat{Q}|\mathrm{RPA}\rangle|^2 . \tag{B7}$$

Many useful quantities and relations can be derived from these moments. For example, the centroid (i.e., the mean energy) $\bar{E}$ and the variance σ of the distribution (B6) are given by

$$\bar{E} = m_1/m_0 , \quad \sigma^2 = m_2/m_0 - (m_1/m_0)^2 . \tag{B8}$$

Upper and lower bounds for these two quantities can be given (Bohigas *et al.*, 1979) by

$$E_1 \le \bar{E} \le E_3 , \quad \sigma \le \sigma_{\max} = \tfrac{1}{2}\sqrt{E_3^2 - E_1^2} \tag{B9}$$

in terms of the two energies E_3, E_1 defined by

$$E_3(\hat{Q})=\left[\frac{m_3(\hat{Q})}{m_1(\hat{Q})}\right]^{1/2},\quad E_1(\hat{Q})=\left[\frac{m_1(\hat{Q})}{m_{-1}(\hat{Q})}\right]^{1/2}. \tag{B10}$$

These energies are particularly easily accessible for the following reason. Under the assumption that $\hbar\omega_n$, $|n\rangle$ are eigenenergies and eigenstates of the total Hamiltonian $\hat{H}$ of the system (which is the assumption of the RPA), the moments m_3 and m_1 can be written as

$$m_1(\hat{Q})=\tfrac{1}{2}\langle \mathrm{RPA}|[\hat{Q},[\hat{H},\hat{Q}]]|\mathrm{RPA}\rangle , \tag{B11}$$

$$m_3(\hat{Q})=\tfrac{1}{2}\langle \mathrm{RPA}|[[\hat{H},\hat{Q}],[\hat{H},[\hat{Q},\hat{H}]]]|\mathrm{RPA}\rangle . \tag{B12}$$

According to a theorem proved by Thouless (1961), the expectation values (B11) and (B12) can be evaluated without loss of accuracy replacing the correlated RPA ground state $|\mathrm{RPA}\rangle$ by the uncorrelated HF ground state $|\mathrm{HF}\rangle$ belonging to the same Hamiltonian. [This holds exactly for a density-independent Hamiltonian. Applied to the Kohn-Sham formalism, the theorem must be generalized to the case of a density-dependent Hamiltonian (due to the form of the exchange and correlation energy functional in the LDA); it can, indeed, be shown (Bohigas *et al.*, 1979) to hold within the quasiboson approximation that is used in all practical RPA calculations.] Thus m_3 and m_1 can be evaluated as HF (or Kohn-Sham) ground-state expectation values without explicit calculation of the RPA spectrum.

Similarly, the RPA moment m_{-1} can be shown (Thouless, 1961; Marshalek and da Providência, 1973) to be proportional to the static polarizability α_{pol} of the HF (or Kohn-Sham) ground state with respect to the external field $\hat{Q}$,

$$m_{-1}(\hat{Q})=\tfrac{1}{2}\alpha_{\mathrm{pol}}(\hat{Q}) . \tag{B13}$$

Exploiting the above relations, it is thus possible to find upper and lower bounds for the centroid and an upper limit for the variance of an RPA excitation spectrum merely from static ground-state wave functions.

Explicit expressions of m_1 and m_3 for the electric dipole operator $\hat{Q}=rY_{L0}(\theta)$ are given in the main text (Sec. IV.C); sum rules for the momentum-dependent excitation operators of the form $j_l(qr)Y_{L0}(\theta)$ have been discussed by Serra *et al.* (1990).

b. Scaling model interpretation of moments m_3 and m_1

The energy E_3 in Eq. (B10) has a simple and transparent physical interpretation in terms of a scaling transformation (Bohigas *et al.*, 1979), if the external excitation operator $\hat{Q}$ commutes with the potential-energy part of the Hamiltonian. This is the case for any *local* operator $\hat{Q}=Q(\mathbf{r})$ in connection with a Coulombic system. One may then define an anti-Hermitian "scaling operator" $\hat{S}$ by

$$\hat{S}=[\hat{H},Q]=[\hat{T},Q]=\tfrac{1}{2}(\nabla\cdot\mathbf{u})+\mathbf{u}\cdot\nabla , \tag{B14}$$

with

$$\mathbf{u}(\mathbf{r})=-\frac{\hbar^2}{m}\nabla Q(\mathbf{r}) . \tag{B15}$$

The moment $m_1(Q)$ is then easily shown by partial integration to equal

$$m_1(Q)=\frac{m}{2\hbar^2}\int \mathbf{u}(\mathbf{r})\cdot\mathbf{u}(\mathbf{r})\rho(\mathbf{r})d^3r , \tag{B16}$$

which is proportional to a hydrodynamical mass parameter if $\mathbf{u}(\mathbf{r})$ is interpreted as a displacement (or static velocity) field [see Eq. (B23) below]. On the other hand, the moment $m_3(Q)$ can be expressed as

$$\begin{aligned} m_3(Q)&=\frac{1}{2}\langle \mathrm{HF}|[\hat{S},[\hat{S},\hat{H}]]|\mathrm{HF}\rangle \\ &=\frac{1}{2}\left[\frac{d^2}{d\alpha^2}\langle \mathrm{HF}|e^{\alpha\hat{S}}\hat{H}e^{-\alpha\hat{S}}|\mathrm{HF}\rangle\right]_{\alpha=0} \end{aligned} \tag{B17}$$

and is thus proportional to the restoring force parameter related to a collective "deformation" variable $\alpha(t)$.

The energy E_3 in Eq. (B10) is therefore identified with the harmonic-oscillator energy $\hbar\omega_\alpha$,

$$E_3=\sqrt{m_3/m_1}=\hbar\omega_\alpha=\sqrt{C/B} , \tag{B18}$$

corresponding to the lowest excitation of a collective Hamiltonian $H_{\mathrm{coll}}(\alpha)$,

$$H_{\mathrm{coll}}(\alpha)=\tfrac{1}{2}B\dot{\alpha}^2+V_{\mathrm{coll}}(\alpha) \tag{B19}$$

in the harmonic approximation. The collective potential energy is the "scaled" HF energy

$$V_{\mathrm{coll}}(\alpha)=\langle \mathrm{HF}|e^{\alpha\hat{S}}\hat{H}e^{-\alpha\hat{S}}|\mathrm{HF}\rangle \tag{B20}$$

obtained by a unitary transformation of the ground state $|\mathrm{HF}\rangle$ through the scaling operator $e^{-\alpha\hat{S}}$. Since $\hat{S}$, as well as $\hat{Q}$, is a single-particle operator, all wave functions $\varphi_i(\mathbf{r})$ are transformed independently in the same way:

$$e^{-\alpha\hat{S}}\varphi_i(\mathbf{r})=\varphi_i(\mathbf{r},\alpha) . \tag{B21}$$

The collective mass parameter B and the restoring force parameter C in (B18) are thus given by

$$B=2\hbar^2m_1(Q) ,\quad C=2m_3(Q) . \tag{B22}$$

The interpretation of $\mathbf{u}(\mathbf{r})$ as the displacement field belonging to the collective flow pattern generated by the scaling transformation (B21) is verified by defining the total velocity field $\mathbf{v}_\alpha(\mathbf{r},t)$

$$\mathbf{v}_\alpha(\mathbf{r},t)=\dot{\alpha}(t)\mathbf{u}(\mathbf{r}) . \tag{B23}$$

Together with the scaled ground-state density

$$\rho_\alpha(\mathbf{r},t)=\rho(\mathbf{r},\alpha(t))=\sum_i|\varphi_i(\mathbf{r},\alpha(t))|^2 , \tag{B24}$$

$\mathbf{v}_\alpha$ is, indeed, found to fulfill the continuity equation

$$\frac{\partial}{\partial t}\rho_\alpha(\mathbf{r},t)+\nabla\cdot[\rho_\alpha(\mathbf{r},t)\mathbf{v}_\alpha(\mathbf{r},t)]=0 . \tag{B25}$$

Note that the above interpretation of the energy E_3 is exact within the HF+RPA approach; the term "scaling model" should therefore not be misunderstood as indicating a further approximation beyond those inherent already in an RPA calculation built on top of the HF ground state. As already mentioned above, all these arguments carry over directly to the case in which the HF calculation for the ground state is replaced by a Kohn-Sham calculation.

The physical meaning of the estimate E_3 for the collective vibrational energy now is clear: It corresponds to a diabatic oscillation of the single-particle states (i.e., here of the valence electrons) around their equilibrium configuration; this oscillation is rapid, so that the mean field (i.e., the HF or Kohn-Sham potential) is not changed during the vibration. All wave functions scale coherently according to Eq. (B21); no change of their nodal structure occurs.

In contrast to this, the energy E_1 in Eq. (B10) contains the *static* polarizability [see Eq. (B13)] in its denominator and thus corresponds to a slow, adiabatic motion of the particles, which adjust their wave functions at any moment to the static external field $\hat{Q}$.

c. Local-current RPA, fluid dynamics, and normal hydrodynamics

Reinhard *et al.* (1990) have shown that the exact RPA equations (B3) are obtained if one makes the energy $E_3(\hat{Q})$ stationary by a variation of the operator $\hat{Q}$ in full particle-hole space. Taking $\hat{Q}$ to be a local function $Q(\mathbf{r})$, one is led to a nonlinear fourth-order differential equation for the velocity field, i.e., the gradient of $Q(\mathbf{r})$ via Eqs. (B15) and (B23) above, which is identical in structure to that of the so-called fluid dynamics approach. This latter approach was initialized by Bertsch (1975) and by Sagawa and Holzwarth (1978) for the description of giant resonances in nuclei, and put in a variational form by Krivine *et al.* (1980) and by da Providência and Holzwarth (1983, 1985). The fluid-dynamical equations have usually been solved for simplified liquid-drop model densities with sharp surfaces (see Lipparini and Stringari, 1989, for a recent review).

An alternative approach, which avoids the numerically difficult solution of the full fluid-dynamical equations and makes use of exact variational (HF, Kohn-Sham, or semiclassical extended Thomas-Fermi) ground-state densities, was recently proposed by Brack (1989) and Reinhard *et al.* (1990) (see also Reinhard and Gambhir, 1992, for an exhaustive presentation of the formalism). Here the variation of $E_3(Q)$ is done on a set of local trial operators $\{Q_i(\mathbf{r})\}$ and leads to a secular equation for coupled harmonic vibrations generated by these operators:

$$\det|\mathcal{K}_{ij}-(\hbar\omega_n)^2\mathcal{B}_{ij}|=0\ . \tag{B26}$$

Here the mass tensor $\mathcal{B}_{ij}$ and the restoring force tensor $\mathcal{K}_{ij}$ are given by

$$\mathcal{B}_{ij}=\langle \mathrm{HF}|[Q_i,[\hat{H},Q_j]]|\mathrm{HF}\rangle\ , \tag{B27}$$

$$\mathcal{K}_{ij}=\langle \mathrm{HF}|[[\hat{H},Q_j],[\hat{H},[Q_i,\hat{H}]]]|\mathrm{HF}\rangle\ . \tag{B28}$$

They are nondiagonal generalizations of the moments m_1 and m_3 in Eqs. (B11) and (B12), so that the secular equation (B26) represents an extension of the simple sum-rule expression E_3 (B10) to the case of several coupled modes. For sufficiently simple operators Q_i, the expressions (B27) and (B28) may be evaluated analytically and lead to integrals involving only HF (or Kohn-Sham) ground-state densities.[23]

Solving the secular equation (B26) then gives a spectrum of eigenenergies $\hbar\omega_n$ that represents an approximation to the RPA spectrum. The corresponding one-phonon states $|n\rangle$ exhaust the m_1 and m_3 sum rules for any external operator that lies in the space spanned by the trial set Q_i. Evaluating the moment m_{-1} also gives, by virtue of Eq. (B13), the static polarizability. The only restriction of this approach with respect to the full microscopic RPA is the choice of a (finite) set of local operators $Q_i(\mathbf{r})$, i.e., the assumption of the local nature of the associated velocity fields or currents.

In fluid dynamics, emphasis has been put on the dynamical distortions of the Fermi sphere in momentum space, which for uniform systems leads to zero sound effects. These effects are fully included in the local-current RPA if the kinetic-energy contribution to the restoring force tensor $\mathcal{K}_{ij}$ (B28) is evaluated microscopically in terms of the scaled single-particle wave functions φ_i (B21) through Eq. (A13) (cf. Brack, 1983). If, however, the kinetic-energy density is evaluated in the Thomas-Fermi or ETF approximation (see Appendix A.2.a), the zero-sound effects are lost, since the momentum distribution is always spherical in the (extended) Thomas-Fermi model, and one obtains standard classical hydrodynamics. For pure electric dipole vibrations, or for monopole vibrations described by the operator $Q_0=r^2$ (leading to a "breathing mode"), there is no difference in the restoring forces obtained by fluid dynamics or ordinary hydrodynamics. For most other modes, however, the differences can become important. A textbook example is the nuclear giant quadrupole mode, in which hydrodynamics gives wrong values and the wrong dependence on the nucleon number A, whereas fluid dynamics leads to an excellent description of the peak energies even with the simple E_3 sum-rule expression (Bohigas *et al.*, 1979; Lipparini and Stringari, 1989; Gleissl *et al.*, 1990).

[23] See Brack (1989) and Reinhard *et al.* (1990) for expressions valid for multipole operators of the form $Q_i(\mathbf{r})=r^{p_i}Y_{L0}(\theta)$ in connection with the spherical jellium model.

REFERENCES

Almbladh, C.-O., and U. von Barth, 1985, Phys. Rev. B **31**, 3231.

Alonso, J. A., and L. A. Girifalco, 1977, Solid State Commun. **24**, 135.

Andreoni, W., 1991, Z. Phys. D **19**, 31.

Ashcroft, N. W., 1966, Phys. Lett. **23**, 48.

Ashcroft, N. W., and N. D. Mermin, 1976, *Solid State Physics* (Holt, Rinehart and Winston, New York).

Baladron, C., M. P. Iñiguez, and J. A. Alonso, 1985, Z. Phys. B **59**, 187.

Balbás, L. C., J. A. Alonso, and A. Rubio, 1991, Europhys. Lett. **14**, 323.

Balbás, L. C., and A. Rubio, 1990, An. Fis. (Spain) A **86**, 207.

Balbás, L. C., A. Rubio, J. A. Alonso, and G. Borstel, 1989, J. Chem. Phys. **86**, 799.

Balian, R., and C. Bloch, 1972, Ann. Phys. (N.Y.) **69**, 76.

Ballone, P., W. Andreoni, R. Car, and M. Parrinello, 1989, Europhys. Lett. **8**, 73.

Ballone, P., C. J. Umrigar, and P. Delaly, 1992, Phys. Rev. B **45**, 6293.

Barberán, N., and J. Bausells, 1985, Phys. Rev. B **31**, 6354.

Barnett, R. N., U. Landman, and C. Rajagopal, 1991, Phys. Rev. Lett. **67**, 3058.

Bartel, J., M. Brack, and M. Durand, 1985, Nucl. Phys. A **445**, 263.

Beck, D. E., 1984a, Solid State Commun. **49**, 381.

Beck, D. E., 1984b, Phys. Rev. B **30**, 6935.

Becke, A. D., 1988, Phys. Rev. A **38**, 3098.

Beckmann, H.-O., J. Koutecký, and V. Bonačić-Koutecký, 1980, J. Chem. Phys. **73**, 5182.

Bernath, M., M. S. Hansen, P. F. Bortignon, and R. A. Broglia, 1993, Phys. Rev. B (in press).

Bernath, M., C. Yannouleas, and R. A. Broglia, 1991, Phys. Lett. A **156**, 307.

Bertsch, G. F., 1975, Nucl. Phys. A **249**, 253.

Bertsch, G. F., 1990, Comput. Phys. Commun. **60**, 247.

Bertsch, G. F., P. F. Bortignon, and R. A. Broglia, 1983, Rev. Mod. Phys. **55**, 287.

Bertsch, G. F., and R. A. Broglia, 1986, Phys. Today **39**, No. 8, 44.

Bertsch, G. F., and W. Ekardt, 1985, Phys. Rev. B **32**, 7659.

Bertsch, G. F., and D. Tomanek, 1989, Phys. Rev. B **40**, 2749.

Bethe, H. A., 1937, Rev. Mod. Phys. **9**, 69.

Bjørnholm, S., J. Borggreen, O. Echt, K. Hansen, J. Pedersen, and H. D. Rasmussen, 1990, Phys. Rev. Lett. **65**, 1627.

Bjørnholm, S., J. Borggreen, O. Echt, K. Hansen, J. Pedersen, and H. D. Rasmussen, 1991, Z. Phys. D **19**, 47.

Bjørnholm, S., T. Døssing, K. Hansen, and H. Nishioka, 1993, Phys. Rep. (in press).

Bjørnholm, S., and J. E. Lynn, 1980, Rev. Mod. Phys. **52**, 725.

Blanc, J., M. Broyer, J. Chevaleyre, P. Dugourd, H. Kuhling, P. Labastie, M. Ulbricht, J. P. Wolf, and L. Wöste, 1991, Z. Phys. D **19**, 7.

Blocki, J., Y. Boneh, J. R. Nix, J. Randrup, M. Robel, A. J. Sierk, and W. J. Swiatecki, 1978, Ann. Phys. (N.Y.) **113**, 330.

Bohigas, O., A. M. Lane, and J. Martorell, 1979, Phys. Rep. **51**, 267.

Bohm, D., and D. Pines, 1953, Phys. Rev. **92**, 609.

Bohr, A., and B. Mottelson, 1975, *Nuclear Structure II* (Benjamin, New York).

Bonačić-Koutecký, V., P. Fantucci, and J. Koutecký, 1988, Phys. Rev. B **37**, 4369.

Bonačić-Koutecký, V., P. Fantucci, and J. Koutecký, 1990, J. Chem. Phys. **93**, 3802.

Bonačić-Koutecký, V., P. Fantucci, and J. Koutecký, 1991, Chem. Rev. **91**, 1035.

Borggreen, J., P. Chowdhury, N. Kebaïli, L. Lundsberg-Nielsen, K. Lützenkirchen, M. B. Nielsen, J. Pedersen, and H. D. Rasmussen, 1993, Phys. Rev. B (in press).

Borstel, G., U. Lammers, A. Mañanes, and J. A. Alonso, 1992, in *Nuclear Physics Concepts in Atomic Cluster Physics,* edited by R. Schmidt, H. O. Lutz, and R. Dreizler (Springer, Berlin), p. 327.

Boustani, I., W. Pewestorf, P. Fantucci, V. Bonačić-Koutecký, and J. Koutecký, 1987, Phys. Rev. B **35**, 9437.

Brack, M., 1983, Phys. Lett. B **123**, 143.

Brack, M., 1984, Phys. Rev. Lett. **53**, 119; 1985, **54**, 851(E).

Brack, M., 1988, unpublished results.

Brack, M., 1989, Phys. Rev. B **39**, 3533.

Brack, M., J. Damgaard, A. S. Jensen, H. C. Pauli, V. M. Strutinsky, and C. Y. Wong, 1972, Rev. Mod. Phys. **44**, 320.

Brack, M., O. Genzken, and K. Hansen, 1991a, Z. Phys. D **19**, 51.

Brack, M., O. Genzken, and K. Hansen, 1991b, Z. Phys. D **21**, 65.

Brack, M., C. Guet, and H.-B. Håkansson, 1985, Phys. Rep. **123**, 275.

Brack, M., and P. Quentin, 1981, Nucl. Phys. A **361**, 35.

Brajczewska, M., C. Fiolhais, and J. P. Perdew, 1993, Int. J. Quantum Chem. (in press).

Bréchignac, C., P. Cahuzac, F. Carlier, M. de Frutos, and J. Leygnier, 1992a, Chem. Phys. Lett. **189**, 28.

Bréchignac, C., P. Cahuzac, M. de Frutos, N. Kebaïli, J. Leygnier, J. P. Roux, and A. Sarfati, 1992b, in *Physics and Chemistry of Finite Systems: From Clusters to Crystals,* edited by P. Jena *et al.* (Kluwer Academic, Dordrecht), Vol. II, p. 853.

Bréchiganac, C., P. Cahuzac, M. de Frutos, J. P. Roux, and K. H. Bowen, 1992c, in *Physics and Chemistry of Finite Systems: From Clusters to Crystals,* edited by P. Jena *et al.* (Kluwer Academic, Dordrecht), Vol. I, p. 369.

Budd, H. F., and J. Vannimenus, 1973, Phys. Rev. Lett. **31**, 1218.

Bunatian, G. G., V. M. Kolomietz, and V. M. Strutinsky, 1972, Nucl. Phys. A **188**, 225.

Car, R., and M. Parrinello, 1985, Phys. Rev. Lett. **55**, 2471.

Chacón, E., and P. Tarazona, 1988, Phys. Rev. B **37**, 4013.

Chou, M. Y., A. Cleland, and M. L. Cohen, 1984, Solid State Commun. **52**, 645.

Christensen, O. B., K. W. Jacobsen, J. K. Nørskov, and M. Manninen, 1991, Phys. Rev. Lett. **66**, 2219.

Cini, M., 1975, J. Catal. **37**, 187.

Clemenger, K., 1985a, Ph.D. thesis (University of California, Berkeley).

Clemenger, K., 1985b, Phys. Rev. B **32**, 1359.

Clemenger, K., 1991, Phys. Rev. B **44**, 12991.

da Providência, J. P., and G. Holzwarth, 1983, Nucl. Phys. A **398**, 59.

da Providência, J. P., and G. Holzwarth, 1985, Nucl. Phys. A **439**, 477.

de Heer, W. A., 1993, this issue, Rev. Mod. Phys. **65**, 611.

de Heer, W. A., W. D. Knight, M. Y. Chou, and M. L. Cohen, 1987, in Solid State Physics, Vol. 40, edited by H. Ehrenreich and D. Turnbull (Academic, New York), p. 93.

de Heer, W. A., and P. Milani, 1990, Phys. Rev. Lett. **65**, 3356.

de Heer, W. A., K. Selby, V. Kresin, J. Masui, M. Vollmer, A.

Chatelain, and W. D. Knight, 1987, Phys. Rev. Lett. **59**, 1805.
Delaly, P., P. Ballone, and J. Buttet, 1992, Phys. Rev. B **45**, 3838.
Denton, R., B. Mühlschlegel, and D. J. Scalapino, 1973, Phys. Rev. B **7**, 3589.
Dirac, P. A. M., 1930, Proc. Cambridge Philos. Soc. **26**, 376.
Dreizler, R. M., and E. K. U. Gross, 1990, *Density Functional Theory* (Springer, Berlin).
Ekardt, W., 1984a, Phys. Rev. Lett. **52**, 1925.
Ekardt, W., 1984b, Phys. Rev. B **29**, 1558.
Ekardt, W., 1985a, Phys. Rev. B **31**, 6360.
Ekardt, W., 1985b, Phys. Rev. B **32**, 1961.
Ekardt, W., 1987, Phys. Rev. B **36**, 4483.
Ekardt, W., and Z. Penzar, 1988, Phys. Rev. B **38**, 4273.
Ekardt, W., and Z. Penzar, 1991, Phys. Rev. B **43**, 1322.
Engel, E., J. A. Chevary, L. D. MacDonald, and S. H. Vosko, 1992, Z. Phys. D **23**, 7.
Engel, E., and J. P. Perdew, 1991, Phys. Rev. B **43**, 1331.
Evans, R., 1979, Adv. Phys. **28**, 143.
Fantucci, P., J. Koutecký, and G. Pacchioni, 1984, J. Chem. Phys. **80**, 325.
Fermi, E., 1928, Z. Phys. **48**, 73.
Fiolhais, C., and J. P. Perdew, 1992, Phys. Rev. B **45**, 6207.
Frauendorf, S., and V. Pashkevich, 1993, Z. Phys. D **26**, S-98.
Gallardo, M., M. Diebel, T. Døssing, and R. A. Broglia, 1985, Nucl. Phys. A **443**, 415.
Galli, G., and M. Parrinello, 1991, in *Computer Simulation in Material Science,* NATO ASI Series E: Applied Sciences, Vol. 205, edited by M. Meyer and V. Pontikis (Kluwer Academic, Dordrecht), p. 283.
Garcia-Prieto, J., G. del Conde, M. Galvan, and O. Novaro, 1984, Phys. Rev. B **30**, 1030.
Genzken, O., 1992, Ph.D. thesis (University of Regensburg).
Genzken, O., and M. Brack, 1991, Phys. Rev. Lett. **67**, 3286.
Genzken, O., M. Brack, E. Chabanat, and J. Meyer, 1992, in *Reactions in and with Clusters,* Bunsen Discussion Meeting, Schliersee (Germany), Ber. Bunsenges. Phys. Chem. **96**, 1217.
Genzken, O., P.-G. Reinhard, M. Brack, H. Bresele, and G. Villing, 1993, Preprint TPR-93-10 (University of Regensburg).
Gilbert, T. L., 1975, Phys. Rev. B **12**, 2111.
Gleissl, P., M. Brack, J. Meyer, and P. Quentin, 1990, Ann. Phys. (N.Y.) **197**, 205.
Goeppert-Mayer, M., 1949, Phys. Rev. **75**, 1969.
Goldhaber, M., and E. Teller, 1948, Phys. Rev. **74**, 1046.
Gross, E. K. U., and W. Kohn, 1990, Adv. Quantum Chem. **21**, 255.
Guet, C., and M. Brack, 1980, Z. Phys. A **297**, 247.
Guet, C., and W. R. Johnson, 1992, Phys. Rev. B **45**, 11283.
Guet, C., W. R. Johnson, and M. Madjet, 1993, Z. Phys. D **26**, S-125.
Gunnarsson, O., M. Jonson, and B. I. Lundqvist, 1977, Solid State Commun. **24**, 765.
Gunnarsson, O., and B. I. Lundqvist, 1976, Phys. Rev. B **13**, 4274.
Gupta, U., and A. K. Rajagopal, 1982, Phys. Rep. **87**, 259.
Gutzwiller, M. C., 1971, J. Math. Phys. **12**, 343.
Haberland, H., 1992, in *Bergmann und Schäfer: Lehrbuch der Experimentalphysik,* Band 5: Vielteilchen-Systeme, edited by W. Raith (de Gruyter, Berlin, New York), p. 549.
Halperin, W. P., 1986, Rev. Mod. Phys. **58**, 533.
Hamamoto, I., B. R. Mottelson, H. Xie, and X. Z. Zhang, 1991, Z. Phys. D **21**, 163.
Hamann, D. R., M. Schlüter, and C. Chiang, 1979, Phys. Rev. Lett. **43**, 1494.
Hansen, M. S., 1989, thesis (Niels Bohr Institute).
Hansen, M. S., and H. Nishioka, 1993, Z. Phys. D **28** (in press).
Haxel, O., J. H. D. Jensen, and H. E. Suess, 1949, Phys. Rev. **75**, 1766.
Hedin, L., and S. Lundquist, 1969, Solid State Phys. **23**, 1.
Hill, D. L., and J. A. Wheeler, 1953, Phys. Rev. **89**, 1102.
Hirschmann, T., J. Meyer, and M. Brack, 1993, Preprint TPR-93-17 (University of Regensburg).
Hoare, M. R., and J. A. McInnes, 1983, Adv. Phys. **32**, 791.
Hodges, C. H., 1973, Can. J. Phys. **51**, 1428.
Hohenberg, P., and W. Kohn, 1964, Phys. Rev. **136**, B864.
Iñiguez, M. P., J. A. Alonso, and L. C. Balbás, 1986, Solid State Commun. **57**, 85.
Iñiguez, M. P., J. A. Alonso, A. Rubio, M. J. López, and L. C. Balbás, 1990, Phys. Rev. B **41**, 5595.
Iñiguez, M. P., M. J. López, J. A. Alonso, and J. M. Soler, 1989, Z. Phys. D **11**, 163.
Jacobsen, K. W., and J. K. Nørskov, 1988, in *The Structure of Surfaces II,* Springer Series in Surface Sciences, Vol. 11, edited by J. F. van der Veen and M. A. van Hove (Springer, Berlin).
Jahn, H. A., and E. Teller, 1937, Proc. R. Soc. London Ser. A **161**, 220.
Jensen, H., 1937, Z. Phys. **106**, 620.
Jones, R. O., 1991, Phys. Rev. Lett. **67**, 224.
Jones, R. O., and O. Gunnarsson, 1989, Rev. Mod. Phys. **61**, 689.
Kawabata, A., and R. Kubo, 1966, J. Phys. Soc. Jpn. **21**, 1765.
Kirkpatrick, S., C. D. Gelatt, and M. P. Vecchi, 1983, Science **220**, 671.
Kirkwood, J. G., 1933, Phys. Rev. **44**, 31.
Kirzhnits, D. A., 1957, Sov. Phys. JETP **5**, 64.
Knight, W. D., K. Clemenger, W. A. de Heer, and W. A. Saunders, 1985, Phys. Rev. B **31**, 2539.
Knight, W. D., K. Clemenger, W. A. de Heer, W. A. Saunders, M. Y. Chou, and M. L. Cohen, 1984, Phys. Rev. Lett. **52**, 2141.
Kohl, H., and R. M. Dreizler, 1986, Phys. Rev. Lett. **56**, 1993.
Kohn, W., and L. J. Sham, 1965, Phys. Rev. **140**, A1133.
Koskinen, M., P. O. Lipas, E. Hammarén, and M. Manninen, 1992, Europhys. Lett. **19**, 165.
Kreibig, U., and L. Genzel, 1985, Surf. Sci. **156**, 678.
Kresin, V., 1988, Phys. Rev. B **38**, 3741.
Kresin, V., 1989a, Phys. Rev. B **39**, 3042.
Kresin, V., 1989b, Phys. Rev. B **40**, 12 507.
Kresin, V., 1990, Phys. Rev. B **42**, 3247.
Kresin, V., 1991, Z. Phys. D **19**, 105.
Kresin,V., 1992, Phys. Rep. **220**, 1.
Krivine, H., J. Treiner, and O. Bohigas, 1980, Nucl. Phys. A **366**, 155.
Kubo, R., 1962, J. Phys. Soc. Jpn. **17**, 975.
Lang, N. D., and W. Kohn, 1970, Phys. Rev. B **1**, 4555.
Lang, N. D., and W. Kohn, 1971, Phys. Rev. B **3**, 1215.
Lang, N. D., and W. Kohn, 1973, Phys. Rev. B **7**, 3541.
Lange, T., H. Göhlich, T. Bergmann, and T. P. Martin, 1991, Z. Phys. D **19**, 113.
Langreth, D. C., and M. J. Mehl, 1983, Phys. Rev. B **28**, 1809; 1984, **29**, 2310(E).
Lauritsch, G., P.-G. Reinhard, J. Meyer, and M. Brack, 1991, Phys. Lett. A **160**, 179.
Lermé, J., M. Pellarin, J. L. Vialle, B. Baguenard, and M. Broyer, 1992, Phys. Rev. Lett. **68**, 2812.
Levy, M., 1979, Proc. Nat. Acad. Sci. USA **76**, 6062.
Levy, M., and J. P. Perdew, 1985, Phys. Rev. A **32**, 2010.
Lipparini, E., and S. Stringari, 1989, Phys. Rep. **175**, 103.

Lipparini, E., and S. Stringari, 1991, Z. Phys. D **18**, 193.
Liu, K. F., and Nguyen Van Giai, 1976, Phys. Lett. B **65**, 23.
López, M. J., M. P. Iñiguez, and J. A. Alonso, 1990, Phys. Rev. B **41**, 5636.
Mahan, G. D., 1980, Phys. Rev. A **21**, 1561.
Mahan, G. D., 1981, *Many-Particle Physics* (Plenum, New York).
Mahan, G. D., and W. L. Schaich, 1974, Phys. Rev. B **10**, 2647.
Maiti, A., and L. M. Falicov, 1991, Phys. Rev. A **44**, 4442.
Maiti, A., and L. M. Falicov, 1992, Phys. Rev. A **45**, 6918.
Makov, G., and A. Nitzan, 1991, J. Chem. Phys. **95**, 9024.
Makov, G., A. Nitzan, and L. E. Brus, 1988, J. Chem. Phys. **88**, 5076.
Manninen, M., 1986a, Solid State Commun. **59**, 281.
Manninen, M., 1986b, Phys. Rev. B **34**, 6886.
Manninen, M., R. M. Nieminen, and M. J. Puska, 1986, Phys. Rev. B **33** 4297.
Marinelli, F., A. Julg, and G. Abbate, 1976, Surf. Sci. **59**, 319.
Marshalek, E. R., and J. P. da Providência, 1973, Phys. Rev. C **7**, 2281.
Martin, T. P., T. Bergmann, H. Göhlich, and T. Lange, 1990, Chem. Phys. Lett. **172**, 209
Martin, T. P., T. Bergmann, H. Göhlich, and T. Lange, 1991a, Chem. Phys. Lett. **176**, 343.
Martin, T. P., T. Bergmann, H. Göhlich, and T. Lange, 1991b, Z. Phys. D **19**, 25.
Martin, T. P., S. Bjørnholm, J. Borggreen, C. Bréchignac, P. Cahuzac, K. Hansen, and J. Pedersen, 1991, Chem. Phys. Lett. **186**, 53.
Martin, T. P., U. Näher, T. Bergmann, H. Göhlich, and T. Lange, 1991, Chem. Phys. Lett. **183**, 119.
Martin, T. P., U. Näher, and H. Schaber, 1992, Chem. Phys. Lett. **199**, 470.
Martins, J. L., J. Buttet, and R. Car, 1985, Phys. Rev. B **31**, 1804.
Martins, J. L., R. Car, and J. Buttet, 1981, Surf. Sci. **106**, 265.
Mermin, N. D., 1965, Phys. Rev. A **137**, 1441.
Mie, G., 1908, Ann. Phys. (Leipzig) **25**, 377.
Migdal, A. B., 1944, J. Phys. USSR **8**, 331.
Monnier, R., J. P. Perdew, D. C. Langreth, and J. W. Wilkins, 1978, Phys. Rev. B **18**, 656.
Mottelson, B., and S. G. Nilsson, 1955, Phys. Rev. **99**, 1615.
Moullet, I., and J. L. Martins, 1990, J. Chem. Phys. **92**, 527.
Moullet, I., J. L. Martins, F. Reuse, and J. Buttet, 1990a, Phys. Rev. Lett. **65**, 476.
Moullet, I., J. L. Martins, F. Reuse, and J. Buttet, 1990b, Phys. Rev. B **42**, 11 598.
Murphy, D. R., and W. P. Wang, 1980, J. Chem. Phys. **72**, 429.
Myers, W. D., and W. J. Swiatecki, 1969, Ann. Phys. (N.Y.) **55**, 395.
Myers, W. D., W. J. Swiatecki, T. Kodama, L. J. El-Jaick, and E. R. Hilf, 1977, Phys. Rev. C **15**, 2032.
Nielsen, O. H., *et al.*, 1992, "Melting of a copper cluster: Critical droplet theory" preprint (Tech. University of Denmark, Lyngby).
Nielsen, O. H., J. P. Sethna, P. Stoltze, K. W. Jacobsen, and J. K. Nørskov, 1992, preprint.
Nilsson, S. G., 1955, K. Dan. Vidensk. Selsk. Mat. Fys. Medd. **29**, No. 16.
Nishioka, H., K. Hansen, and B. R. Mottelson, 1990, Phys. Rev. B **42**, 9377.
Nørskov, J. K., 1982, Phys. Rev. B **26**, 2875.
Nørskov, J. K., and N. D. Lang, 1980, Phys. Rev. B **21**, 2131.
Ortiz, G., and P. Ballone, 1991, Phys. Rev. B **43**, 6376.
Pacheco, J. M., and R. A. Broglia, 1989, Phys. Rev. Lett. **62**, 1400.
Pacheco, J. M., R. A. Broglia, and B. R. Mottelson, 1991, Z. Phys. D **21**, 289.
Pacheco, J. M., and W. Ekardt, 1992, Z. Phys. D **24**, 65; Ann. Phys. (Leipzig) **1**, 254.
Pedersen, J., S. Bjørnholm, J. Borggreen, K. Hansen, T. P. Martin, and H. D. Rasmussen, 1991, Nature **353**, 733.
Pedersen, J., J. Borggreen, P. Chowdhury, N. Kebaïli, L. Lundsberg-Nielsen, K. Lützenkirchen, M. B. Nielsen, and H. D. Rasmussen, 1993, Z. Phys. D **26**, S-281.
Penzar, Z., and W. Ekardt, 1990, Z. Phys. D **17**, 69.
Penzar, Z., W. Ekardt, and A. Rubio, 1990, Phys. Rev. A **42**, 5040.
Perdew, J. P., 1979, Chem. Phys. Lett. **64**, 127.
Perdew, J. P., 1985, in *Density Functional Methods in Physics,* edited by R. M. Dreizler and J. da Providência (Plenum, New York), p. 309.
Perdew, J. P., 1986, Phys. Rev. B **33**, 8822; **34**, 7406(E).
Perdew, J. P., 1988, Phys. Rev. B **37**, 6175.
Perdew, J. P., 1989, in *Condensed Matter Theories, Vol. 4,* edited by J. Keller (Plenum, New York), p. 149.
Perdew, J. P., 1991a, in *Electronic Structure of Solids '91,* edited by P. Ziesche and H. Eschrig (Akademie, Berlin).
Perdew, J. P., 1991b, Physica B **172**, 1.
Perdew, J. P., J. A. Chevary, S. H. Vosko, K. A. Jackson, M. R. Pederson, D. J. Singh, and C. Fiolhais, 1992, Phys. Rev. B **46**, 6671.
Perdew, J. P., and V. Sahni, 1979, Solid State Commun. **30**, 87.
Perdew, J. P., H. Q. Tran, and E. D. Smith, 1990, Phys. Rev. B **42**, 11 627.
Perdew, J. P., and Y. Wang, 1986, Phys. Rev. B **33**, 8800.
Perdew, J. P., Y. Wang, and E. Engel, 1991, Phys. Rev. Lett. **66**, 508.
Perdew, J. P., and A. Zunger, 1981, Phys. Rev. B **23**, 5048.
Persson, J. L., R. L. Whetten, H.-P. Cheng, and R. S. Berry, 1991, Chem. Phys. Lett. **186**, 215.
Pogosov, V. V., 1990, Solid State Commun. **75**, 469.
Przyblyski, H., and G. Borstel, 1984a, Solid State Commun. **49**, 317.
Przyblyski, H., and G. Borstel, 1984b, Solid State Commun. **52**, 713.
Puska, M. J., R. M. Nieminen, and M. Manninen, 1985, Phys. Rev. B **31**, 3486.
Rao, B. K., and P. Jena, 1985, Phys. Rev. B **32**, 2058.
Reimann, S., and M. Brack, 1993, in *Theory of Atomic and Molecular Clusters,* edited by E. Hilf, P. Borrmann, and H. Barth (in press).
Reimann, S., M. Brack, and K. Hansen, 1993, Z. Phys. D **28** (in press).
Reinhard, P.-G., 1992, Phys. Lett. A **169**, 281.
Reinhard, P.-G., M. Brack, and O. Genzken, 1990, Phys. Rev. A **41**, 5568.
Reinhard, P.-G., and Y. Gambhir, 1992, Ann. Phys. (Leipzig) **1**, 598.
Reinhard, P.-G., S. Weisgerber, O. Genzken, and M. Brack, 1992, in *Nuclear Physics Concepts in Atomic Cluster Physics,* edited by R. Schmidt, H. O. Lutz, and R. Dreizler (Springer, Berlin), p. 254.
Röthlisberger, U., and W. Andreoni, 1991, J. Chem. Phys. **94**, 8129.
Rowe, D. J., 1968, Rev. Mod. Phys. **40**, 153.
Rubio, A., L. C. Balbás, and J. A. Alonso, 1990, Solid State Commun. **75**, 139.

Rubio, A., L. C. Balbás, and J. A. Alonso, 1991a, Physica B **168**, 32.
Rubio, A., L. C. Balbás, and J. A. Alonso, 1991b, Z. Phys. D **19**, 93.
Rubio, A., L. C. Balbás, and A. Vega, 1989, Z. Phys. D **12**, 209.
Sagawa, H., and G. Holzwarth, 1978, Prog. Theor. Phys. **59**, 1213.
Saito, S., S. B. Zhang, S. G. Louie, and M. L. Cohen, 1990, J. Phys. Condensed Matter **2**, 9041.
Saunders, W. A., 1986, Ph.D. thesis (University of California, Berkeley).
Schöne, W.-D., 1991, Diploma thesis (Bielefeld University).
Seidl, M., K.-H. Meiwes-Broer, and M. Brack, 1991, J. Chem. Phys. **95**, 1295.
Seidl, M., M. E. Spina, and M. Brack, 1991, Z. Phys. D **19**, 101.
Selby, K., V. Kresin, J. Masui, M. Vollmer, W. A. de Heer, A. Scheidemann, and W. D. Knight, 1991, Phys. Rev. B **43**, 4565.
Serra, Ll., F. Garcias, M. Barranco, N. Barberán, and J. Navarro, 1990, Phys. Rev. B **41**, 3434.
Serra, Ll., F. Garcias, M. Barranco, J. Navarro, L. C. Balbás, and A. Mañanes, 1989a, Phys. Rev. B **39**, 8247.
Serra, Ll., F. Garcias, M. Barranco, J. Navarro, L. C. Balbás, A. Rubio, and A. Mañanes, 1989b, J. Phys. Condensed Matter **1**, 10391.
Smith, J. M., 1965, Am. Inst. Aeronaut. Astronaut. J. **3**, 648.
Snider, D. R., and R. S. Sorbello, 1983a, Solid State Commun. **47**, 845.
Snider, D. R., and R. S. Sorbello, 1983b, Phys. Rev. B **28**, 5702.
Snider, D. R., and R. S. Sorbello, 1984, Surf. Sci. **143**, 204.
Sorbello, R. S., 1983, Solid State Commun. **48**, 989.
Spina, M. E., M. Brack, 1990, Z. Phys. D **17**, 225.
Spina, M. E., M. Seidl, and M. Brack, 1990, in *Symposium on Atomic and Surface Physics (SASP90)*, edited by T. D. Märk and F. Howorka (Innsbruck, University, Innsbruck), p. 426.
Sprung, D. W. L., 1972, Adv. Nucl. Phys. **5**, 225.
Stampfli, P., and K. H. Bennemann, 1987, in *Physics and Chemistry of Small Clusters*, edited by P. Jena, B. K. Rao, and S. N. Khanna (Plenum, New York), p. 473.
Sternheimer, R. M., 1957, Phys. Rev. **107**, 1565.
Stocker, W., and M. Farine, 1985, Ann. Phys. (N.Y.) **159**, 255.
Stott, M. J., and E. Zaremba, 1980, Phys. Rev. A **21**, 12.
Strutinsky, V. M., 1968, Nucl. Phys. A **122**, 1.
Strutinsky, V. M., 1975, Nukleonika (Poland) **20**, 679.
Strutinsky, V. M., A. G. Magner, S. R. Ofengenden, and T. Døssing, 1977, Z. Phys. A **283**, 269.
Strutinsky, V. M., and A. S. Tyapin, 1964, Sov. Phys. JETP **18**, 664.
Szasz, L., 1985, *Pseudopotential Theory of Atoms and Molecules* (Wiley, New York).
Tarazona, P., and E. Chacón, 1989, Phys. Rev. B **39**, 10366.
Thomas, L. H., 1927, Proc. Cambridge Philos. Soc. **23**, 542.
Thorpe, M. A., and D. J. Thouless, 1970, Nucl. Phys. A **156**, 225.
Thouless, D. J., 1961, Nucl. Phys. **22**, 78.
Tiggesbäumker, J., L. Köller, H. O. Lutz, and K.-H. Meiwes-Broer, 1992, Chem. Phys. Lett. **190**, 42; reprinted in *Nuclear Physics Concepts in Atomic Cluster Physics, 1992,* edited by R. Schmidt, H. O. Lutz, and R. Dreizler (Springer, Berlin), p. 247.
Treiner, J., and H. Krivine, 1986, Ann. Phys. (N.Y.) **170**, 406.
Utreras-Diaz, C. A., and H. B. Shore, 1984, Phys. Rev. Lett. **24**, 2335.
Utreras-Diaz, C. A., and H. B. Shore, 1989, Phys. Rev. B **40**, 10345.
von Barth, U., and L. Hedin, 1972, J. Phys. C **5**, 1629.
von Steinwedel, H., and J. H. D. Jensen, 1950, Z. Naturforsch. A **5**, 413.
von Weizsäcker, C. F., 1935, Z. Phys. **96**, 431.
Wigner, E. P., 1932, Phys. Rev. **40**, 749.
Wigner, E. P., 1934, Phys. Rev. **46**, 1002.
Wood, D. M., 1981, Phys. Rev. Lett. **46**, 749.
Yannouleas, C., and R. A. Broglia, 1991a, Phys. Rev. A **44**, 5793.
Yannouleas, C., and R. A. Broglia, 1991b, Europhys. Lett. **63**, 255.
Yannouleas, C., and R. A. Broglia, 1992, Ann. Phys. (N.Y.) **217**, 105.
Yannouleas, C., R. A. Broglia, M. Brack, and P. F. Bortignon, 1989, Phys. Rev. Lett. **63**, 255.
Yannouleas, C., J. M. Pacheco, and R. A. Broglia, 1990, Phys. Rev. B **41**, 6088.
Yannouleas, C., E. Vigezzi, and R. A. Broglia, 1993, Phys. Rev. B **47**, 9849.
Zangwill, A., and P. Soven, 1980, Phys. Rev. A **21**, 1561.